UNIVERSIDADE DO ALGARVE

Faculdade de Ciências e Tecnologia

FUNCTIONAL STUDY OF AVE SECRETED GENES DURING MOUSE EMBRYOGENESIS: INSIGHTS ON THE ROLE OF mADTK1

Lisa Gonçalves Dias da Silva

Tese orientada por Professor Doutor José António Belo

Doutoramento em Biologia

Biologia Molecular

2009

Dissertação de Candidatura ao Grau de Doutor em Biologia, Área de Biologia Molecular, pela Universidade do Algarve

PhD Thesis proposal in Biology, Molecular Biology, by the Universidade do Algarve (Portugal)

As opiniões expressas nesta publicação são da exclusiva responsabilidade do seu Autor.

The contents of this dissertation are of the exclusive responsibility of its Author.

(Lisa Gonçalves Dias da Silva)

In theory, there is no difference
between theory and practice.
In practice, however, there is.

unknown

Acknowledgments

I would like to thank Prof. José António Belo for accepting me at his lab at Instituto Gulbenkian de Ciência when I was just graduated, and for providing such an enriching scientific experience at his lab. Thank you for all the support and guidance, for all the educating scientific discussions and for believing I could carry out this project, even at the most difficult times.

To Faculdade de Ciências e Tecnologia of the Universidade do Algarve, thank you for the vote of confidence by accepting me as PhD student. To Centro de Biologia Molecular e Estrutural at Universidade do Algarve, thank you for provide such good facilities.

Fundação para a Ciência e Tecnologia, thank for the financial support, without which I couldn't have carried out this work.

I also want to acknowledge Intituto Gulbenkian de Ciências for its fantastic facilities, and support provided by all staff members and the scientific support all groups from *Zheng Ho* wing gave me when my lab was in transition to Faro. Particularly to Moises Mallo, who colaborated in the study of *mADTK1*, and Miguel Godinho who helped me with the Southern Blots.

Ana Cristina Borges, thank you for all the support you gave me when I first arrived at IGC. You made mouse basic embryology techniques seem much easier than they really are, thank you all you taught me. Thank you for all the patience.

Zé Inácio and Sara Marques, thank you for thoroughly reviewing this manuscript, for all comments, explanations and corrections. Without you it would have proved very difficult to deliver this manuscript. I also want to acknowledge Zé Inácio for performing all the transfection assays, and Sara Marques for helping me with the newborn analysis.

To all the members in the lab (the ones who are currently in lab and the ones who already left it), thank you for all the suggestions, advices and friendship; when experiments didn't work go as good as they should, you always gave the support to go on and try again, and again.

To all my friends and family, particularly to Hugo and Lucia, thank you for all the support, love and friendship. Thank you for listening and trying to understand those unique moments of great joy and frustration when an experiment finally works, or doesn't.

To my mother and brother, thank you for all the patience, advices, unconditional support, comprehension and love. Thank you for sharing the moments of joy and worry, and for sharing all the setbacks and all the achievements I accomplished during this PhD. Thank you for reviewing this manuscript, for all the corrections and suggestions. Without you I couldn't have made it. Thank you.

Resumo

Sendo os organismos vertebrados caracterizados por serem organizados assimetricamente sobre três eixos distintos, anterior-posterior (A-P), dorsal-ventral (D-V) e proximal-distal (P-D), é bastante importante estudar o momento em que estes eixos se formam. Durante o desenvolvimento embrionário existem várias vias de sinalização envolvidas neste acontecimento crucial, entre elas encontra-se a superfamília "Transforming Growth Factor-β" que engloba moléculas de elevada importância, tais como Nodal e proteínas morfogenéticas do osso (BMPs).

Em ratinho, são consideradas duas estruturas organizadoras para o tronco e cabeça. O centro organizador para o tronco é o nó, uma estrutura transiente que aparece ao sétimo dia do desenvolvimento embrionário, durante o processo de gastrulação, enquanto a linha primitiva se extende.

A Endoderme Visceral Anterior (AVE) é considerada o centro organizador para a cabeça e as estruturas anteriores, sendo portanto uma estrutura de imensa importância durante o desenvolvimento embrionário. É com a formação da AVE que começam a ser aparentes as primeiras evidências de assimetria, e que se inicia a formação do primeiro eixo, o eixo A-P. É nesta estrutura embrionária que vários genes de grande importância para a correcta organização dos eixos e desenvolvimento do embrião são expressos. Entre eles encontra-se *Hex*, *goosecoid, otx2*, *Hesx1/Rpx, lim1, dkk1, lefty1* e *cerberus-like1* (*cerl1*).Este último é um antagonista de Nodal e BMPs, e é um membro da superfamília TGF-β.

Mutantes homozigóticos para o *cerl1* não aparentam ter qualquer tipo de fenótipo, são viáveis e férteis. Contudo, é preciso salientar o facto de a ausência de fenótipo não ser sinónimo de pouca importância. Durante o desenvolvimento embrionário, vários genes compensam o papel uns dos outros, actuando sinergisticamente.

cerl1 é um gene que desempenha um papel central na regulação da via de sinalização Nodal. Estudos prévios demonstraram que o *cerl1* age em cooperação com genes *lefty*, também conhecidos pelo seu carácter antagonista em relação a Nodal. A via de sinalização Nodal é necessária para que o processo de gastrulação ocorra, e é essencial para a correcta formação dos eixos embrionários.

Com o intuito de aprofundar o estudo da via de sinalização Nodal, e uma vez que esta é extremamente importante durante o desenvolvimento embrionário, numa primeira

fase efectuaram-se estudos a fim de avaliar potenciais interacções entre *cerl1* e *cripto*, um co-receptor necessário para a transdução de sinais Nodal. Curiosamente, a análise destas possíveis interacções sugere uma via de sinalização Nodal independente do co-receptor Cripto. O estudo de duplos mutantes para *cerl1* e *cripto*, levou à conclusão que neste caso, a via de sinalização Nodal é parcialmente recuperada. O que indica uma potencial via de sinalização Nodal não canónica, provavelmente através do receptor serina/treonina tipo I, ALK7.

Na tentativa de caracterizar e entender melhor o papel da AVE durante o desenvolvimento embrionário de ratinho, no que diz respeito aos genes que nela são expressos, foi efectuado no laboratório um *screening* diferencial, onde foram seleccionados os genes que se encontravam sobre expressos na região da AVE.

Entre os vários novos genes descobertos, encontram-se o *shisa* e *ADTK* (Anterior Distal Tyrosine Kinase).

Os ortólogos, s*hisa-1* e s*hisa-2* em *Xenopus*, demonstraram estar envolvidos na formação de estruturas anteriores e sómitos, respectivamente. Ainda mais, revelaram ter um papel inibitório das vias de sinalização Wnt e Fibroblast Growth Factors (FGF). Foi publicado um estudo onde demonstraram que Shisa1 se liga aos receptores de FGF e Wnt no retículo endoplasmático impedindo deste modo a maturação dos receptores e, consequentemente, a sua translocação para a superfície celular, onde estes receptores desempenham as suas funções. No que diz respeito ao Shisa-2 estudos efectuados no laboratório levaram à conclusão que a expressão nos sómitos e zona pré-somítica estava directamente correlacionada com o seu papel. Experiências revelaram que baixos níveis deste gene dá origem a sómitos mais estreitos e ao deslocamento rostral de marcadores específicos da mesoderme pré-somítica posterior.

De modo a conhecer os potenciais papéis desempenhados por este gene em ratinho, foi efectuada uma análise comparativa exaustiva do padrão de expressão durante o desenvolvimento embrionário de ratinho e galinha. Verificou-se que o *shisa* de ratinho e de galinha têm um padrão de expressão muito idêntico, o que indica que este gene é mantido inter-espécies. Ainda mais, verificou-se que o *shisa* está presente em tecidos como o olho, sómitos e membros, que, tipicamente, requerem a modulação das vias de sinalização Wnt e FGF. Contudo, recentemente foi publicado um estudo em que eliminaram todas as isoformas existentes do *shisa* em ratinho, e nenhuns defeitos a nível

dos sómitos, olho ou membros, foram identificados. Ainda mais, nenhum defeito a nível da cabeça, como é sugerido em experiências efectuadas com *shisa-1* em *Xenopus*.

A grande parte deste trabalho concentrou-se no estudo do novo gene *ADTK1*. Este gene codifica uma proteína com domínio catalítico tirosina cinase serina/treonina. Uma vez que os processos de fosforilação são etapas determinantes para o correcto desenvolvimento embrionário, que os domínios serina/treonina desempenham papéis fulcrais na transdução de sinal, e sendo este gene expresso na AVE, (região que contém tantos genes de particular interesse para o vários processos essenciais à embriogénese), seria do maior interesse fazer uma análise pormenorizada do padrão de expressão deste gene durante as várias fases do desenvolvimento embrionário, bem como uma análise funcional. Deste modo, verificou-se que o gene *ADTK1* está expresso desde muito cedo no desenvolvimento embrionário, e permanece expresso até mais de metade do processo. O padrão de expressão do *ADTK1* intrigou-nos desde logo, uma vez que está presente em várias estruturas de particular interesse para o desenvolvimento. Verificou-se que este gene está presente na AVE, o que é um controlo positivo para o *screening* efectuado, aparece pontualmente na linha primitiva quando esta ainda não se encontra na sua extensão completa, depois do qual fica restrito à parte anterior do embrião, marcando zonas como dobras neurais, primórdios do olho, sómitos, arcos faríngeos, pericárdio, membros superiores e inferiores. Tais resultados sugeriram um potencial papel na regulação de estruturas como a cabeça, tubo neural, coração e desenvolvimento dos membros. Dados preliminares em *Xenopus* e galinha corroboraram esta hipótese, uma vez que os ortólogos de *Xenopus* quando subexpressos, apresentam dificuldades em fechar o tubo neural, enquanto os ortólogos de galinha, quando subexpressos, apresentam defeitos a nível do coração. Procedeu-se então à inactivação do *ADTK1* em ratinho através de recombinação homóloga. Os animais heterozigóticos não apresentam quaisquer tipos de defeitos, são viáveis e férteis. O cruzamento destes animais gerou homozigóticos que foram sacrificados nas primeiras 48 horas. Pelo menos durante este período de tempo, os animais homozigóticos são viáveis e não apresentam comportamentos diferentes dos restantes animais da mesma ninhada. A análise dos homozigóticos para o *ADTK1* demonstra que a maioria destes animais não exibe qualquer defeito exterior óbvio. A cabeça apresenta-se bem fechada, os membros parecem estar bem formados e o tubo neural está correctamente fechado. No entanto, em alguns mutantes verificaram-se alterações no olho e orelha. Uma análise preliminar

do esqueleto dos mutantes demonstrou que os ossos dos membros são menores do que os correspondentes animais wild-type. Ao analisar os órgãos internos, verificou-se que estes se posicionavam correctamente, e não foram identificadas diferenças significativas a nível do coração, pulmões, fígado, intestinos e estômago. Ao comparar os rins dos animais homozigóticos com os correspondentes wild-type, observou-se que todos os animais analisados apresentavam rins maiores e com uma cor mais vermelha. A análise histológica preliminar dos rins, sugere deficiências ao nível da zona medular do rim, e diminuição de estruturas glomerulares. Comparando com a literatura, verificou-se que o fenótipo obtido nos rins de homozigóticos *ADTK1*, é bastante semelhante ao descrito para o gene *wnt4*. Animais mutantes para o *wnt4* apresentam defeitos nas células do estroma medular do rim. Este gene está envolvido no processo de desenvolvimento dos rins, nomeadamente no desenvolvimento e proliferação de células do músculo liso. Tal sugere um potencial papel na regulação do desenvolvimento dos rins. Este é um processo bastante complexo e que ainda se encontra muito pouco estudado, sabendo-se que as vias de sinalização Wnt, FGF e BMP estão envolvidas neste processo.

Tal como acontece com tantos outros genes, o gene *ADTK1* não reproduz os defeitos que os correspondentes ortólogos em *Xenopus* apresentam. É provável que tal se deva ao facto de, nos mamíferos, existirem genes que compensam as funções uns dos outros, de modo a minimizar as anomalias, e ultrapassar possíveis defeitos que dessem origem à interrupção do desenvolvimento embrionário.

Palavras-chave: AVE, ratinho, desenvolvimento embrionário, gastrulação, *ADTK1*, *shisa*, *cerl1*, tirosina cinase.

Abstract

The vertebrate organisms are characterized by being asymmetrically organized in three different axes, it is important to study the onset of these axes. Several pathways are involved in this crucial event, among them is Transforming Growth Factor-β (TGF-β) superfamily which comprises several key molecules as Nodal and Bone Morphogenetic Proteins (BMP).

The Anterior Visceral Endoderm (AVE) is a very important structure during mouse embryonic development, where first asymmetries start to show and axes start to be established. Several genes such as mouse *cerberus-like,* a member of the TGF-β superfamily, and a Nodal and BMP antagonist, are expressed in this tissue and are of major importance for correct development of the embryo. *cerl-1* is a critical player in the Nodal signaling pathway, which is of major importance during gastrulation and the onset of axes establishment. Interestingly, the analysis of potential interactions between Cer-l and Nodal co-receptor Cripto, suggested the possibility of a Cripto independent Nodal signaling pathway, in establishing the anterior-posterior (A-P) and dorso-ventral (D-V) axes during embryonic development.

In an attempt to further study the AVE a pool of novel genes upregulated in this tissue was discovered by a differential screening. Among these were found *shisa* and *ADTK1*.

Previous work in *Xenopus* has shown that Shisa-1 inhibits both FGF and Wnt signaling pathways, by regulating the maturation of their receptors. Downregulation of Shisa-1 leads to defects in anterior structures. In the lab, it was demonstrated that Shisa-2 is involved in the correct development of somites. During this work, it was performed an exhaustive comparative analysis of s*hisa* expression patterns in mouse and chick. Cross-species comparison showed that the expression pattern is conserved in mouse and chick, indicating that the Shisa family genes are typically expressed in tissues known to require the modulation of Wnt and FGF signaling, such as somites, eye and limbs.

The largest part of this work consisted of the analysis of *ADTK1* role in mouse. A detailed analysis of its expression pattern was performed, indicating several processes in which this gene might be involved in, such as the formation of anterior structures, limb and heart development and neurulation. This hypothesis was consistent with data from *Xenopus* and chick orthologs, where downregulation of *ADTK1* leads to defects in neural tube closure and heart development, respectively.

In order to evaluate *ADTK1* biological function, a targeted inactivation was performed. Although the majority of *ADTK1* null mutants presented no visible phenotype, some presented defects in the eye and ear. Skeletal analysis of *ADTK1* null mutants demonstrated defects in bone length; these mutants present shorter limbs than their wild-type littermates. Regarding the internal organs, defects in kidney development were detected in all analyzed mutants. *ADTK1* mutant kidneys were larger and had a reddish color, comparing to the wild-type littermates. Furthermore, preliminary histological analysis suggests that the kidney medullar region is affected, and that glomerular structures are diminished, when comparing to the wild type. The process of kidney development is a complex one, not yet fully understood. Several signaling pathways, such as Wnts, Shh, BMPs and FGFs, are involved in the process of nephrogenesis.

Once again, as it happens with so many genes, *ADTK1* null mutants don't mimic the defects presented by downregulation in *Xenopus* and chick orthologs. It is possible that the lack of striking phenotype can be accounted for the fact that, in mammals, there are several genes with redundant activity, preventing, this way, potential anomalies, and overcoming defects that could lead to embryonic development arrest.

Keywords: AVE, mouse, embryonic development, gastrulation, *ADTK1*, *shisa*, *cerl1*, tyrosine kinase.

Table of Contents

Table of Figures

Abbreviations

µL	-	Microliter
µm	-	Micrometer
3’	-	3 prime
5’	-	5 prime
aa	-	Amino acid
Ab	-	Antibody
ADE	-	Anterior Definitive Endoderm
ADTK	-	Antero Distal Tyrosine Kinase
AER	-	Apical Ectodermal Ridge
AP	-	Anterior-posterior
ASE	-	Asymmetric Intronic Enhancer
AVE	-	Anterior visceral endoderm
BMP	.	Bone Morphogenetic Protein
bp	-	Base pair
cDNA	-	Coding DNA
CDS	-	Coding Sequence
cerl	-	Cerberus-like
Chd	-	Chordin
CNS	-	Central Nervous System
Dhh	-	Desert hedgehog
DIG	-	Digoxigenin
Dkk	.	Dickkopf
DLHP	-	Dorsolateral hinge point
DMEM	-	Dulbecco’s Modified Eagle Medium
DNA	-	Deoxyribonucleic acid
dpc	-	Days post coitum
DV	-	Dorso-Ventral
DVE	-	Distal Visceral Endoderm
E	-	Embryonic day
EGO	-	Early Gastrula Organizer
EPI	-	Epiblast

ER	-	Endoplasmatic Reticulum
ES	-	Embryonic stem
FBS	-	Fetal Bovine Serum
FD	-	Faraday
FGF	-	Fibroblast growth factor
Fw	-	Forward
Fz	-	Frizzled
h	-	Hour
HPRT		hypoxanthine guanine phosphoribosyl transferase
ICM	-	Inner Cell Mass
Ihh	-	Indian hedgehog
JNK	-	Jun-N terminal Kinase
LPM	-	Lateral Plate Mesoderm
L-R	-	Left-Right
LRP	-	Low-density-lipoprotein Receptor-related Protein
MAP	-	Mitogen-Activated Protein
MEF	-	Mouse Embryonic Fibroblast
MGO	-	Mid Gastrula Organizer
MHP	-	Medium hinge point
min	-	Minute
mL	-	Milliliter
NTD	-	Neural tube defect
Oep	-	one eye pinhead
ON	-	Overnight
Otx2	-	Orthodenticle-related homeobox
PBS	-	Phosphate-buffered saline
PCP	.	Planar Cell Polarity
PCR	-	Polymerase Chain Reaction
P-D	-	Proximal-Distal
PE	-	Primitive Endoderm
PFA	-	Paraformaldehyde
PKC	-	Protein Kinase C
PSM	-	Presomitic Mesoderm

Ptc	-	Patched
RA	-	Retinoic Acid
Rev	-	Reverse
RNA	-	Ribonucleic acid
RT	-	Reverse Transcription
RT	-	Room Temperature
RTK	-	Receptor tyrosine kinases
SDS	-	Sodium dodecyl sulfate
SFRP	-	Secreted Frizzled Related Protein
Shh	-	Sonic hedgehog
SMART	-	Simple Modular Architecture Research Tool
Smo	-	Smoothed
TE	-	Trophoectoderm
TGF-β	-	Transforming Growth Factor-beta
UTR	-	Untranslated Region
UV	-	Ultraviolet
V	-	Volt
VE	-	Visceral Endoderm
WISH	-	Whole mount in situ hybridization
ZPA	-	Zone of Polarizing Activity

1. Introduction

The origin of life is still poorly understood. As for the origin of life concerning the animal kingdom, much is already known, but much still remains to unravel.

Embryonic development has been fascinating the human being for a very long time. Aristotle, in 384 B.C., was the first person ever to write about embryology, suggesting the two theories that would prevail for long. At that time, the debate was whether the embryo was a preformed miniature individual (a homunculus) or an undifferentiated form that gradually became specialized when fertilized: preformation versus epigenesis. According to the preformation theory, an embryo or miniature individual preexists in either the female's egg or the male's sperm and begins to grow when properly stimulated. Some preformationists believed that all the embryos that would ever develop had been formed by God at the Creation. From the analysis of chick embryos Aristotle preferentially supported the theory of epigenesis.

The subject of embryo development was then left forgotten until the 13th century, when Albertus Magnus, a scholastic, started to study fish development. This reappraisal opened the way to the scientific movement of the Renaissance, when in the 15th century Leonardo da Vinci played an essential role, approaching the development of the human embryo with a series of sketches that supported the preformation theory (Fig. 1.1) (da Vinci 1510-1513).

Figure 1.1 - The dwarf embryo as imagined by Leonardo da Vinci in the 15th century
Adapted from Studies over embryos, da Vinci 1510-1513.

With the use of the microscope, and the discovery of sperm in 1677 by Hartsoeker and Leeuwenhoek, the theory of epigenesis proved the more difficult to defend: Hartsoeker proposed a spermatozoid structure where a tiny human being was concentrated (Fig 1.2) (Hartsoeker 1694). However a question remained, how could complex organisms, as human beings, develop from such simple organisms?

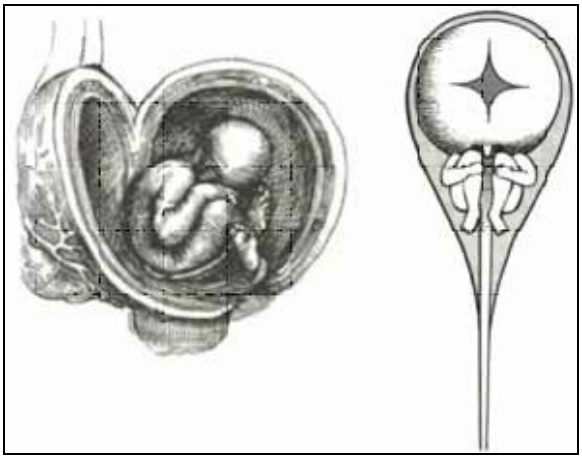

Figure 1.2 - The sperm as miniature human being by Hartsoeker from the 17th century
Adapted from Hartsoeker 1694.

It wasn't until two centuries later, in 1827, when Karl Ernst von Baer discovered the mammalian egg by identifying a yellowish spot within the follicle, which was only visible with a microscope (von Baer 1827), that Aristotle's theory of epigenesis was again supported. In the late 19th century, in 1890, Wilhelm Roux and Hans Driesch founded the experimental embryology. Roux tried to prove the preformation theory when, in a two-cell stage frog embryo, he destroyed half the embryo with a hot needle and obtained just half an embryo after letting the embryo develop. He believed that the fertilized egg receives substances that represent different characteristics of the organism, which, as cell division occurs, are asymmetrically distributed to daughter cells. This qualitative division fixes the fate of the cells and their descendants, because some of the determinants are lost at each division. The destruction of a single cell in an embryo with a hot needle was a revolutionary technique that would be the base of several experiments many years later (Kirschner 2003).

Driesch refuted this theory when he himself, instead of destroying one of the cells, separated a two cell stage of a sea urchin embryo into two individual cells, and allowed

them to develop: both cells developed into complete sea urchins. Driesch concluded, then, that each cell retains all the developmental potential of the zygote (Oppenheimer 1970).

Later on, in the 20th century, Hans Spemann and Hilde Mangold performed a series of experiments on the newt that opened a new field towards the understanding of the embryonic development, namely the organization and the process of axis formation. These experiments led to the beginning of developmental biology, an area of science where much is still to discover and understand (Spemann and Mangold 1924, Spemann 1931).

During the last fifty years, since the finding of DNA in 1953 by Watson and Crick (Watson and Crick 1953), and then the discovery of the translation system which gave a Nobel Prize in 1968 to Holley, Khorana and Nirenberg, there were many breakthroughs towards understanding cell signaling and molecular biology. Furthermore, much has been achieved with the sequencing of the genome. The first draft of the human genome was published in 2001 and was completed in 2006, whereas the complete mouse genome was published in 2002. This only came to unravel the large amount of work that remains to be done with the about 24.000 genes identified in mouse; nowadays, the true work lies on interpreting the proteins translated and the interactions between them, understanding therefore the signaling cascade processes that occur outside and inside the cells.

1.1 MOUSE EMBRYOGENESIS

The mouse is a widely used model when studying developmental biology and inherent molecular processes. However, mouse embryos are small and are not produced in large numbers in comparison to *Xenopus* or chick; furthermore, mouse embryos develop relatively slowly, complete mouse gestation takes about three weeks, and the embryos are inaccessible to experimental manipulation because development takes place *in utero*. In spite of all these drawbacks, mice are mammals, easy to handle, and of low maintenance cost, when compared with other mammalian model organisms.

Being mammals ourselves, we have a particular interest in understanding mammalian development. Furthermore, comparing with *Xenopus* and chick, the mouse genome has a higher homology to the human genome and proteins share similar functions.

1.2 EARLY MOUSE DEVELOPMENT

The fertilized egg divides and develops as it travels along the oviduct to the uterus. In mice this process takes about 4 to 5 days (Fig 1.3). The egg has a protective membrane called the *zona pellucida*, which stops it from implanting in the oviduct wall (Beddington and Robertson 1999).

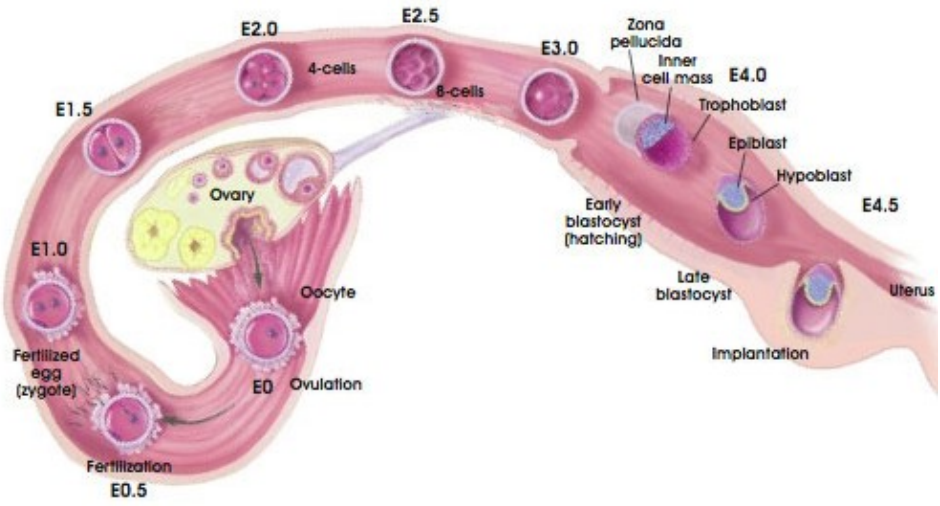

Figure 1.3 - Development of the pre-implantation blastocyst in mice

Schematic view of the processes which the embryo undergoes until it is implanted into the uterine wall. E-embryonic day. Adapted from Regenerative Medicine 2006.

By the time it reaches the uterus, the egg has undergone many cell divisions. Cleavage culminates in blastulation right after the morula stage, by day 3.5 to 4.5 (Beddington and Robertson 1999). The blastocyst hatches from the *zona pellucida* to implant into the uterine wall. The morula stage is reached at 16 cell stage when the outside cells increase contact with each other through a process known as compaction

(Zernicka-Goetz 2005). With blastulation two distinct types of tissues are formed: extraembryonic and embryonic. The extraembryonic tissue consists of the trophectoderm (TE) and is called extraembryonic because it does not contribute with any descendant cells in the future body. The embryonic tissue is called the inner cell mass (ICM) (Beddington and Robertson 1999, Zernicka-Goetz 2002). The ICM is said to be pluripotent, as each cell can be differentiated into any cell type. These pluripotent cells are characterized by expressing three transcription factors, Oct4, Nanog and Stat3 that are essential for maintaining the pluripotency of the ICM and for the formation of the embryo. The trophectoderm is characterized by the expression of the T-box transcription factor eomesodermin and the caudal-like transcription factor Cdx2, which are responsible for the downregulation of Nanog and Oct4 (Fig 1.4) (reviewed by Zernicka-Goetz, et al. 2009).

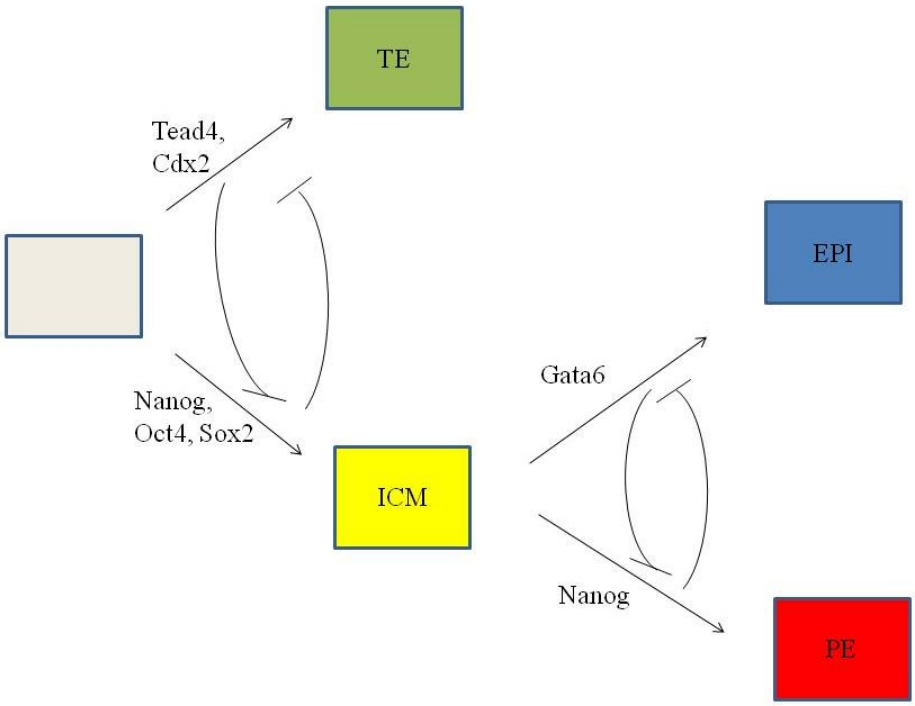

Figure 1.4 - Transcriptional circuitry of cell fate decisions

TE- trophectoderm, ICM- inner cell mass, EPI- epiblast, PE- primitive endoderm. ICM-specific gene expression (yellow; such as *Nanog*, *Oct4*, *Sox2*) represses TE-specific genes (green; such as *Tead4*, *Cdx2)* that in turn could repress ICM genes. The ICM then differentiates into EPI (blue; for example, *Nanog*) and PE (red; such as *Gata6*), where there is similar reciprocal antagonism of gene expression. Adapted from Zernicka-Goetz, 2009.

Later on after implantation, the ICM gives rise to the epiblast (EPI) and the primitive endoderm (PE), which produces the visceral endoderm lining the extraembryonic yolk sac (Tam and Loebel 2007).

Immediately after hatching, the blastocyst is caught by the endometrium where a network of collagen, laminins and fibronectin form an extracellular matrix that, along with the trophoblast enzymes, allow the embryo to attach and bury in the uterine wall (Gilbert 2006).

When the mouse embryo implants, it changes its form and size rather dramatically; it starts being a vesicular structure consisting of ICM inside the trophectoderm and, within 3 days, the polar trophectoderm and the ICM develop into an elongated structure that is made up of the ectoplacental cone and the extraembryonic ectoderm (Fig 1.5). The proliferating polar trophectoderm will originate the extra-embryonic ectoderm that seems to 'push' the proliferating ICM complex into the blastocyst cavity. It is this inward growth, which is characteristic of rodent embryos, that transforms the embryo into the elongated cylindrical structure called the egg cylinder (Zernicka-Goetz 2002). It is at this stage, when the extraembryonic and embryonic regions are well defined, that the polarized proximo-distal (P-D) axis is delineated. More, the prospective dorso-ventral (D-V) axis can also be detected at this stage, the surface of the epiblast that faces the proamniotic cavity corresponds to the future dorsal side and the outer surface of the VE marks the future ventral side of the embryo (Beddington and Robertson 1999).

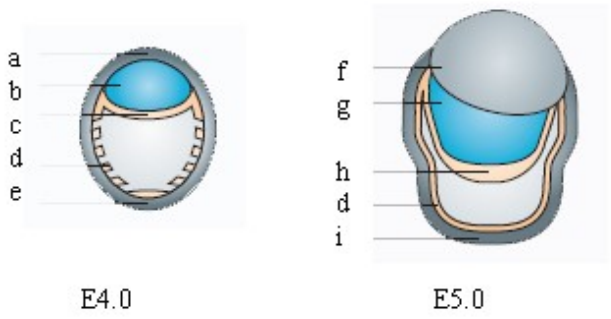

Figure 1.5 – Implanting blastocyst to pre-DVE stage

a. Polar trophectoderm; b. Inner Cell Mass; c. Primitive endoderm; d. Parietal endoderm; e. Mural trophectoderm; f. Extraembryonic ectoderm; g. Epiblast; h. Visceral endoderm; i. Trophoblast. Adapted from Tam and Loebel 2007.

The primitive endoderm, also called hypoblast, is a transitory cell layer that appears along the blastocoelic surface of the embryo between E4.0 and E5.0 dpc (days post coitum) (Fig 1.5) (Tam and Loebel 2007). These cells are of great importance, as they are the origin of two important and distinct extraembryonic cell types, the parietal endoderm and the visceral endoderm. The first, along with trophectoderm, is responsible for the synthesis of the extracellular matrix type IV proteins, collagen and laminins. These proteins will then assemble into Reichert's membrane, a specialized membrane that surrounds the embryo and passively filters nutrients (Bielinska, et al. 1999). The second, the visceral endoderm (VE), is associated with the epiblast. The VE cells have microvilli and contain numerous phagocytic and pinocytic vesicles that will grant the absorption and digestion of maternal nutrients. Another feature of VE is that these cells still retain the ability to differentiate into parietal endoderm (Bielinska, et al. 1999).

Curiously, the morphology of VE cells are different along the endoderm layer: the ones overlying the lower or distal pole of the egg cylinder have a squamous morphology, while more proximal visceral endoderm cells are cuboidal (Bielinska, et al. 1999); furthermore, it is also known that the function of these cells also varies. For instance, in the distal tip of the embryo several Nodal antagonists responsible for axis formation are present (Belo, et al. 1997), whereas in posterior proximal region of the VE genes related with hematopoietic commitment such as *wnt3* and *bmp2* can be detected (Baron 2005).

Asymmetry generation begins very early during embryonic development, even before gastrulation, with the generation of polarity, mostly from maternal information inheritance in the extra embryonic ectoderm (Zernicka-Goetz 2005).

1.2.1 Gastrulation

Gastrulation is a stage in which the embryo faces massive reorganization due to a wide cell movement, from a simple spherical ball of cells, the blastula, into a multi-layered organism. Although the details of gastrulation differ between various groups of animals, the cellular mechanisms involved in gastrulation are common to all animals. Gastrulation involves changes in cell motility, cell shape, and cell adhesion (reviewed in Gilbert 2006, Wells and Melton 1999).

In the early post implantation mouse embryo, the process of gastrulation converts the epiblast into the three primary germ layers: endoderm, mesoderm and ectoderm, from which all the fetal tissues will develop (Fig 1.6). Briefly, from these layers, the ectoderm will generate skin and the central nervous system; mesoderm will give rise to the blood, bone and muscle and the endoderm will be the origin of the respiratory and digestive tracts (reviewed by Wells and Melton 1999).

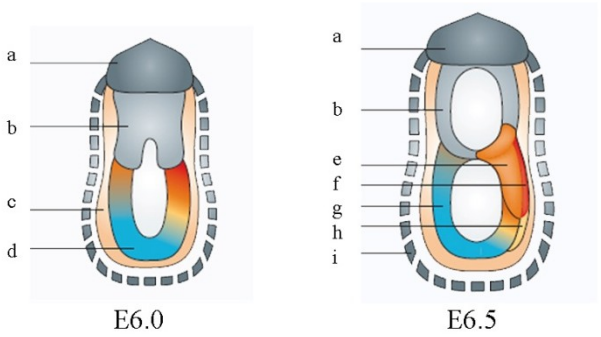

Figure 1.6 - Early post-implantation development in the mouse: Post DVE to early streak stage
a. Ectoplacental Cone; b. Extraembryonic Ectoderm; c. AVE; d. Epiblast; e. Mesoderm; f. Primitive Streak; g. Ectoderm; h. Definitive Endoderm; i. Parietal yolk sac and Reichert's membrane. Adapted from Tam and Loebel 2007.

Gastrulation begins at 6.5 dpc with the formation of a characteristic transient structure, the primitive streak (PS), at the posterior end of the epiblast (Fig 1.7). Embryos that fail to form PS, also fail to proceed with gastrulation and are not viable (Conlon, et al. 1994). During this critical step of embryonic development, several morphogenetic cell movements occur in order to transform a two germ layer into a three germ layer epiblast. In the proximal region of the epiblast, the mesendodermal cells ingress and, as the PS extends, mesoderm, definitive endoderm, and axial mesendoderm precursors arise in the streak by 7.0 dpc, and undergo coordinated morphogenetic movements that lead to their eventual placement in posterior and anterior positions (Tam and Loebel 2007). Mesodermal cells move immediately adjacent to the overlying epiblast, while definitive endoderm cells constitute the outer-most layer (Tam and Loebel 2007, Tam, et al. 2006). The anterior and proximal movement of definitive endoderm cells displaces visceral endoderm to extraembryonic locations. On the other

hand, the mesodermal cells that arise in the anterior end of the primitive streak at 7.0 dpc, except for the node, constitute the presumptive heart mesoderm, and have moved to the anterior-most embryonic region by 7.5 dpc where the heart will be formed (Baron 2005).

The PS is marked by the expression of several genes such as *Nodal, brachyury, cripto* and *wnt3* among others (Rivera-Pérez and Magnuson 2005, Conlon, et al. 1994, Barrow, et al. 2007). It is involved in cell fate specification, whereby endoderm and mesoderm precursors migrate through the PS in the process of differentiating. It is known that the generation of the primitive streak is regulated by multiple pathways, including Nodal, Wnt and Bmp (Conlon, et al. 1994, Barrow, et al. 2007).

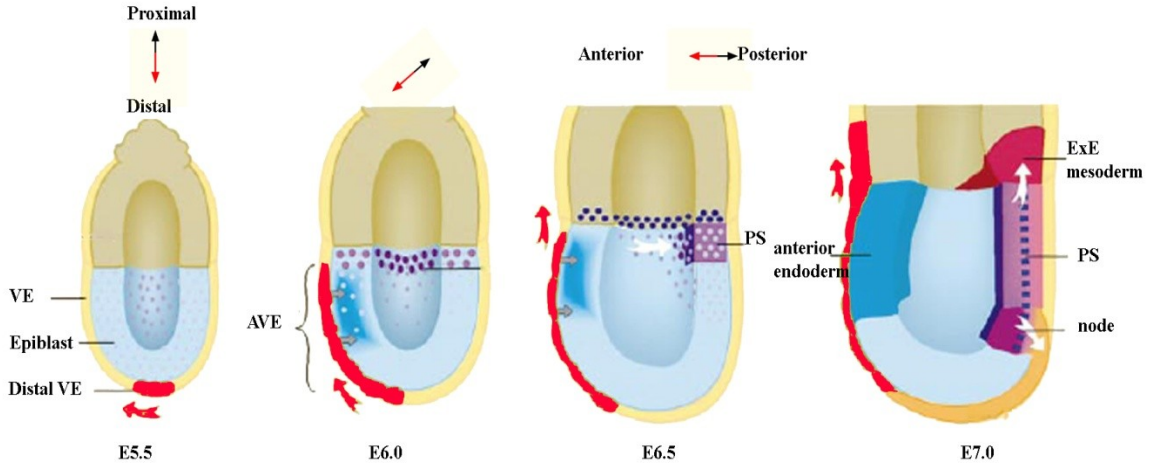

Figure 1.7- Cell Movements and Molecular Signals Controlling Axis Formation

AVE- Anterior Visceral endoderm, ExE- Extraembryonic; PS- Primitive streak,VE- Visceral endoderm. At E5.5, distal VE cells (red), marked by *Hex* expression, give rise only to anterior progeny, which populate the AVE and eventually move into the extraembryonic region (red arrows). The AVE induces anterior character in the underlying epiblast. Transcripts of future markers of the PS such as *Cripto* are ubiquitously expressed in the epiblast at E5.5 but restricted to the proximal rim of epiblast at E6.0, where other markers of the PS, such as *brachyury* (deep purple) start to be expressed. Caudal cell movement in the proximal epiblast (white arrow) results in the PS forming opposite the AVE at E6.5. By E7.0 extraembryonic mesoderm is produced from the posterior aspect of the streak while anteriorly the node forms. Adapted from Beddington and Robertson 1999.

Also during gastrulation, a transient structure named node is formed (Fig 1.7) (Beddington 1994, Lee and Anderson 2008, McGrath, et al. 2003). This structure is formed from the mesoderm, at the most anterior part of the PS. As the streak elongates, the subsequent mesendodermal cells that pass through the node will differentiate into anterior definitive endoderm (ADE), prechordal mesendoderm and notochord. (Beddington 1994). By the end of gastrulation, the prechordal plate is preceded posteriorly by the notochord and followed anteriorly by the definitive endoderm. At this time, convergent extension, a combined movement of mesoderm and definitive endoderm, is required for the midline tissues anterior to the node to extend. By this time, the endoderm consists of one thick cell layer of approximately 500 cells, which covers the mesoderm and ectoderm of the embryo (Zernicka-Goetz 2005).

As said before, the definitive endoderm constitutes the precursor of the embryonic gut: the visceral endoderm during gastrulation is replaced by definitive endoderm which ingresses through the anterior segment of the PS; the visceral endoderm only makes a minor contribution to the foregut (Tam, et al., 2003).

Before gastrulation, although it is difficult to identify the anterior-posterior (A-P) axis of the embryo by morphology, the expression of some genes is already asymmetrically established on one side of the VE. This side corresponds to the future anterior end of the embryo, hence its name, the anterior visceral endoderm (AVE).

1.2.2 The origin of body axis and the organizer

Early studies by Spemann and Mangold showed that in amphibian embryos the dorsal blastopore lip, a region that was subsequently named the "Spemann organizer" or "Organizer", could induce a complete secondary axis, when grafted in the ventral side of an embryo (Spemann and Mangold 1924). In addition, it was also observed that this transplanted tissue could induce the surrounding cells to acquire a new fate, organizing this way the formation of a novel central nervous system (CNS) and notochord, and also contributing to the dorsalization of mesoderm and generation of somites (Spemann and Mangold 1924).

Studies of body axis formation led to the discovery of similar inducing centers in other vertebrates, which were called Hensen's node in chick (Waddington 1933), the

embryonic shield in zebrafish (Ho 1992), and the node and AVE in mouse (Beddington and Robertson 1999). While grafts of the early Spemann organizer can induce a complete, head-containing secondary axis, grafts of late organizer tissue give rise to the trunk region without a head (Spemann 1931).

The node was the first organizing center proposed in mouse; however, node transplantation in the mouse embryo resulted in the formation of incomplete axis without anterior structures, suggesting then the existence of another organizer for the anterior structures (Beddington 1994).

Until quite recently, anterior patterning of the developing central nervous system in the mouse had been attributed solely to the influence of axial mesoderm or definitive endoderm derived from the node during gastrulation (Beddington 1981, Blum, et al. 1992). Over the past few years it has become apparent that murine AVE, which overlies the future anterior embryonic region, plays an active role in the specification of the A-P axis, as well as in heart formation and positioning of the yolk sac (Thomas and Beddington 1996, Belo, et al. 1997). Accordingly, the AVE was suggested to be an early organizer that specified anterior identity prior to and early in gastrulation (Belo, et al. 1997, Beddington and Robertson 1998).

The gastrula stage has been associated to head formation for a long time. During gastrulation, the AVE organizer assures anterior gene expression, which is essential to the development of the early head, and the beginning of the formation of neural tissues (Anderson 2002)

This way, two distinct organizing centers for the head and trunk have been postulated for the development of the A-P axis in mammals (Belo, et al. 1997). These head and trunk inducing activities are suggested to reside within the AVE and node/primitive streak, respectively. These structures are clearly separated in mouse, contrary to the amphibian embryos where the head and trunk organizer are spatially close, residing in the Spemann organizer (Beddington 1994, Spemann and Mangold 1924, Belo, et al. 1997).

The process of normal left-right (L-R) patterning of the vertebrate embryo can be described in three different stages. The first is the establishment of L-R asymmetry with respect to the D-V and A-P axes in the embryo. This results in a global L-R axis for the embryo such that asymmetries are consistently oriented in the body. Subsequently, this global L-R patterning information is transmitted to developing organ primordia, through

signaling molecules. And finally, the organ primordia must correctly interpret the positional cues and execute appropriate morphogenetic responses. When perturbations of L-R development occur, numerous defects result including bilateral symmetry, isomerism, heterotaxia, *situs inversus*.

1.2.3 The Node

The mouse node is a structure that is formed at the distal tip of the E7.0 embryo, when some groups of columnar cells with small apical surfaces become visible (Beddington 1994). The node is composed of two columnar epithelial layers with adjoining basal surfaces: the dorsal node is adjacent to the surrounding epiblast, whereas the ventral node is contiguous with adjacent endodermal epithelium (Lee and Anderson 2008). There are about 250 cells in a mature node. The node pit consists of a dorsal layer of ectoderm over a ventral layer of cells each with a single *monocilium* on their apical surface; these cells present apical basal polarity (Lee and Anderson 2008, McGrath, et al. 2003).

At this structure, a leftward fluid flow of great importance to the establishment of the L-R axis, will be generated. This flow depends on two different cellular processes: motility of the cilia and morphogenesis of the node itself (Lee and Anderson 2008). Mutant mouse embryos, that completely lack cilia, or have immotile cilia, such as *iv* mutants, show an abnormal L-R patterning (McGrath, et al., 2003). *Inv* mutants have 20% of the cilia pointed anteriorly rather than posteriorly and a nodal flow that moves slowly and not in a polarized way. These mutants do not show a randomization but a complete inversion of the L-R pattern, which is called *situs inversus*. Moreover, when an artificial flow with reversal of the nodal flow direction is imposed, this leads to the reversal of L-R patterning, suggesting that the flow per se is responsible for subsequent L-R patterning events. (reviewed in Shiratori and Hamada 2006; Lee and Anderson 2008). It is important to mention the presence of an increased influx of Ca^{2+} ions on the left periphery of the node, which appears to be linked with the nodal flow. This asymmetry in the Ca^{2+} influx is correlated with the asymmetric activation of *nodal* expression in the left lateral plate mesoderm (McGrath et al., 2003; Tanaka et al., 2005).

This nodal flow is quite conserved between vertebrate. In zebrafish, motile cilia which generate a unidirectional flow have been detected in Kupffer's vesicle; whereas

in *Xenopus*, there are cilia present in the gastrocoel roof plate, which also generate a leftward unidirectional flow (reviewed in Lee and Anderson 2008).

In the *HNF-3β* null mutants, absence of the node allows limited neural induction in some embryos (Levine and Brivanlou 2007). Despite the loss of the node, and with it the loss of the genes that are normally expressed in the node (for instance *noggin* and *chordin*), *chordin* is still expressed briefly in the mid gastrula organizer in these mutants, which may account for the limited neural induction (Klingensmith, et al. 1999). Also in *fgf8* and *cripto* mutants, which are again characterized by lacking the node, there is anterior neural induction (Ding, et al. 1998, Sun, et al. 1999). Consequently, the node itself is not required for neural induction. However, the same cannot be said of its predecessor: the node precursors are located at the advancing anterior tip of the primitive streak, as it elongates during gastrulation. This precursor of the node is more potent than the node itself in promoting early anterior neural development (Tam and Steiner 1999). At mid-streak stage, when the primitive streak is elongated midway, grafts of the anterior primitive streak are able to induce anterior brain markers. On the other hand, grafts from earlier or later stages induce more posterior markers (Yang and Klingensmith 2006). These tissues are considered the early gastrula organizer (EGO) and mid gastrula organizer (MGO).

The node of the late-gastrula embryo has been shown to possess organizing activity by virtue of its ability to induce axis formation following heterotopic transplantation. When the node of the mouse is tested for its organizing activity by transplantation, the induced axis is typically made up of the graft-derived tissues in the notochord and somites, and neural tissues that are derived from the host, are morphologically characteristic of the trunk neural tube (Beddington 1994).

Although structurally different, the mouse node shares signaling properties with Hensen's node in chick, Kupffer's vesicle in zebrafish and the Spemann's Organizer in amphibians (Gilbert 2006, Lee and Anderson 2008).

Organizer cell properties, through different vertebrate species, are conserved. In vertebrates such as *Xenopus*, chicken and mouse, one can detect in these cells the presence of transcription factors such as *goosecoid* and *HNF3β* (Zhu, et al. 1999, Belo, et al. 1998), and secreted molecules such as *noggin* and *chordin* (Anderson 2002). Furthermore, these cells share similar fates as they become notochord, prechordal mesoderm and gut mesoderm. Moreover, both chicken, *Xenopus* and mouse organizer

cells can induce secondary axis when transplanted, although the mouse node, as said before, induces an incomplete axis, lacking anterior structures (Beddington 1994, Beddington and Robertson 1998).

1.2.3 Anterior visceral endoderm

The VE, which surrounds the epiblast and the extraembryonic endoderm, forms at the distal tip of the egg cylinder at the embryonic day 5.5. The following unilateral polarized movement of these cells towards the proximal region of the embryo establishes the future anterior pole and imparts anterior identity upon the underlying epiblast, becoming the AVE (Fig 1.7) (Rodriguez 2005, Srinivas 2004, Thomas, et al. 1998, Tam and Loebel 2007).

This movement is accompanied by asymmetric gene expression and is the first phenomenon that marks the end of the radial symmetry in the mouse embryo (Zernicka-Goetz 2002). However, recently, it has also been suggested that the intrinsic information within the embryo is involved in the orientation of AVE migration and therefore the orientation of the AP axis (Torres-Padilla 2007). Nevertheless, these changes in cell movement and gene expression mark the conversion of the P-D axis of the embryo into the A–P axis of the embryo.

From the moment it is established, the AVE performs an essential role in the primordial induction of the anterior neuroectoderm.

During mid-gastrulation, as the AVE emerges from the anterior primitive streak and intercalates into the outer VE layer, a population of anterior mesendoderm cells that expresses a similar subset of genes, signals to the anterior epiblast, to pattern the neuroectoderm (Lu, et al. 2001).

This early patterning is processed and transduced into cascades of asymmetric gene expression that will characterize the subsequent phases of dorso-ventral and left-right asymmetry generation in the embryo (Hamada, et al. 2002). It sets off with the expression of some genes in the AVE, encoding for transcription factors like *lim1*, the homeobox containing genes such as *hex*, *goosecoid, otx2* and *Hesx1/Rpx* (Thomas and Beddington 1996, Thomas, et al. 1998), and several repressors of Nodal and Wnt signaling such as *cer1, lefty1, dkk1, sfrp5* and *sfrp1* (Belo, et al. 1997, Perea-Gomez 2002, Yamamoto, et al. 2004). These *Nodal* antagonists force the initial homogenous

expression of *Nodal*, to the posterior part of the embryo, beginning in this step an asymmetry in the embryo (Belo, et. al 1997, Perea-Gomez 2002).

The study of *Hex* gene was the first experiment to show how the AVE is formed. Initially *hex* is expressed in the PE, but by 5.5 dpc it starts being expressed only in the VE at the distal tip of the embryo. Subsequently, it marks the unilateral movement of these cells, as its expression shifts towards the anterior side of the embryo (Thomas, et al. 1998).

Initially there were doubts regarding the origin of AVE population, and whether the VE might be the first tissue to acquire A-P polarity in the mouse conceptus; in order to confirm that the VE cells are indeed the precursors of the AVE, DiI was injected at the distal tip of the endoderm, and tracing confirmed VE as the origin of the AVE cells (Thomas, et al. 1998).

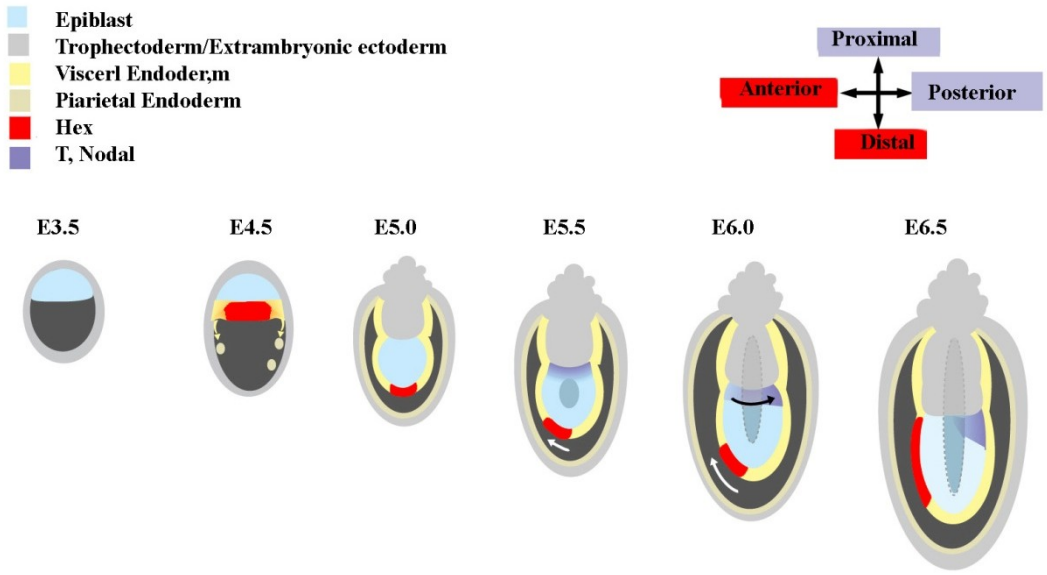

Figure 1.8 - A model for anteroposterior axis formation in the mouse embryo

Hex expression (red) is initiated in the nascent PE of the 4.5 dpc blastocyst and at 5.0 dpc is restricted to a few VE cells at the distal tip of the egg cylinder. At 5.5 dpc this P-D asymmetry is converted into A-P asymmetry by the unilateral movement of the distal *Hex*-positive cells (white arrow). At this time, *T* and *Nodal* expression patterns (purple) are symmetrical in the proximal epiblast. Subsequently, *T* and *Nodal* expression resolve to the opposite side of the egg cylinder from the AVE (black arrow). Adapted from Thomas, et al. 1998.

Before gastrulation, expression markers are already expressed asymmetrically. The distal tip of the embryo is patterned with anterior genes, whereas the proximal region of the embryo expresses genes that are characteristic markers of the primitive streak, such as *brachyury*, *Nodal* and *fgf8*. Furthermore, it is shortly after the VE cells shift towards the anterior region, that a movement from the proximal region and towards the posterior side of the epiblast starts (Thomas, et al. 1998) (Fig 1.8).

There are considered three organizing centers besides the AVE, that are responsible for the correct formation of the head (Anderson 2002). The prechordal plate, an organizing center derived from the mesendodermal cells of the node, confers dorso-ventral patterning to overlying tissue through its secreted molecules; among these molecules is sonic hedgehog (Shh) (Chiang, et al. 1996). The other organizers for head development are the anterior neural ridge and the isthmic organizer; they act in the neural ectoderm (Rubenstein and Beachy, 1998). The first induces and promotes forebrain character, whereas the second is responsible for neural tissues contiguous to the midbrain/hindbrain boundary. These organizers also express morphogens such as FGF8 (Crossley and Martin 1995).

It has been shown the importance of these three organizing centers in head development: when they and their effector molecules are removed, the result is a mispatterning and hypoplasia of the developing forebrain (reviewed by Beddington and Robertson, 1998).

Previous studies suggest an important role in forebrain induction. AVE alone is insufficient to induce forebrain in grafting experiments, but can do so in concert with posterior epiblast fragments (Tam and Steiner 1999). The AVE functions to inhibit the expression of posterior genes (Yamamoto et al., 2004), but much still remains unknown about how it promotes forebrain fates.

Although the AVE is not sufficient to induce forebrain character in explants from the early streak stage, it does promote forebrain gene expression in explants from the mid and late streak stages. This is consistent with findings from other species: the chick equivalent of the AVE, the hypoblast, induces transient neural character.

In addition, surgical ablation of the AVE at early gastrulation stages E6.5 leads to the loss of expression of forebrain markers such *hesx1* (Thomas and Beddington 1996). Null alleles of genes encoding transcription factors expressed in the AVE such as *otx2* and *lim1* lead to loss of the forebrain and midbrain (Perea-Gomez, et al. 2001, Shawlot, et al. 1999).

1.3 THE IMPORTANCE OF SIGNALING PATHWAYS

Right from the onset of cell division, several molecules from different cascades and signaling pathways, act simultaneously in order to obtain the correct development of an embryo. Although it is often referred one or other pathways, none of the signaling pathways exists completely by itself; development is an entanglement of several pathways, which are translated into signal transduction cascades.

The most common target of signaling in development is transcription. Different pathways activate or repress different genes at distinct times and places in the embryo (Gilbert 2006).

All signaling pathways are important at a certain point during development, being sometimes more, sometimes less significant, according to the stage of gestation and signals required at that time.

In development, there are five major signaling pathways, which are grouped on the basis of their structure: the fibroblast growth factor (FGF), the Hedgehog, Notch, Wnt family, and the TGF-β superfamily (Gilbert 2006).

To date, the FGF family consists of twenty three members, all of which contain a conserved 120 amino acid (aa) core region. The members of this family act extracellularly through four tyrosine kinase FGF receptors: the FGF receptor binds to a FGF dormant kinase, which will then be activated and phosphorylate some other proteins (Powers, et al. 2000). FGF signaling, although it stands for fibroblast growth factors, is not limited to cell growth. This family of cytokines, even though induces fibroblast proliferation, is also known to play important roles in several critical

processes such as hematopoiesis, angiogenesis, cancer and development (Vasiliauskas and Stern 2004). During development, FGF signaling members play a role in numerous key events, such as gastrulation and organogenesis including somite, kidney, brain and limb development (Perantoni, et al. 2005). One important member of this family is *fgf8* which is first expressed in the pre-gastrulation epiblast and then in the primitive streak (Crossley and Martin 1995). Null mutants for *fgf8* fail to gastrulate (Sun, et al. 1999), whereas *fgf8* hypomorphic alleles or tissue-specific gene inactivation result in several defects such as aberrant cell death of the prospective midbrain and cerebellum (Chi, et al. 2003), abnormalities in cardiovascular and smooth muscle development (Abu-Issa, et al. 2003), defects in limb development and the onset of nephrogenesis (Crossley, et al. 1996). *fgf8* is not the only important member of the FGF signaling pathway, FGF receptors are of major importance in signaling transduction, as other member as *fgf10* and *fgf4,* that are involved in limb development (Capdevila and Izpisúa Belmonte 2001).

There are three members of the vertebrate Hedgehog family: Desert hedgehog (Dhh), Indian hedgehog (Ihh) and Sonic hedgehog (Shh) (Cohen 2003). Hedgehog proteins undergo autocatalytic processing and modification that is critical for their signaling activity. The precursor protein is cleaved and gives rise to an N-terminal domain and a C-terminal domain. The auto-processing of Hedgehog causes the covalent attachment of cholesterol to the C-terminal side of the N-terminal domain; it is this attachment with the cholesterol molecule that transforms the Hedgehog protein into a completely functional protein (Jiang and Hui 2008, Ma et al. 2008). The Hedgehog reception system consists of a 12-span transmembrane protein, Patched (Ptc), as the Hedgehog receptor and a 7-span transmembrane protein, Smoothened (Smo), as the obligatory signal transducer across the plasma membrane (Cohen 2003).

These three members all contribute to correct development during embryogenesis: it is already known that Shh is a major player during embryonic development, being involved in several processes such as the development of the CNS, in establishing lateral asymmetry and the anterior posterior limb axis (Chiang 2001), and in the process of nephrogenesis; it is of major importance as it is one of few morphogens known (Cohen 2003). As for Ihh signaling, it is involved in bone development, especially the

cartilage, regulating chondrocyte proliferation and differentiation. Dhh is essential for the development of spermatogenesis and the Schwann cells in peripheral nerves (Ma, et al. 2008).

Briefly, Notch signaling is known to be important for specifying cell fates, regulating pattern formation, and defining boundaries between different cell types. Notch proteins are transmembrane receptors for the Jagged and Delta transmembrane ligands. Notch, Delta, and Jagged proteins have EGF domains in their extracellular structures. Notch can act as both a ligand-binding receptor and a nuclear factor that regulates transcription. This pathway has been implicated in several processes such as neural development, apoptosis, and hematopoiesis, among others (Shi and Stanley 2006). One important feature is the ability of the Notch signaling to activate Nodal in the node through its downstream targets which will be a critical step in breaking the symmetry of the embryo (Krebs, et al. 2003). It is also of major importance regarding the epithelial to mesenchymal transition, which is essential, for example, in processes as PS cell migration (Takeuchi, et al. 2007).

After the interaction of Notch with its ligands, the signal induced by ligand binding is transmitted intracellularly, where nuclear translocation of the intracellular domain of the Notch family protein will occur. Once in the nucleus, the Notch intracellular domain will form a complex with the RBP-J protein (Krebs, et al. 2003). This complex activates transcription of downstream target genes such as *Nodal*, a member of the TGF-β superfamily that is of major importance in embryonic development and will be further discussed ahead.

The Wnt signaling pathway is a highly conserved signal transduction cascade that has a central role in embryonic development. Three different pathways are believed to be activated upon Wnt receptor activation: the canonical Wnt/β-catenin cascade, the non-canonical planar cell polarity (PCP) pathway, and the Wnt/Ca2+ pathway (Clevers 2006, Qian, et al. 2007). Target cell populations respond to secreted Wnt morphogens in a concentration dependent manner, such that the gradient of Wnt concentration determines the resulting gene expression and cellular differentiation. These actions

make Wnt molecules central to the signal transduction pathways which underlie cell proliferation, survival and differentiation.

The Wnt ligands are a family of nineteen molecules that are secreted, vary in length between 350 and 400 aa, possess 22 to 24 conserved cysteines, and show 20%-85% aa identity within the family (Bejsovec 2000, Bejsovec 2005).

As this signaling pathway is so important for the correct development of an embryo, it will be discussed more thoroughly ahead.

The TGF-β superfamily is of enormous importance during embryonic development. Several key genes reside within this family as, for example, Smads, BMPs, activin receptors and Nodal signaling pathways (Gilbert 2006). These ligands are synthesized as pre-propeptides. The N-terminal pro-region is cleaved prior to secretion, and the secreted C-terminal mature segment has six or seven spatially conserved cysteines, which form a cysteine knot structure in the monomer. The mature segments will then form dimers via disulfide links (with some exceptions, such as *lefty1*), which will subsequently serve as the active ligand.

1.3.1 Nodal signaling

During embryonic development, an important step is the establishment of the L-R axis. It has been shown that Nodal signaling is essential for this asymmetry to be processed: it is required the asymmetric activation of the Nodal signaling cascade in the left side of the body wall (reviewed in Hamada, et al. 2002), the left Lateral Plate Mesoderm (LPM).

Nodal starts being expressed very early. Transcripts can be detected in ES cells *in vitro*, however, *in vivo* it is not until shortly after implantation, at E5.5, that *Nodal* can be seen in the VE and epiblast (Varlet, et al. 1997). Also at this time, the AVE is formed and starts to dislocate towards the anterior side of the embryo. In the AVE several *Nodal* antagonists are expressed, such as *cerl-1* and *lefty1* (Fig 1.8, Fig 1.9) (reviewed by Yamamoto, et al. 2004). Later on, at E6.0 *Nodal* is strongly detected in the proximal ring of the epiblast, while in the VE low levels of *Nodal* can be detected. As the primitive streak starts to be formed, at E6.5, *Nodal* can be seen pushed towards the

posterior side of the embryo, where the mesoderm is to be formed (Meno, et al. 1999) (Fig 1.8, Fig 1.9), a feature of the responsibility of *Nodal*'s antagonists expressed in the AVE. At E7.5, when the primitive streak is completely formed, *Nodal* transcripts can be detected in the perinodal region. This early expression is necessary for *Nodal* posterior activation in the left LPM later on, at E8.0 (Lowe, et al. 1996), activating its downstream targets and also leading to an asymmetric expression in the node (Brennan, et al. 2001).

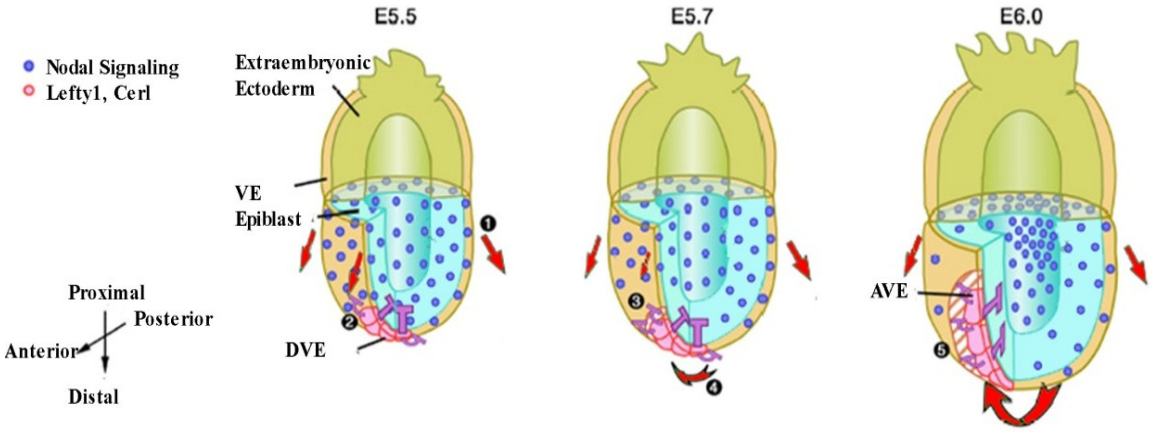

Figure 1.9 - Model for A-P determination by Nodal antagonists

In the wild-type embryo at E5.5, Nodal signals in the epiblast and overlying VE regulate cell proliferation of VE in a symmetric manner (Step 1; red arrows represent putative migration force generated by cell proliferation). Nodal antagonists (*Lefty1 and cerl*) in DVE whose expression domains are already inclined toward the prospective anterior side start to inhibit the Nodal signals in the region adjacent to the DVE (step 2). Cell proliferation will be inhibited in the VE regions that have received the Nodal antagonists (step 3). This would generate higher migration force on the posterior side and induce the DVE to migrate toward the anterior side (step 4). Migration of the DVE toward the anterior side further establishes A-P asymmetries in Nodal signaling and cell proliferation (step 5). Adapted from Yamamoto, Saijoh, et al. 2004.

Very briefly, as a member of the TGF β superfamily, Nodal is first a proprotein; this proprotein is processed extracellularly by convertases PACE4 and Furin. Nodal signaling is activated by the interaction of mature Nodal ligand with activin receptors (ActRIIB, ALK4) and EGF-CFC co-receptors, and it is inhibited by *leftys* and *Cerberus* family genes (Cheng, et al. 2004, Belo, et al. 1997, Belo, et al. 2000). Nodal signaling is

transmitted intracellularly by phosphorylation of Smad2 and its association with Smad4 and transcription factors such as FoxH1, which will regulate the expression of genes such as *Nodal* itself, *lefty*, *pitx2*, among others (Fig 1.10).

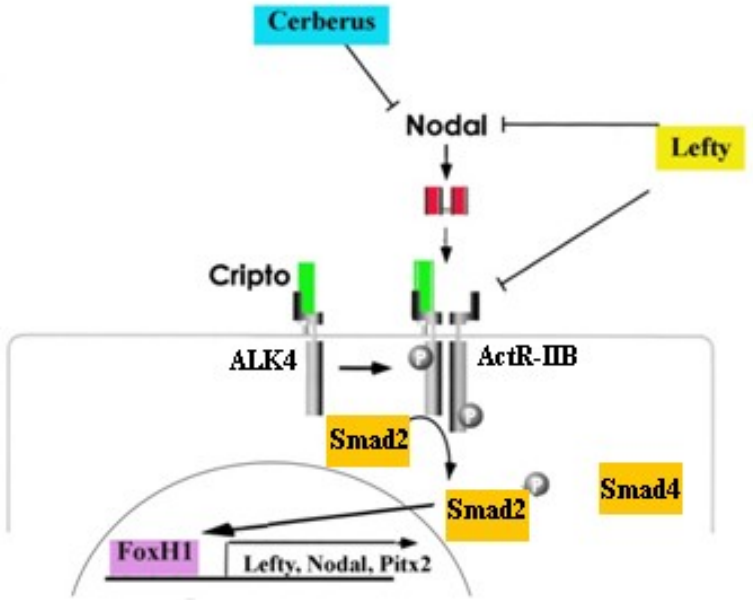

Figure 1.10 - Schematic representation of Nodal signaling

In order to transduce intracellular signals, Nodal interacts with EGF-CFC factors and type I and II receptors (Alk4 and ActRIIB).This complex activates Smad2 protein which, together with Smad4, activates gene expression, associating with FoxH1. Cerberus and Lefty prevent Nodal biding to the receptor complex either by binding directly to Nodal or interacting with its receptor or co-receptor. Adapted from (Schier 2003, Yeo and Whitman 2001).

Nodal was shown to be required for mesoderm formation. Mouse Nodal mutants lack a primitive streak and most mesoderm, displaying only sporadic formation of some posterior mesoderm (Conlon, et al. 1994, Schier and Shen 2000).

The EGF-CFC gene family is a group of structurally related proteins that serve as important competence factors during early embryogenesis. It encodes for extracellular proteins with a modified epidermal growth factor (EGF)-like motif and a conserved cysteine-rich (CFC) motif (Saloman, et al. 2000). This family comprises protein like zebrafish *one eye pinhead* (*oep*) and mouse *cripto* and *cryptic* (Shen, et al. 1997,

Shen and Schier 2000). EGF-CFC proteins play a major role in Nodal signaling, as they are components of Nodal receptor complexes.

Although EGF-CFC independent Nodal signaling has already been suggested (Liguori, et al. 2008); genetic studies both in zebrafish and in mouse show that null mutants for *oep* and *Cripto* resemble the double mutants for Nodal factors *cyclops* and *squint* and the *Nodal* mutant, respectively (Gritsman, et al. 1999, Ding, et al. 1998). These mutants lack the PS and embryonic mesoderm, just as *Nodal* mutants (Yeo and Whitman 2001, Reissman, et al. 2001).

There are several extracellular inhibitors that can regulate the activity of *Nodal*. Some of them are Cerl-1, Cerl-2, Lefty1 and Letfty2, and BMPs.

The Lefty subfamily belongs to the TGF-β superfamily, although their structure diverges a little from the other TGF-β molecules. Lefty proteins are thought to act as monomers, as they lack a cysteine residue and a long α-helix, critical for the assembly and stabilization of TGF-β homo and heterodimers (Meno, et al. 1998, Meno, et al. 1999). In the Nodal signaling pathway, Lefty proteins can act directly with both Nodal, EGF-CFC co-receptors and Activin type IIB (Chen and Shen 2004, Cheng, et al. 2004).

There are two Lefty genes in mouse, *lefty1* and *lefty2*. *lefty1* mutants display laterality defects, whereas *lefty2* mutants show an oversized PS and laterality defects which can be overcome downregulating Nodal activity (Meno, et al. 1999).

The *cerberus/Dan* subfamily belongs to the TGF-β superfamily. Cerberus was identified in *Xenopus* as an inducer of the head structures, and an antagonist of Nodal, BMP and Wnt signals. In mouse, cerl-1 is able to inhibit Nodal and BMP, but not Wnt signals.

Furthermore, *cerl-1* null mutants show no apparent phenotype (Belo, et al. 2000), although it is not a synonymous of being a less important gene. On the contrary, it was shown to play a major role in the establishment of A-P axis, together with *lefty1* (Yamamoto, et al. 2004). *Lefty1* null mutants, like *cerl-1*, show no obvious phenotype, however, in *lefty1;cerl-1* null mutants, the VE fails to migrate anteriorly, suggesting a redundant or synergist activity of these genes.

Regarding *Nodal* expression in the node and LPM, the signaling cascade still remains incompletely explained. Nodal's perinodal expression is induced by the Notch signaling cascade in the following way: an intracellular form of Notch forms a complex with RBP-Jk that, once in the nucleus, will activate the transcription of *Nodal* gene

(Krebs, et al. 2003). The transition between symmetric and asymmetric expression in the node is the object of several studies; it is already clear that a leftward flow of the cilia in the node contributes to this characteristic expression pattern; however it is not the only thing contributing to this asymmetry in the node.

Although it is not yet completely clear how it is processed, at a certain point, a gene of the *cerberus/Dan* family, c*erl-2* is essential to restrict Nodal activity to the left side of the node (Marques, et al. 2004). Like *Nodal*, *cerl-2* transcripts can be firstly detected in a horse-shoe shaped pattern in the perinodal region of the E7.0 mouse embryo; by late headfold stage, expression of *cerl-2* begins to decrease in intensity on the left side and by E8.0 it is mostly detected in the right side of the node, which is a complementary expression pattern to *Nodal* at this stage (Marques, et al. 2004, Belo, et al. 2008).

This asymmetrical expression of *cerl-2* seems to restrict the Nodal activity to left side, stopping this way any additional activation of *Nodal*, *lefty2*, and *pitx2* in the right LPM (Marques, et al. 2004).

In the absence of Cerl-2 antagonistic activity in the node, *Nodal* may be also activated in the right LPM, leading to bilateral or ectopic expression of this genetic cascade in the right LPM. *cerl-2* null mutants present laterality defects, however, *Nodal* is still asymmetrically expressed on the left side of the node in *cerl-2* mutants (Marques, et al. 2004).

As said above, although there are different signaling pathways, they don't act independently. For instance, in the mouse, *Shh* also influences Nodal signaling in the correct establishment of left-right asymmetry. It is required for the formation of the midline and floorplate, without Shh embryos loose *lefty1* expression showing a defective midline, which leads to bilateral *Nodal* expression in the LPM (Echelard, et al. 1993).

1.3.2 BMP signaling

The BMPs comprise a large family of secreted signaling molecules which are related to members of the TGF-β superfamily, as they are synthesized as large precursors that are processed to yield mature protein dimers.

BMPs are expressed during gastrulation; based on their expression studies and genetic studies, some members of this family are believed to be essential for initiation of gastrulation and patterning of mesoderm. BMP signaling is required at an early stage for differentiation of the primitive endoderm into the embryonic VE, while it inhibits DVE formation, restricting it to the distal region, at a later stage (Yamamoto, et al. 2009). Several BMP genes and their downstream signal transducers are expressed in early mouse embryos before and during gastrulation. These include *bmp2, bmp4, bmp5, bmp7, bmp8b, alk2, alk3, bmprII, actrIIa, actrIIb, smad1, smad5*, and *smad8*.

Signal transduction studies have revealed that Smad1, 5 and 8 are the immediate downstream molecules of BMP receptors and play a central role in BMP signal transduction.

Like in Nodal signaling, BMP also signals through type I (ALK2, ALK3 or BMPRIA and ALK6 or BMPRIB) and type II receptors (BRII, ActRIIA and ActRIIB) (Kishigami and Mishina 2005). Usually, the type I receptors are the high-affinity binding receptors, whereas the type II receptors bind BMPs with low affinity. Type II receptors activate type I receptors. When BMPs bind to type I receptors, it results in the phosphorylation of downstream Smad proteins, triggering the intracellular signal cascade. The BMP signal activates Smad1, Smad5 and Smad8, which upon phosphorylation can associate with Smad4 (Nie, et al. 2006, Di-Gregorio, et al. 2007).

Among all genes in BMP signaling pathway, *alk3* is the one that shows a more striking phenotype, as when it is removed embryos die before E7.0 with impairment of the epiblast and reduced mesoderm.

All through embryonic development, *bmp4* is the most widely expressed, being detected as early as E3.5. BMP2 and BMP4 show over 90% identity. *Bmp4* null mutants lack the primordial germ cells, show a reduction in the extraembryonic mesoderm, lack or present a very thin allantoid and have heart defects. As for *bmp2* null mutants, they share the *bmp4* null mutants' phenotype, only with a bit less severity considering the primordial germ cells: instead of completely lacking them, they show a reduced number (Zhao 2003). Furthermore, *bmp8b* is also involved it primordial germ cell formation. It

is interesting that *bmp2*$^{+/-}$;*bmp4*$^{+/-}$ mutants show a further reduction in primordial germ cell number when compared to single heterozygous; moreover, *bmp2*$^{+/-}$;*bmp8b*$^{+/-}$ mutants do not show a further reduction in primordial germ cells number when compared to single heterozygous. This suggests that BMP2 and BMP4 signal through a similar pathway, while BMP8B uses a separate pathway in primordial germ cells formation (Zhao 2003)

BMP signals are redundant and seem to compensate for one another. Besides the case of BMP2 and BMP4, also BMP5 and 7 show this compensation. Single null mutants for *bmp5* and *bmp7* do not show significant defects in mesoderm formation. However, double homozygous manifest severe defects in extraembryonic mesoderm formation, including short allantoid (reviewed by Kishigami and Mishina 2005).

One could say that BMP signaling functions as a complement of Nodal signaling. The first functions to enhance epiblast proliferation (*alk3* mutants show a very small epiblast), whereas Nodal signaling acts to inhibit the proliferation of the epiblast (*Nodal* mutants present an initial hyper-proliferation of the epiblast followed by developmental arrest) (Zhao 2003).

It is already known that BMP antagonism is crucial for the correct development of the embryo (Sasai and De Robertis 1997). Chordin, noggin, follistatin and Cerberus are inhibitors of the activity of BMP4 binding directly to it. Both *noggin* and *chordin* are expressed in the node of the mouse embryo, at late gastrula stage. Later they are co-expressed at the level of the notochordal and prechordal plates (Anderson 2002, Bachiller, et al. 2000).

Noggin null mutants display a vast number of defects in spinal cord and somites, whereas *chordin* null mutation results in stillborn animals which show abnormalities in ear development, pharyngeal and cardiovascular organization (Stottmann, et al. 2006). Being already severe mutations, these two genes act synergistically, compensating for one another. When double null mutant are originated, defects at the level of the forebrain development in addition to defects related to L-R patterning and mesoderm maintenance are observed (Bachiller, et al. 2000); also, these mutants fail to form correct A-P and D-V axes. Furthermore, although at the onset of gastrulation AVE markers such as *cerl-1, lim1* and *hesx1/rpx* are present in *noggin;chordin* double null mutants, by early headfold stage *cerl-1* and *hesx1/rpx* are not present (Bachiller, et al. 2000).

As mentioned in section 1.3.2, BMPs are involved in Nodal signaling. Although *bmp4*, which is required for L-R patterning, is expressed symmetrically, BMP signal transduction is higher in the right LPM, and BMP antagonists, noggin and chordin, are expressed at higher levels in the left LPM. In *chrd;nog* double mutants BMP signaling is increased on both sides of LPM, and *Nodal* expression is absent. Furthermore, ectopic expression of *noggin* in the left LPM of *chrd;nog* double mutants leads to correct expression of *Nodal* (Mine, et al. 2009).

Altogether, these results suggest that BMP antagonists secreted at the level of the node have a head inducing activity, by maintaining the anterior patterning which is initiated by the AVE, and are required for normal L-R morphogenesis and asymmetric expression of left-side determinants in LPM.

1.3.3 Wnt signaling

Together with other families of secreted factors such as FGF, TGF-β, and Hedgehog proteins, Wnt proteins are implicated in a wide variety of biological processes. Activation of the Wnt pathway controls a wide variety of processes in embryonic development and adult homeostasis (Bejsovec 2005).

Wnt proteins form a family of highly conserved secreted signaling molecules that regulate cell-to-cell interactions during embryogenesis. They signal across the plasma membranes by interacting with serpentine receptors of the Frizzled (Fz) family and members of the low-density-lipoprotein receptor-related protein (LRP) family (Bejsovec 2005).

Wnt proteins can activate at least three different signaling pathways: the canonical or Wnt/β-catenin, the planar cell polarity (PCP) and the Wnt/calcium pathways (Bovolenta, et al. 2008) (Fig 1.11).

As currently understood, Wnt proteins bind to receptors of the Fz and LRP families on the cell surface. In the canonical pathway, through several cytoplasmic relay components, the signal is transduced to beta-catenin, which enters the nucleus and forms a complex with TCF to activate transcription of Wnt target genes (Bejsovec 2000).

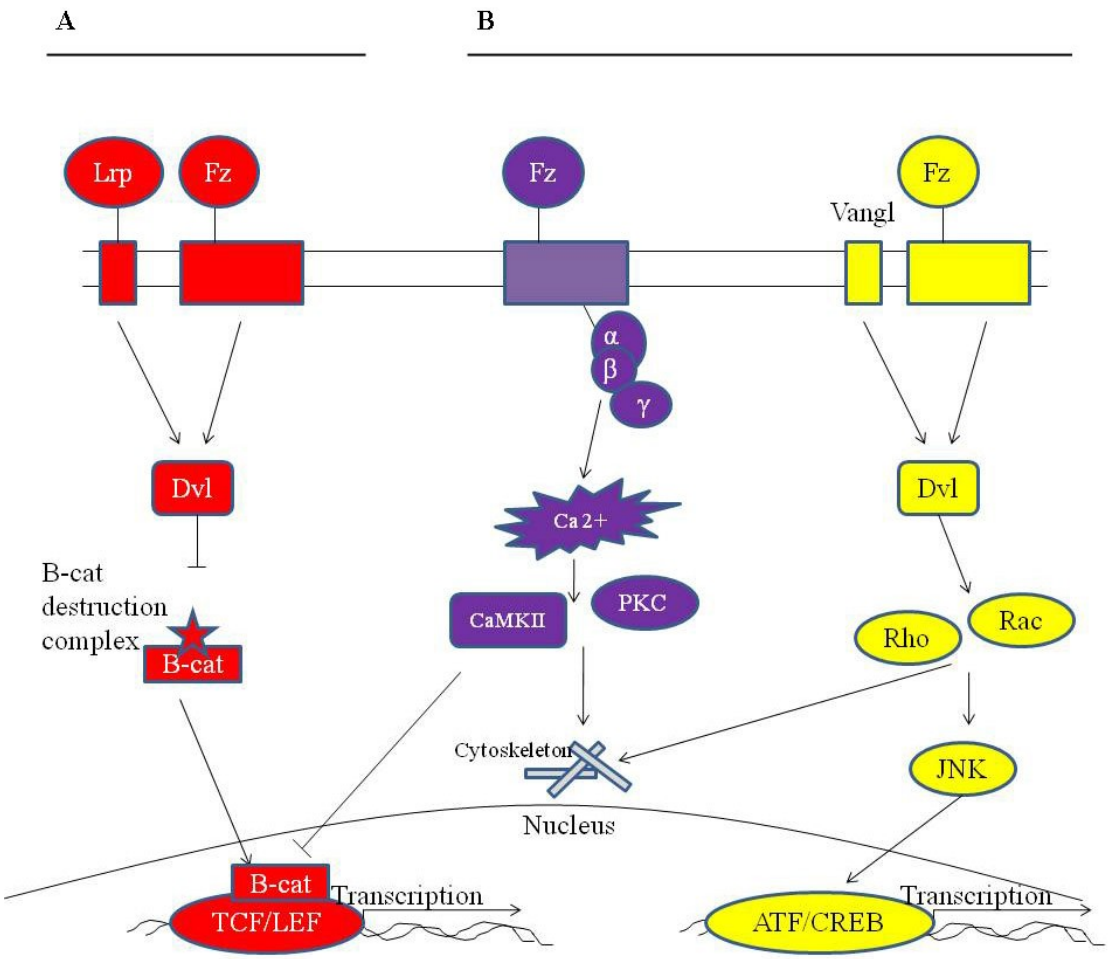

Figure 1.11 - Wnt signaling pathways

(A) Canonical Wnt signaling (red); (B) Non-canonical Wnt signaling involves at least two pathways: the Ca^{2+}/protein kinase C (PKC) (purple) and RhoA/JNK pathways. Adapted from Cohen, Tian and Morrisey 2008.

Although there is controversial data regarding the role of Wnt signaling during early embryogenesis, it has been established that it is of major importance as early as right after the implantation process. It is known that the maintenance of pluripotency requires suppression of Wnt signaling which promotes differentiation. Formation of mesoderm from the pluripotent epiblast depends upon canonical Wnt β-catenin signaling.

There is abundant evidence that many developmental decisions are controlled by Wnts, from gastrulation and early pattern formation to organogenesis. Although Wnts are known to influence cell behavior through several different signaling pathways, many act by regulating the stability and subcellular localization of β- catenin (Cadigan 2008).

The Wnt–β-catenin pathway revolves around the stability of β-catenin, with higher levels of this protein promoting activation of Wnt targets. β-catenin is also essential for cell adhesion, forming this way a link between E-cadherin and the actin cytoskeleton. In addition to this membrane-bound pool of β- catenin, there is a cytoplasmic pool that rapidly turns over in unstimulated cells. It is this β-catenin pool that is regulated by Wnt stimulation, although there is evidence of a more dynamic interaction between cytosolic and membrane-bound β-catenin in some cells, suggesting a direct link between Wnt–β-catenin signaling and cell adhesion (Cadigan 2008).

Activation of Wnt signaling is further controlled by different antagonists, including Wnt inhibitory factor-1, Cerberus and members of the Dickkopf1 (Dkk1) and Secreted Frizzled Related Protein (SFRPs) families. While Dkk1 proteins interfere with Wnt activity and antagonize canonical signaling by binding to LRP5/LRP6, Wnt inhibitory factor-1, Cerberus and SFRPs can interact directly with Wnt proteins (Kawano and Kypta 2003). *dkk1* is expressed in the AVE, node and axial mesendoderm (Glinka, et al. 1998). As it happens with BMP antagonists, *dkk1* null mutants lack head structures anterior to the midbrain and at late streak stage show no expression of the neuroectoderm marker *hesx1/rpx.* Thus, Dkk is proposed to be involved in the induction of rostral neuroectoderm.

Interestingly, double heterozygous mutants for *dkk1* and *noggin*, show severe head defects, presenting no head structures anteriorly to the mid-hindbrain boundary, due to a defective anterior mesendoderm which fails to pattern the rostral epiblast (Mine, et al. 2009).

This is a clear example of the redundant and synergistic functions of the different pathways. The Wnt and BMP antagonists secreted by the node play an important role, particularly in the induction of the head structures.

One example of Wnt signaling being required for correct gastrulation is the *wnt3* null mutant, which shows absent PS, mesoderm and node, and lacks A-P patterning, despite AVE markers being correctly positioned (Liu, et al. 1999). Furthermore *β-catenin* deficient mice also have defects in establishing the A-P axis, the mesoderm and head structure are not formed and AVE markers remain distal. In sum, canonical Wnt pathway is of great importance in the formation of the A-P axis.

Members of the PCP pathway are highly conserved in vertebrates where they have been implicated in controlling the process of convergent extension during gastrulation

and neurulation (which will be discussed further ahead), through the non-canonical Wnt/frizzled pathway (Kibar, et al. 2007).

Although the Ca^{2+}/PKC and RhoA/JNK pathways mediate most β-catenin-independent, non-canonical Wnt signaling, it remains unexplained whether these two pathways can be indeed separated from one another, and the combinations of effectors that mediate this signaling often vary (Cohen, et al. 2008).

1.4 LATER EMBRYONIC DEVELOPMENT

Early embryonic development is critical for the embryo formation. Wrong or absent expression of key genes during these stages may lead to the arrest of embryonic development. However, these early stages are not the only important ones. Later stages of development are also of major importance, as during these stages, incorrect or absent activity of important genes, may not only arrest the development of the embryo, but also may lead to several severe birth defects.

1.4.1 Neurulation

Neurulation in vertebrates results in the formation of the neural tube, which gives rise to both the spinal cord and the brain. Neural crest cells are also created during neurulation. Neural crest cells migrate away from the neural tube and give rise to a variety of cell types, including pigment cells and neurons.

Neurulation begins with the formation of the neural plate, a thickening of the ectoderm caused when cuboidal epithelial cells become columnar. This change in shape and movement, results in convergence toward the midline and extension of the tissue along the A-P axis, and is highly influenced by the non-canonical Wnt pathway. Changes in cell shape and cell adhesion causes the plate edges to fold and rise, meeting in the midline to form a tube. The cells at the tips of the neural folds come to lie between the neural tube and the overlying epidermis. These cells become the neural crest cells. Both epidermis and neural plate are capable of giving rise to neural crest cells (Harris and Juriloff 1999, Kibar, et al. 2007, Ybot-Gonzalez, et al. 2007).

Formation of the neural plate is described as neural induction. During this process the dorsal midline ectoderm is differentiated into the neuroepithelium. Usually, BMPs prevent the ectoderm to form neuroectoderm and instruct it, instead, to form epidermis; however, during neural induction there is the suppression of this epidermal fate by the activity of BMP antagonists, including chordin, noggin and follistatin. These, emanate from the primitive node, thus allowing the ectoderm to form neuroectoderm. FGF and the canonical Wnt signaling pathways are also implicated in neural induction. FGF activates the MAPK cascade, which results in the phosphorylation of a crucial linker region of the BMP effector Smad1, which acts as an inhibitor of the BMP pathway (Stern 2005, Stern 2006, Kibar, et al. 2007)

Throughout neurulation, the process in which the neural plate bends and fuses in order to give rise to the neural tube, different molecules such as Shh, Noggin, BMP family and BMP related molecules, are involved in order to give rise to a correct neural tube development. Neural tube closure is believed to proceed bi-directionally in the same way as zipper. This phase of the embryonic development occurs between six and thirty somite stages. It is an important step during embryogenesis, as it is essential in establishing the central nervous system (CNS), and is responsible for one of the most common birth defects, the neural tube defects (NTDs). These NTDs can be subdivided in two, depending on the region that has failed to close the neural tube; it can be *spina bifida*, when it fails to close the most posterior region, or anencephaly, when it fails to close the most anterior region, the brain. Failure of neural tube closure during neurulation at any level of the body axis from the brain up to the sacral spine leads to an open NTD.

The formation of the hollow CNS starts with the elevation of the lateral edges of flat sheet of the thickened epithelial cells that lay on the dorsal side of the embryo. These elevated edges, the neural folds, will move persistently towards the dorsal midline, where they meet and then fuse to complete the conversion of the sheet into a tube (Wallingford 2005).

This neurulation process can be divided in three phases regarding the neural tube closure and according to the structures formed during the bending process (Shum and Copp 1996).

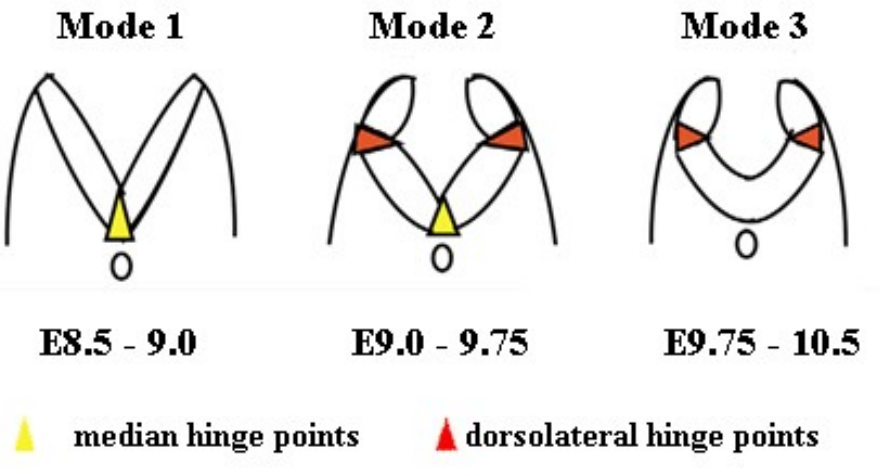

Figure 1.12 - Model for neural tube bending

In mode 1 there is the presence of median hinge point structure; in mode 2 both the median and dorsolateral hinge points are present; in mode 3 the median hinge point structures disappear and only the dorsolateral hinge point structures remain. Adapted from (Ybot-Gonzalez, et al. 2007)

In the first phase, the neural tube acquires a v-shape form, bending at the medium hinge points (MHP). At this phase, Shh is released from the notochord very strongly and inhibits *noggin* expression. Being noggin, a BMP signaling antagonist, and downregulated, *bmp2* expression is kept high, preventing the tube to close. During the second phase, there is the establishment of dorsolateral hinge points (DLHP) in the neural folds where these structures start bending, maintaining the MHP. Through phase three, at the most-caudal level of the spinal axis, the MHP disappear and the neural plate bends exclusively at the DLHP (Fig 1.12). During phases two and three of neurulation, Shh signals from the notochord diminish, causing BMP antagonists to be active. This way, BMP2 is inhibited allowing the neural plate to bend (Greene and Copp 2009, Ybot-Gonzalez, et al. 2007).

Besides being involved in neural tube closure, Shh, along with Gli proteins (which are the primary transcriptional mediators of Shh target genes), is also important regarding the patterning of ventral cell types present in the neural tube (Lei, et al. 2005). Five primary neuronal classes have been identified ventrally, each deriving from a unique and characteristic progenitor domain. These progenitors can be subdivided into two groups based on their response to Shh: Class II proteins are induced by Shh and

placed ventrally, while Class I proteins are repressed by high levels of Shh activity and located dorsally to Class II proteins. Together with graded Shh-Gli expression, Wnt signals also contribute to the neuronal fate (Lei, et al. 2005).

1.4.2 Somitogenesis

As reported in section 1.2, during gastrulation there is the formation of the third germ layer, the mesoderm. At the neurula stage, the trunk mesoderm can be divided in four subcategories: the chordamesoderm which forms the notochord, the intermediate mesoderm which will give rise to the urogenital system, the LPM that is involved in the formation of the heart, blood vessels, and the paraxial or somitic mesoderm (Gilbert 2006).

During neurulation, the vertebrate embryo body is sequentially segmented along its A-P axis, the paraxial mesoderm on both sides of the embryo becomes subdivided into a series of repeating epithelial, round embryonic structures that are called somites. These structures can be divided into three compartments: the sclerotome which forms the vertebrae and rib cartilage; the myotome which is responsible for the formation of the muscles of the back, the ribs and limbs; and the dermatome, which gives rise to the dermis of the back (Aulehla and Herrmann 2004, Dubrulle and Pourquié 2004). Although somites are merely transient embryonic structures, they are of unequivocal importance for the layout of the vertebrate body plan.

Somitogenesis is tightly coupled with axis formation via a system involving dynamic gradients of morphogens, such as FGFs, Notch, Wnts and retinoic acid (RA).

The somite number, as well as the pace at which each somite is formed, is species dependent. The mouse has sixty five pairs of somites, and each pair takes 120 minutes to be formed, although some variations have been reported.

The mechanism by which this constant periodic pattern progresses from head to tail, is called the “clock-and-wavefront model”. In short, this system consists of two components: the clock, which is a constant, periodic oscillator that flips between two states, permissive and non-permissive; and the “wavefront,” which moves at a constant rate from the head towards the tail. As the “wavefront” slowly moves down, it triggers any tissue it has passed through, to transform from PSM to somite, but only if the “clock” in that tissue is in the permissive phase. This way, the wavefront determines

where the somite will form, and the clock determines when it will form. The first evidence for such segmentation clock came from the observation of the periodic expression in PSM cells of chick *hairy1*, which is expressed as a wave sweeping the unsegmented mesoderm in a posterior to anterior fashion, once, during each somite formation (Palmeirim, et al. 1997). Although several other cyclic genes were identified, until now all the genes involved in this mechanism belong to the Notch and Wnt signaling pathways (Dubrulle and Pourquié 2004).

In mutants for *fgf8* and *fgfr1*, no paraxial mesoderm is formed, and the territory of the axial mesoderm is enlarged, which suggests that paraxial mesoderm cells are converted to an axial fate (Deng, et al. 1994, Sun, et al. 1999). Therefore FGF signaling seems to be essential for the specification of paraxial mesoderm identity. Additionally, Wnt signaling also appears to be correlated with the process of somitogenesis: in *wnt3a* null mutants and *TCF;Lef1* double mutants (Fig1.11), somitogenesis is disrupted after the formation of the first 5 to 6 somites (Pourquie 2001, Aulehla, et al. 2003).

A number of genes that pattern somite segmentation, appear to function together in the Notch signaling pathway. Mutations in the receptors (*notch1*), ligands (*dll1*, *dll3*) and downstream transcription factors (*rbpsuh*, *mesp2*), cause defects in somite segmentation (Correia and Conlon 2000).

1.4.3 Limb Formation

The vertebrate limb bud starts to be formed from the somites. It involves several cell and axis specification and patterning processes, which are directed by specialized structures such as the zone of polarizing activity (ZPA), the apical ectodermal ridge (AER), and the non-ridge ectoderm. The vertebrate limb is a complex organ with an asymmetrical organization in all three axes. The first axis to be developed is the P-D, where the limb grows, accentuating the differences between shoulder and finger, or hip and toe. Then the A-P axis develops, marking the differences between the digits. At last, the D-V axis distinguishes the palm for the knuckles (reviewed in Gilbert 2006).

Once again, BMP, FGF, Notch, Shh and Wnt signaling pathways, are all involved in the formation of these structures (Robert 2007, Li and Muneoka 1999, Hill, et al. 2003, Galceran, et al. 1999). The AER is a major signaling center for limb outgrowth. It forms at the boundary between the dorsal and ventral domains of the lateral ectoderm,

thus constituting compartments. The ZPA is a posteriory localized signaling centre, which is responsible for the patterning of the digits.

Shh is asymmetrically expressed in the posterior margin of the limb bud, in the ZPA. Null mutants for this gene present several defects, among them the forelimb is represented by a single distal cartilage element whereas the hindlimb consists of a single digit (Hill, et al. 2003). Complementary, *bmp4* mutants show polydactyly defects (Robert 2007). Shh is responsible for the activation of *fgf4* in the AER, by inducing a FGF inhibitor in the proximal region, Gremlin, Shh restricts FGFs to the AER (Zúñiga, et al. 1999). Together with *fgf8, fgf4* is involved in the proliferation of the mesenchymal limb bud cells in the progress zone (Capdevila and Izpisúa Belmonte 2001). Additionally, FGFs in the AER are partially responsible for maintaining Shh in the ZPA (Li and Muneoka 1999). Therefore, there is a feedback loop where Shh signaling in the ZPA modulates FGF4 signaling in the posterior AER, which in turn maintains the polarizing region.

Wnt signaling is also critical in controlling the induction of the AER Mouse embryos lacking the *Wnt/* β-*catenin* pathway components, *LRP6* or simultaneously *Lef1* and *Tcf1*, exhibit defects in the formation of the AER (Galceran, et al. 1999). Moreover, Wnt-7a is also required for anterior-posterior patterning

Remarkably, as occurs in somitogenesis, the presence of oscillatory genes can also be detected in limb formation, although the correlation between the formation of one segment and an oscillation cycle is not as clear as that observed during somitogenesis. The role of this limb clock in the periodic production of limb elements remains to be established (Aulehla and Pourquié 2008).

1.4.4 Heart Development

Congenital heart disease represents the most common birth defects with a rate of about 1 in 100 live births and even higher in miscarriages (Hoffman 1995). The heart is the first organ to form during embryogenesis and its circulatory function is critical from early on for the viability of the development embryo. During mouse gastrulation, mesodermal cells destined to form the heart are located in the anterior region of the primitive streak, then they migrate and coalesce anterior-laterally to form the cardiogenic regions now regarded as the primary heart field. The heart arises from cells

in the anterior LPM of the early embryo, arranged in bilateral fields on either side of the prechordal plate and rostral notochord (Tirosh-Finkel, et al. 2006), forming the cardiac crescent, where differentiated myocardial cells are already detectable. The cardiac crescent fuses at the midline and forms a heart tube, which then connects with the body through a posterior inflow and an anterior outflow. The heart tube undergoes asymmetrical growth and remodeling, to form its characteristic structures (Meilhac, et al. 2004).

Prior to the development of the heart, the embryo is already organized in its three different axes: A-P, D-V and L-R. For the process of heart formation it is required the correct L-R patterning of the embryo. It is known that several genes, which are correlated to the establishment of the L-R axis of the embryo, also affect the heart morphogenesis.

BMPs and FGFs act as potent inducers of cardiac differentiation during early stages of heart formation (Schlange, et al. 2000), whereas members of the canonical Wnt signaling pathway can block cardiac differentiation during these stages (Foley, et. al 2000, Foley, et al. 2007, Schneider and Mercola 2001). Homozygous loss of *chordin* (a BMP antagonist as referred in section 1.3.2) in mice causes septation defects, very similar to those caused by *tbx1* null mutants (Bachiller, et al. 2003). Furthermore, it has been shown that in *chordin* null mutants, *tbx1* and *fgf8* expression was reduced or absent in the pharyngeal region. This might suggest that *chordin* could function upstream of *tbx1*. However, the molecular cascade by which Chordin regulates *Tbx1* expression is still unknown (Xu and Baldini 2007).

In *Xenopus*, ectopic expression of *dkk-1*, a Wnt antagonist, in the ventral marginal zone can induce abundant expression of *nkx2.5* and *tbx5*, two homeobox genes that mark the early heart field. Cerberus homologs are expressed in heart-inducing tissues in mouse, chick, and *Xenopus* (Belo, et al. 1997, Shawlot, et al. 1999) and can induce expression of *nkx2.5* in *Xenopus* animal cap tissue (Belo, et al. 1997). Despite this, Cerberus does not induce expression of terminal cardiac differentiation markers, and hearts develop properly in null mutants for the murine homolog of Cerberus *cerl*. The same cannot be said for *cerberus-like2*, where its null mutants exhibit several heart defects (Marques, et al. 2004).

1.4.5 Kidney Development

Along with the heart, kidney is one of the most important organs, as it is responsible for filtering toxins and waste products from the blood.

The process of kidney development starts at E9.5 when the nephric mesenchyme arises in the region contiguous to the hindlimb. (Mugford, et al. 2009). The first kidney-like structure during development first is the mesonephros, a temporary structure derived from the intermediate plate mesoderm. The pronephros, a rudimentary transient kidney, starts to be formed when signals from the somites and surface ectoderm, induce the cells in the intermediate mesoderm to form the nephric bud. (Bouchard, et al. 2002). The definitive kidney, also called metanephros, is not fully developed until approximately the third week after birth (reviewed in Kaufman and Bard, 1999).

At E10.5, the metanephric mesenchyme induces a single ureteric bud from the nephric duct near the hind limb (Dressler 2006). Afterwards, the ureteric bud elongates and branches within the metanephric mesenchyme, giving rise to the collecting ducts, pelvis, and ureter (Dressler 2006). At the tip of the ureteric bud, local metanephric mesenchyme is stimulated to condense and differentiate into nephron epithelia. Furthermore, regions of stromal mesenchyme also surround the developing nephrons.

Several signaling pathways are involved in kidney development. Member from Wnt signaling, such as, β-catenin, Wnt6, Wnt7b, Wnt9b and Wnt11, have already been described as being essential for the correct branching morphogenesis (Bridgewater, et al. 2008). Furthermore, Wnt4, along with BMP4 and Shh, is known to play a role in the differentiation of the kidney medullary stromal cells (Itäranta, et al. 2006, Yu, et al. 2002).

Other genes such as *lim1* and *c-ret* typically pattern the urogenital system (Bridgewater, et al. 2008). FGF signaling is also present in nephrogenesis, *fgf7* and *fgf10* null mutants present small kidneys, whereas *fgf2* promotes condensation of the ureteric tubules (Hains, et al. 2008). *eya1, wt1, pax2, six1* and *gdnf* characterize the metanephric mesenchyme, and in each of these mutants, hypotrophy or agenesis of the kidney is observed (Bouchard, et al. 2002, Yu, et al. 2004, Mugford, et al. 2009).

Although many players have been identified in kidney development, it is not yet completely clear how the different molecules and signaling pathways interact, in order to correctly develop such an important organ.

1.5 OBJECTIVES

1.5.1 Nodal signaling pathway

As one can see all through this chapter, although a large amount of work as been done, much remains to explain regarding the Nodal signaling pathway. There are many players in this process and though much is already known, the interactions between the players and the possibility of redundant activities are still not completely clear, as well as the possibility of a Nodal signaling independent from EGF-CFC proteins.

In the effort of studying this pathway a little deeper, I participated in the experiments described in chapter 3.

1.5.2 The importance of AVE secreted genes

It is already known that the AVE plays a major role during mouse embryonic development being responsible for the secretion of *Nodal* antagonists and thus initiating the process of anterior-posterior axis establishment.

Several signaling pathways present in the different stages and structures of embryonic development are already known. However, several key genes that might be regulating some signaling pathways, or making the bridge between different signaling pathways, remain to be discovered.

As said before, *mcerl-1* is expressed in the AVE; previously, in the lab, as a challenge to characterize the genes expressed in such an important region, a differential screening was performed in order to unravel novel genes expressed in AVE (Filipe et al., unpublished). The results presented in chapters 4 and 5 were based on two of these genes, *Shisa* and *ADTK1*.

Xenopus Shisa, which is expressed in the organizer and anterior endomesoderm as well as in the anterior neuroectoderm, is able to inhibit Wnt and FGF signals in a cell-autonomous manner. In chapter 4 a comparative analysis of *Shisa* and its chicken homolog was performed, and its expression pattern was studied in detail.

Being ADTK1 an unknown serine/threonine tyrosine kinase, and knowing that phosphorylation of several substrates are key processes for signal transduction during embryonic development, in chapter 5 a thorough analysis of *ADTK1* expression pattern was performed, in an attempt to discover the potential signaling pathways this novel gene might be inserted in, and the signaling pathways it may be regulating. Additionally, sequence analysis was performed and it was made an attempt to assess whether ADTK1 two distinct isoforms play a different role during development. Furthermore, a targeted mutation (knockout) of this gene was performed in order to evaluate its importance during development, and its potential partners.

2. Materials and Methods

2.1 PREPARATION OF EMBRYOS

At several stages of mouse embryonic development,embryos were dissected in cold PBS DEPC. They were transfered after dissected to a glass vial containing 4% paraformaldehyde (freshly made in PBSw DEPC) and left to fix overnight at 4ºC. The next day, embryos were washed two times with PBSw DEPC. Then they were dehydrated with methanol series (25%, 50%, 75% in PBSw, 100%). Methanol 100% solution was changed two times and then the embryos were stored at -20°C.

2.2 mRNA ANTISENSE PROBE PREPARATION AND LABELING

Antisense probes were prepared according to the protocol described in Belo *et al.* (1997).

Plasmids containing the DNA of molecular markers of interest were linearized using restriction enzymes that cut at the 5' end. The DNA was run on a 0.8% agarose gel to check if the linearization was right, then the DNA was purified with QIAGEN® miniprep columns: a PB® volume 2.5 bigger than the sample was added and this was put on a column a centrifuged 1 min at 13000 rpm, the supernatant was discharged and 700µL of Ethanol Buffer was added to the column. This was centrifuged twice for 1 min at 13000 rpm, always discharging the supernatant. The DNA on the column was then eluted in RNase free water, centrifuging 1 min at 13000 rpm. DNA inserts corresponding to the gene of interest (total or partial) were transcribed using an according RNA polymerase (T3, T7 or SP6) (Roche) in order to produce an antisense transcript. The transcription reactions were incubated at 37ºC during 1h30. The RNA probes were spun through Quick Spin Columns (Boehringer Mannheim) to remove unincorporated nucleotides. 1uL of the probes was run on a 2% agarose gel in order to confirm if the transcription reaction was successful.

The list of the probes used, and how they were made is in appendix (Table 7.2).

2.3 WHOLE MOUNT *IN SITU* HYBRIDIZATION

Whole mount *in situ* hybridizations were carried out according to the protocol described in Belo *et al.* (1997).

Day 1

Embryos were dehydrated the embryos through 75, 50 and 25% methanol series in PBSw DEPC for 5 min each step. Then, embryos were washed two times for 5 min with PBSw DEPC. The embryos were bleached in 6% hydrogen peroxide (freshly made in PBSw DEPC), for 1h in the dark, at RT. After this embryos were washed three times for 5 min with PBSw DEPC. Subsequently, embryos were incubated with 10µg/ml pK, in PBSw DEPC, RT (3 min for E6.0, 5 min for E7.5, 6 min for E8.5, 7 min for E9.5, 9 min for E10.5, 10 min for E11.5). Digestion was stopped by washing in freshly prepared 2mg/ml glycine in PBSw DEPC during 5 min.

Embryos were then rinsed twice in PBSw DEPC for 5 min. After rinsing, embryos were refixed in 4% PFA 0.2% glutaraldehyde in PBSw DEPC for 15 min. Next, embryos were again rinsed in PBSw DEPC for 5 min, three times. Following, embryos were pre-hybridized samples for 3h at 65 °C with pre-hybridization solution (see in *Appendix*). After these 3h, embryos were hybridized with a RNA probe in hybridization solution (see in *Appendix*), at 65ºC overnight.

Day two

Hybridization solution was removed, pre-heated WISH solution I (see in *Appendix*) was added and embryos were left to wash for 30 min at 65ºC. This step was repeated once. WISH solution I was removed and replaced by WISH solution II, embryos was (see in *Appendix*) left to wash for 30 min at 65ºC. This step was repeated once. Embryos were then washed three times with MABT (see in *Appendix*) for 5 min at RT. Embryos were blocked for 2h at RT, while rocking, in WISH blocking solution (see in *Appendix*) and then incubated with WISH antibody (Roche) solution (see in *Appendix*) at 4ºC ON, rocking.

Day three

Antibody solution was removed and replaced by MABT, embryos washed for 45 min at RT, rocking. This step was repeated four times. Embryos were then washed for 10 min in NTMT (see in *Appendix*) at RT, twice. NTMT solution was removed and developing solution (BM purple, NBT/BCIP or BCIP) was added. Embryos develop in the dark. The reaction was stopped by removing the developing solution and adding PBS. PBS solution was changed twice.

In the case of a WISH where a single probe was used embryos were fixed and stored for posterior analysis.

In the case of a WISH where two probes were used the experiment continues.

Day four

The first antibody was inactivated through a series of methanol (25%, 50%, 75% in PBSw, 100% and to 25% again), 5 min each at RT and then two washes in PBSw during 5 min each were performed. This solution was replaced by MABT and embryos were left washing for 5 min at RT. This step was repeated. Embryos were blocked for 2h at RT, while rocking, in WISH blocking solution and then incubated with WISH antibody solution for the second probe at 4ºC ON, rocking.

Day five

Antibody solution was removed and replaced by MABT, embryos washed for 45 min at RT, rocking. This step was repeated four times. Embryos were then washed for 10 min in NTMT at RT, twice. NTMT solution was removed and developing solution (BM purple, NBT/BCIP or BCIP) was added. Embryos develop in the dark. The reaction was stopped by removing the developing solution and adding PBS. PBS solution was changed twice.

2.4 HISTOLOGY

Embryos were used for histology after mRNA *in situ* hybridization. There were two different processes of inclusion: in gelatin for cryosectioning and in paraffin for microtome sectioning.

2.4.1 Gelatin embedding

Embryos were placed in a 15% sucrose (SIGMA) solution at 4ºC until they "sank" to the bottom of the vial, and then embed in a 7.5% gelatin (SIGMA) in 15% sucrose (SIGMA) at 37ºC for 1h. The gelatin was left to solidify and the embryos were then oriented according to the sectioning desired (sagital, coronal or transverse). The blocks that included the embryos were frozen on cool isopentan and stored at -80ºC. Blocks were cut at 6µm using a cryostate. Sections were left at -20ºC after what gelatin was removed. Sections were washed in PBS at 40ºC for 10 min, and then washed three times in PBS for 5 min at RT. Slides were mounted using Aquatex (Merck). After 24h sections were analyzed at the microscope.

2.4.2 Paraffin embedding

Embryos previously fixed and rehydrated in PBS were washed in a 0.85% NaCl (SIGMA) solution at 4ºC for 15 min. This solution was removed and replaced by a 1:1 0.85% NaCl and ethanol (Panreac), embryos were washed for 15 min at 4ºC. Embryos were dehydrated through a series of ethanol 70%, 85%, 95% and 100%, 15 min each step at 4ºC. When in 100% ethanol, embryos were washed three times. Toluol was added, and embryos were washed three times during 10 min at RT. A pre-heated solution of toluol and paraffin (Merck) 1:1 was added and embryos were left at 60ºC for 15 min. Embryos were washed twice in paraffin at 60ºC for 20 min and then once more for 1h or ON. The embryos were then orientated in mould according to the orientation desired. The paraffin solidified and moulds were stored at 4ºC. Depending on the size of the embryos, sections were performed from a range of 6µm to 10µm.

Sections were placed on slides and left to dry at 37ºC until the paraffin became invisible (a few hours to overnight, depending on the thickness of the sections). Paraffin was removed by washing twice in xilol for 10 min each. Slides were mounted with DPX (Fluka). After 24h sections were analyzed at the microscope.

2.4.3 Kidney histology

Kidneys were removed and fixed O/N in 4% PFA, after what they were included according to what described in section 2.4.2. Sections were performed at 12 µm. After the sectioning, paraffin was removed by washing twice with xylene for 10 min at RT. Sections were then rehydrated through a ethanol series of 100, 95, 75%, 5 min for each step, and then washed in distilled water for 5 min. The tissues were stained using the haematoxylin and eosin. Sections were immersed for 30 sec in haematoxylin, and briefly washed with tap water with a few drops of 4M ammonia, following, they were immersed in eosin for 2 min. Subsequently, sections were washed again with tap water with a few drops of acetic acid and then distilled water. Sections were then dehydrated through graded ethanol series (75, 95 and 100%), 5 minutes each, and then immerse in xylene twice for 10 min each. Slides were mounted with DPX (Fluka). After 24h sections were analyzed at the microscope.

2.5 TARGETING CONSTRUCT

A C57BL/6 mouse Bacterial Artificial Chromosome (BAC) genomic clone, RP24-360O6, containing *ADTK1* exons, was obtained from BACPAC Resources, Children's Hospital Oakland Research Institute. Using the BAC DNA as a template, a 5' homologous region ranging from 4779 to 284 bp upstream of the transcription start site of exon 1, and a 3' homologous region ranging from 2328 to 3916 bp downstream of the end of exon 1 were isolated by PCR. These genomic fragments were fully sequenced and cloned in a PGK neo floxI, to both sides of a PGK-Neo-pA cassette, a HSV-TK cassette was also added to the vector to the beginning of the 5' arm. The vector was linearized with SalI and was used as the targeting vector.

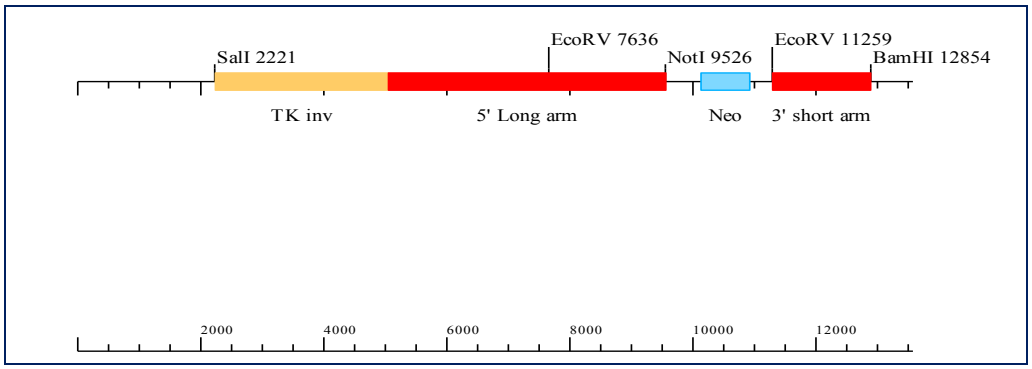

Figure 2.1 - Construct scheme

Using PGK neo flox I plasmid vector, a 5' homologous region upstream of the transcription start site of exon 1, and a 3' homologous region downstream of the end of exon 1, were cloned flanking the neo cassette. A HSV-TK gene was cloned upstream of the 5'recombination arm.

2.6 MOUSE EMBRYONIC FIBROBLASTS PREPARATION

Mouse Embryonic Fibroblast (MEF) cells are required to support the growth of undifferentiated ES cells, thus they are also called feeder cells. These cells stop dividing after a couple of passages, so embryonic fibroblasts need to be isolated freshly from time to time. This requires pregnant female mice at embryonic day 12 or 13. MEF cells are isolated from mouse embryos.

The pregnant female is sacrifice between days 12 and 13 dpc by cervical dislocation or CO_2.The uterine horns are removed, and briefly rinsed and placed into a Petri dish containing PBS. Embryos are removed to a clean Petri dish containing PBS and all placenta and surrounding membranes are removed. The head is cut as are all the internal organs (lungs, heart, liver, intestine, stomach, etc.). The remaining embryo is washed through several Petri dishes containing sterile PBS (Gibco) in order to remove all blood residues.

At this stage, the embryos were placed in a clean Petri dish and put inside the laminar flow chamber; they were washed through a series of five plates with PBS. Embryos were cut with a razor blade in as little pieces as possible and put in a plate with 15mL of trypsin-EDTA (Gibco), This was resuspended roughly by pippeting up and down for five or six times and then put in the incubator and left to act at 37ºC during 15min. Passed that time, another 5mL of trypsin-EDTA were added, resuspended and left to digest for another 10min. This digested tissues were

homogenized and passed through a net with very small porous into a new plate. The net was washed with 5mL of PBS and what went through the net was placed on a falcon, and the plate was washed with 10mL of PBS; that was put also in the falcon and all the content was centrifuged for 8min at 1000rpm and 10ºC. The supernatant was rejected and the pellet was resuspended in MEFs culture medium (see in *Appendix*), filling the necessary volume in order to obtain about one flask of 175cm^2 per two dissected embryos.

The cells were plated and left to grow. The medium was changed on the following day and the cells were passed when a confluence of 80% was reached.

After two passages the cells were frozen in a concentration of about 1million per vial in a 1:1 MEFs culture medium, 2x freezing medium (see in *Appendix*). First they were put on a -80ºC freezer and on the following day they were stored in liquid nitrogen.

2.7 ES CELL TARGETING

C57Bl6 Bruce4 embryonic stem (ES) cells were thawed and grown on inactivated MEFs in ES cell medium (see in *Appendix*). They were fed every day and split every two days in a proportion of 1:5.When an amount of 10^7 cells were reached, ES cells were carefully trypsinized and centrifuged 5 min at 1000 rpm, RT. The pellet was washed in 5 ml of sterile PBS in order to remove all the salts and centrifuged again in the same conditions. The pellet was then resuspended in 800µL of sterile PBS and the linearized construct DNA was added. This suspension was put in an electroporation cuvette and electroporation occurred at the conditions of 500µFD and 0.24V. The cells were removed from the cuvette and gently mixed in 5 mL ES cell medium. This suspension was then carefully mixed in 20 mL of pre-heated ES cell medium and plated on five 6 cm cell plates, previously coated with inactivated MEFs. On the following day the medium was changed, and on the day after the medium was replaced by the ES cell medium enriched with 5mg of G418 and 2 µM GANG. This medium was used for the following eight days in order to positively and negatively the ES cells. In the presence of GANG, cells that contain the HSV-TK gene die, whereas only cells which contain the neo cassette survive in the presence of G418. Ten days after the electroporation

occurred, ES cell colonies that survived the conditioned medium were picked, trypsinized and put in 96 well plates and were culture with regular ES cell medium. These plates were trypsinized and resuspended in α-ES medium (see in *Appendix*), then were split 1:3 where two plates were maintained in culture, adding regular ES medium and the other was kept frozen at -80ºC adding β-ES medium (see in *Appendix*). The two plates were maintained in culture until they were 100% confluent, in order to extract the DNA.

After the 3' recombination arm was screened by PCR, selected clones were thawed directly to a well of a 24 well plate and were allowed to grow. Cells were expanded three times, in order to have 2 wells of a six well plate. The cells from one of the wells were frozen and stored in liquid nitrogen, whereas the cells from the other well were maintained in culture until they were 100% confluent, in order to extract the DNA, which will be used in southern blot analysis.

2.8 DNA EXTRACTION FROM ES CELLS

ES cells were washed with 100µL of PBS and then digested with 50µL of ES cell lysis buffer with 1mg/mL pK, ON, at 60ºC, in a closed humid box. The following day 100µL of a solution of 150µL 5M NaCl in 10 mL ethanol was added. The DNA was left to precipitate for 1h at RT. The 96 well plates were inverted very quickly in order to discharge the supernatant and the pellet was washed twice with 150µL of chilled 70% ethanol. The pellet was left to dry at RT and the resuspended.

2.9 SOUTHERN BLOT

DNA samples were digested with different restriction enzymes according to the results desired for specific probes, at 37ºC O/N. The following day, gel electrophoresis was performed: digested DNA samples were ran on a 0.7% agarose gel in TAE for 5h at 80V, in order to separate the desired bands.

The gel was washed in a 0.25M HCl solution for 15 min with agitation, in order to break the bonds between the gel and the DNA, afterwards this solution was replaced by

a denaturing solution (see in *Appendix*), where the gel remained for 30 min and then the gel was washed in a neutralizing solution (see in *Appendix*) for 30 min. These steps were performed at RT. The gel was then briefly washed in 10x SSC and transferred into a membrane according to the scheme presented in *Appendix* (Fig 7.1). The membrane was washed briefly in SSC 2x and crosslinked in a UV crosslinker. Alternatively, the DNA was fixed in the membrane by baking for 3h at 80ºC.

There were two different procedures in what membrane hybridization was concerned: the radioactive and the non-radioactive one (using DIG).

2.9.1 Radioactive Hybridization

The membrane was pre-hybridized in ExpressHyb™ Solution (Clontech) for 2hrs at 65ºC with agitation. Meanwhile, the DNA radioactive probe was prepared. About 200ng of DNA in 23µL of distilled water was denaturated at 100ºC for 5min and immediately put on ice where it was added to 2µL of dATP solution, 2µL of dGTP solution, 2µL of dTTP solution, 15µL of Random Primer Buffer Mixture (Invitrogen) and 5µL (50µCi) of [α^{32}P] dCTP. All this was mixed and 5U of Klenow fragment was added and incubated at 37ºC for 1h. After the incubation period, 5µL of stop buffer was added. The probe was purified through a G-50 sephadex™ column and eluted in 400µL of TE. This was denaturated at 100ºC for 5min, then put on ice and added to 10mL of ExpressHyb™ Solution. The pre-hybridization solution was removed and replaced the ExpressHyb™ Solution with the radioactive probe. The membrane was left to hybridize O/N at 65ºC, with agitation.

The following day the hybridization solution was removed and the membrane was washed briefly with SSC 2x at RT. Then it was left to wash with Southern Wash Solution I (see in *Appendix*) for 1h at 65ºC with agitation. This solution was then removed and replaced by Southern Wash Solution II (see in *Appendix*) for 1h at 65ºC with agitation. This last step was repeated once. The membrane was then removed from Wash Solution II and rinsed briefly in SSC 2x at RT. It was left to expose in an Amersham™ screen for 24h and was developed (scanned) in Molecular Imager.

2.9.2 Non-Radioactive Hybridization - DIG High Prime DNA Labeling

The membrane was pre-hybridized in DIG Easy Hyb buffer ™ Solution (Roche) for 2hrs at 45ºC with agitation. Meanwhile, the DNA-DIG probe was prepared. A 1µg of template DNA in 16µl of double distilled water was denaturated at 100ºC for 10 min and then put on ice where 4µl of DIG-High Prime was added (Roche). The reaction was incubated at 37ºC for 3hrs and stopped by adding 2µl of 0.2M EDTA at pH 8.0 and then heating to 65ºC for 10min.

The DIG-labeled DNA probe was denatured for 5min at 100ºC, put on ice, and the added to about 10mL of DIG Easy Hyb buffer™ Solution. The pre-hybridization solution was removed and replaced by this one. The membrane was left to hybridize O/N at 50ºC with agitation.

The following day the membrane was washed two times for 5min at 65ºC with Southern Wash Solution I (see in *Appendix*) and two times for 15min at RT with Southern Wash Solution II (see in *Appendix*), always with agitation. After these washes, the membrane was rinsed briefly in Southern Washing Solution (see in *Appendix*) and incubated in blocking solution (dilution of 10x blocking solution (Roche) in Southern Maleic Acid Buffer) for 30min at RT with agitation. Blocking solution was removed and replaced by Antibody solution (Anti-Digoxigenin-AP 1:10000 (75mU/ml) (Roche) in Blocking Solution) and left to incubate for 1hr at RT, with agitation. After the Antibody solution, membrane was washed twice for 15min with Southern Washing Solution, and then equilibrated in Detection Buffer (see in *Appendix*) for 5min.

The membrane was removed from the recipient and placed with the DNA side up, and 1ml of CSPD ready-to-use™ (Roche) was applied; the membrane was covered with a plastic sheet to spread the substrate evenly and without air bubbles, and left to incubate for 5min at RT. The excess of liquid was squeezed out and the membrane was put in a cassette with a film and left to expose for about 3hrs.

The film was then developed in a dark room, using developing solution (Sigma) and then the fixing solution (Sigma). The film was left to dry at RT and was evaluated for its contents.

2.10 GENOTYPING

2.10.1DNA extraction from the tail

About 0.5 cm of the tail of mice between 15-21 days of age were cut into eppendorfs and posteriorly were incubated in 750 µl of tail buffer and proteinase K (Boheringer), O/N at 55ºC, in a water bath. For each 750 µl of tail buffer 20 µl from a stock of pK at 20mg/ml were added.

On the following day, the tubes were removed from the bath and mixed for 5 min in the shaker. Then 250µl of a saturated NaCl solution was added and left to mix for 10 min. Then the tubes were centrifuged during 10 min at 13200 rpm. The top phase was replaced into a new tube and 750 µl of isopropanol was added and then mixed for about 5 min in the shaker. The eppendorfs were spinned for 5 min at 13200 rpm and the supernatant was discharged. At this point a pellet could be seen at the bottom of the tube. The DNA was wash with 750µl of 70% ethanol, and centrifuged for 5 min at 13200 rpm. The supernatant was discharged and the pellet was left to dry at RT. The DNA was subsequently ressuspended in 250 µl of TE, at RT with low agitation.

2.10.2DNA extraction from mouse embryos

The pos *in situ* hybridization embryos were washed two times in PBS and were put each inside a 1,5ml tube. PBS was discharged with 1ml syringe with needle under the stereoscope, and embryos were incubated in embryo buffer with pK (final concentration of 0.5 mg/ml) O/N at 55ºC.

For E6.5 embryos was used a final volume of 20µl/embryo, for E7.5 was used 30µl/embryo and for E8.5 embryos use a final volume of 40µl/embryo.

On the following day, pK was inactivated at 95ºC for 10 min; the tubes were put immediately on ice and centrifuged at full speed for 10 min.

The top phase was used to do the PCR.

2.10.3PCR mix

All PCR were prepared on ice according to the following table (Table 2.1).

Table 2.1 - PCR mix

Reagent	Volume
Buffer #10	2.5 µL
dNTPs 2mM	2.5 µL
Primer Fw	1.0 µL
Primer Rev	1.0 µL
Nuclease Free Water	16.7 µL
Taq (Fermentas)	0.3 µL
DNA	1.0 µL
Total Volume	25.0 µL

The PCR programs vary in the annealing temperature and in the extension time, according to the primers in question (Table 2.3). Other than that, all PCRs follow the same program, according to the following table (Table 2.2).

Table 2.2 - PCR program

Temperature	Time	
96ºC	4 min	
94ºC	1 min	x30
Annealing temp	1 min	
72ºC	Depending on the size of the band	
72ºC	10 min	
4ºC	∞	

After the PCR, samples were analyzed after a gel electrophoresis was performed, using an agarose gel.

Table 2.3 - List of primers used in genotyping

Gene	Primer	Sequence	Band size
ADTK1	ADTK wt fw ADTK wt rev ADTK neo fw	CACCGACTACACCTACAAC ACCACCACCAGGAAGCATGA CTCGACTGTGCCTTCTAGTT	WT: wt fw-wt rev 864 bps Null neo fw- wt rev 544 bps
Cripto	CRAE3G CRAIS2 KOTPNEO	GCCAAGAGCCATGACAGAGATGG GGGGACAGGGCTGCTCAGTGTCGC AGCGCATGCTCCAGACTGCCTT	WT: CRAE3G-CRAI2S 308 bps Null: CRAI2S-KOTPNEO 125 bps
Nodal	F1 R4 3F3	AAGAGAGGAAAGTAGGCTTGC GCGAACAGAAGCGAGAAGC GCACATAAGAACTGATGGTGGTGCCTG	WT: F1-3F3 240 bps Null: F1-R4 560 bps
Otx2	Otx up Otx low1 Otx neo Otx low5	GTGACTGAGAAACTGCTCCC GTGTCTACATCTGCCCTACC TGCTGTGTTCCAGAAGTGTT GCTCAAAGACAGACCTCAATATC	WT: Otx up-Otx low1 150 bps Null: Otx neo-Otx Low5 500 bps
cerl1	EcoF1 L4 IRES2 Lacz2	GACGAATTCACCCACCTGCTGACCACCT GCTTCC CTCTTTCTATTTTGCCGTTTGTC CGTTGTGAGTTGGATAGTTGTGG GATAGGTTACGTTGGTGTAGATGG	WT: EcoF1-L4 700 bps Null: IRES2-Lacz2 525 bps

2.11 RNA EXTRACTION

Embryos were dissected at the desired stages and put on a tube with PBS. After all embryos were dissected, PBS was removed from the tube and replaced by 500µL of Trizol Reagent. The sample was well homogenized and 200µL of chloroform was added. The tube was shaken vigorously and centrifuged for 10 min at 13200rpm and 4ºC. The upper colorless phase was collected into a new tube and 500µL of 2-propanol

was added and well mixed. The tube was placed at -20ºC during 1h after what it was centrifuged for 15 min at 13200rpm and 4ºC. The supernatant was discharged and 500µL of 75% ethanol was added. The tube was then put briefly on the vortex and centrifuged for 5 min at 13200rpm and 4ºC. The supernatant was removed and pellet was left to dry at RT. The RNA was dissolved in 20µL of nuclease free water and 0.5µL of the sample was used in a gel electrophoresis, using a 2% agarose gel in order to verify if the RNA was well extracted. One should see two different bands in the gel, corresponding to the two different sedimentation coefficients of RNA.

2.12 REVERSE TRANSCRIPTION PCR

Reverse transcription-polymerase chain reaction (RT-PCR), is a sensitive method for the detection of mRNA expression levels.

RT-PCR involves two steps: the RT reaction and PCR amplification.

RNA is first reverse transcribed into cDNA using a reverse transcriptase: to 1µg of RNA is added 0.2µg/µL in a volume of 12µL and incubated for 5 min at 70ºC, following this, 4µL of 5x Reaction Buffer, 2µL of 10mM dNTP mix and 20U of RNase Inhibitor were added to the mix and incubated at 25ºC for 5 min. After the incubation period was ended, 200U of RevertAid™ H Minus M-MuLV RT was added. This reaction was incubated first 10 min at 25ºC, then 1h at 42ºC, 10 min at 72ºC and left to cool down till 4ºC.

The resulting cDNA is used as templates for subsequent PCR amplification using primers specific for one or more genes. Housekeeping gene, HPRT (hypoxanthine guanine phosphoribosyl transferase) crosses introns, in order to be sure the cDNA is not contaminated with genomic DNA. After PCR, the samples were separated through gel electrophoresis, in order to verify the obtained product length.

Table 2.4 - List of primers used in RT-PCR

Gene	Primer	Sequence (5' – 3')
ADTK1	E1aFW	CGTCCTCAACGTGCTCTTCG
	E1aREV	AGATCGTGGCCGCTGAAGTC
	E1bFW	CTGCAGCTCTATGGCTATTG
	E1bREV	CTGAGGCAGATTCGGAATCG
	E1FW	AAACGTCCTCAACGTGCTCTTCG
	E1REV	AAAGCTCCAGCAGCACCATCTCT
	E2E3FW	AAAGATCCAGCTGTTGCAGACTT
	E2E3REV	AAAGTAGGCATTGTAGAGGTTCC
	E4E6FW	AAATCCGACCTCTCCTGGATAGC
	E4E6REV	AAAAGGCACGACACTGAGCATGG
	E1E7FW	AAATCCGTCCTCAACGTGCTCTT
	E1E7REV	AAAATGCAGCAGCAGTGTTCTGG
	E1E6FW	AAACGAGGAGGTGCAGCGCTATT
	E1E6REV	AAAAGGCACGACACTGAGCATGG
HPRT	HPRT FW	GCTGGTGAAAAGGACCTCT
	HPRT REV	CACAGGACTAGAACACCTGC

2.13 SKELETAL ANALYSIS

For the skeletal analysis of the neonates, Alcian blue/Alizarin red staining was performed according to what is described in Belo et al. (1998). Skin and viscera were removed from the newborn mice, and the tissue was fixed ON in ethanol 95%. The following day were stained for three days with 0,045% Alcian blue, 80% ethanol and 20% acetic acid. After three days, alcian stain was washed with 95% ethanol for 6h. This solution was then replaced with 2% KOH for 24h. Specimens were stained with 0,03% Alizarin red (Sigma) in 1% KOH for 12h. Specimens were cleared with 1% KOH, 20% glycerol, and passed through a glycerol/ethanol storage solution series: 50%, 80% and finally 100% glycerol.

3. **Results I -** Cripto-Independent Nodal Signaling Promotes Positioning of the A-P Axis in the Early Mouse Embryo

Cripto-Independent Nodal Signaling Promotes Positioning of the A-P Axis in the Early Mouse Embryo

Giovanna L. Liguori[2,4], Ana Cristina Borges[1,3,4], Daniela D'Andrea[2], Annamaria Liguoro[2], Lisa Gonçalves[1,3], Ana Marisa Salgueiro[1,3], M. Graziella Persico[2,5] and José Antonio Belo[1,3,5]

[1]Instituto Gulbenkian de Ciência, 2781-901 Oeiras, Portugal

[2]Institute of Genetics and Biophysics "A. Buzzati-Traverso", CNR, Via Pietro Castellino 111, 80131 Naples, Italy;

[3]IBB-Institute for Biotechnology and Bioengineering, Centro de Biomedicina Molecular e Estrutural, Universidade do Algarve, Campus de Gambelas, 8005-135 Faro, Portugal;

[4]these authors contributed equally to this work

[5]these authors contributed equally to this work

Published in Developmental Biology 315 (2008) 280–289

3.1 ABSTRACT

During early mouse development, the TGF-β-related protein Nodal specifies the organizing centers that control the formation of the Antero-posterior (A-P) axis. EGF-CFC proteins are important components of the Nodal signaling pathway, most likely by acting as Nodal co-receptors. However, the extent to which Nodal activity depends on EGF-CFC proteins is still debated. *Cripto* is the earliest EGF-CFC gene expressed during mouse embryogenesis and is involved in both A-P axis orientation and mesoderm formation. To investigate the relation between Cripto and Nodal in the early mouse embryo, we removed the Nodal antagonist *cerberus-like1 (cerl1)* and simultaneously *cripto,* by generating *cerl1;cripto* double mouse mutants. We observed that two thirds of the *cerl1;cripto* double mutants are rescued in processes that are severely compromised in *cripto-/-* embryos, namely A-P axis orientation, anterior mesendoderm and posterior neuroectoderm formation. The observed rescue is strongly reduced in *cerl1;cripto;Nodal* triple mutants, suggesting that Nodal can signal extensively in the absence of Cripto, if *cerl1* is also inhibited. This signaling activity drives A-P axis positioning. Our results provide evidence for the existence of Cripto-independent signaling mechanisms, by which Nodal controls axis specification in the early mouse embryo.

3.2 INTRODUCTION

A signaling pathway centered on Nodal, a member of the Transforming growth factor-β (Tgf-β) superfamily, is responsible for crucial events in the configuration of the vertebrate embryo, such as the definition of both Anterior-Posterior (A-P) and Left-Right (L-R) axes and the formation of mesoderm and endoderm germ layers (Schier, 2003). In the mouse embryo, the A-P axis becomes explicit during gastrulation with the appearance of the primitive streak, marking the posterior extreme of the embryo (Beddington and Robertson, 1998). However, before the onset of gastrulation, some genes, such as *cerberus-like 1* (*cerl1*) and *lefty1*, begin to be expressed in the distal visceral endoderm (DVE), while other genes, such as *cripto*, *brachyury* and *fgf8* are specifically expressed in the proximal epiblast (Beddington 1998, Beddington and Robertson 1998, Beddington and Robertson 1999, Ding, et al. 1998, Yamamoto, et al. 2004). This gene expression asymmetry defines a proximal-distal (P-D) polarity inside

the mouse embryo, before gastrulation (Beddington 1998, Beddington and Robertson 1998, Beddington and Robertson 1999). Later, the DVE cells migrate asymmetrically towards the prospective anterior side of the egg cylinder, giving rise to the anterior visceral endoderm (AVE); in the meantime, the expression of the proximal genes is restricted to the posterior embryonic pole, which will give rise to the primitive streak (Ang and Constam 2004, Beddington 1998, Beddington and Robertson 1998, Beddington and Robertson 1999). The unilateral migration of the DVE converts the P-D to an A-P axis, presumably by directing cell movements and regulating gene expression in the epiblast (Ang and Constam 2004, Perea-Gomez, et al. 2002, Yamamoto, et al. 2004). Nodal is required both to specify the DVE, which moves anteriorwards to form the AVE, and to pattern the epiblast (Lu and Robertson 2004). In fact, *Nodal* null mutants fail to form a P-D axis (Brennan, et al. 2001, Conlon, et al. 1994). Later on, Nodal signaling provides the driving force for DVE migration and thus promotes the conversion of the initial P-D polarity into the A-P axis (Yamamoto, et al. 2004). Nodal signaling depends upon interaction with EGF-CFC cofactors and Activin type I and II receptors (ActRI and II) (Schier 2003, Shen 2007, Whitman 2001). Nodal activity is also tightly limited in space and time by inhibitory factors, such as Cerl1, Tomoregulin, Drap1, Lefty1 and Lefty2 (Schier 2003, Shen 2007, Whitman 2001). The EGF-CFC founder member Cripto, together with the Nodal antagonists Cerl1 and Lefty1, direct the proper orientation of the A-P axis, and gastrulation movements (Ding, et al. 1998, Xu, et al. 1999, Perea-Gomez, et al. 2002, Yamamoto, et al. 2004, Liguori, et al. 2003). In fact, *cripto* null mutants fail to convert the initial P-D into an A-P axis and also fail to form embryonic mesoderm (Ding, et al. 1998, Liguori, et al. 2003). This phenotype is striking, because *cripto* expression has never been detected in the visceral endoderm (Shen and Schier 2000). Moreover, analysis of chimeras consisting of wt epiblast and *cripto-/-* extraembryonic tissues clearly demonstrates that *Cripto* is not essential in visceral endoderm (Kimura, et al. 2001). On the other side, Cerl1 and Lefty1 synergistically act to determine the direction of migration of the DVE cells (which define the future anterior pole of the embryo) as well as to restrict primitive streak formation in the embryo to the posterior pole (Perea-Gomez, et al. 2002, Yamamoto, et al. 2004).

The EGF-CFC molecules are membrane-attached extracellular proteins, found only in vertebrates (Persico, et al. 2001, Shen and Schier 2000). Family members have been

characterized in mouse (Cripto and Cryptic), human (CRIPTO and CRYPTIC), chick (Cripto), zebrafish (oneeyed pinhead [oep]), and frog (FRL-1) (Persico, et al. 2001, Shen and Schier 2000). Biochemical studies indicate that Cripto and Cryptic form a complex with Nodal, ActRIB (ALK4) and ActRIIB (Reissman, et al. 2001, Yeo and Whitman 2001, Whitman 2001). Mechanistically, EGF-CFC factors appear to function as co-receptors, enhancing Nodal binding to the type I/II receptor complex. However the extent to which Nodal activity depends on EGF-CFC proteins remains unresolved. On the one hand, *in vitro* studies show that Cripto interaction with ALK4 is necessary both for Nodal binding to the ALK4/ActRIIB receptor complex and for Smad2 activation by Nodal (Yeo and Whitman 2001). Studies in zebrafish also suggest that EGF-CFCs are absolutely required for Nodal signaling, since Nodal has no apparent effect on *oep* mutants (Gritsman, et al. 1999). Moreover, Vg1 and Gdf1 signaling in zebrafish also depends on EGF-CFCs proteins, suggesting that multiple Tgf-β signals converge on ActR/EGF-CFC complexes (Cheng, et al. 2003). On the other hand, cell culture assays indicate that Nodal signaling via the ActRIA (ALK7) receptor is enhanced by EGF-CFC proteins but does not absolutely require them (Reissman, et al. 2001). In addition, the mouse *cripto* null mutation does not precisely phenocopy the *Nodal* loss of function. In particular, the *Nodal*$^{-/-}$ mouse embryo is not able to specify an A-P axis (Conlon, et al. 1994), whereas in *Cripto* null mutants, the rudiment of an A-P axis is recognizable, even though it is not correctly oriented (Ding, et al. 1998, Liguori, Echevarría, et al. 2003). Recent experiments have also shown that unprocessed Nodal proprotein is able to bind both ALK4 and ActRIIB receptors in transfected 293T cells, even though neither Cripto nor other EGF-CFC factors are co-transfected (Ben-Haim, et al. 2006). The purified recombinant Nodal proprotein is also able to induce *Bmp4* and *PACE4* expression in mouse extraembryonic ectoderm explants, although neither *Cripto* nor *Cryptic* genes are expressed in extraembryonic ectoderm (Ding, et al. 1998, Kimura, et al. 2001, Shen, et al. 1997, Ding et al., 1998, Kimura et al., 2001; Shen et al., 1997); this activity has been shown to be ALK4-dependent (Ben-Haim, et al. 2006). Cripto is also able to act non cell autonomously both *in vitro* in cell coculture assays and *in vivo* during mouse embryogenesis (Yan, et al. 2002, Chu, et al. 2005). These data suggest that Cripto can also function in trans as an intercellular mediator of Nodal signaling activity (Chu, et al. 2005). Finally, Cripto is thought to promote tumour growth via Nodal-independent mechanisms, such as activation of a ras/raf/MAP kinase pathway or

inhibition of Tgf-β and Activin signaling (Bianco, et al. 2003, Adkins, et al. 2003, Gray, et al. 2003, Strizzi, et al. 2005). In summary, both Nodal and Cripto are multifunctional signaling proteins, involved in numerous physiological and pathological processes. Therefore, the relation between Cripto and Nodal constitutes a crucial point for the reciprocal regulation of their activity and this relation needs further characterization.

To investigate the extent to which Cripto is required for Nodal signaling in the mouse embryo, we designed a double mutant mouse strategy, taking advantage of both *Cripto* and *Cerl1* null mutants (Belo, et al. 2000, Liguori, et al. 2003). Cerl1 is a Nodal inhibitor that antagonizes Nodal by direct interaction in the extracellular space (Belo, et al. 2000). Therefore, the removal of Cerl1 should increase the level of free Nodal ligand, by releasing Nodal from Cerl1 inhibition. If Cripto is absolutely required for Nodal signaling, this increase in Nodal level should have no effect, and the *cerl1; cripto* double mutants should have the same phenotype as *cripto* null mutants. Alternatively, if the increased level of Nodal protein can bypass Cripto function, the outcome would be a rescue of the *cripto*$^{-/-}$ early lethal phenotype. We chose Cerl1 from among the different Nodal antagonists for two important reasons. First of all, Cerl1 exerts its action without interacting with Cripto (in contrast, Lefty1, Lefty2 and Tomoregulin antagonize Nodal signaling by blocking Cripto and preventing the formation of the receptor complex; (Cheng, et al. 2004, Harms and Chang 2003). Secondly, the *Cerl1* null mutation produces no evident phenotype in the mouse embryo (Belo, et al. 2000); hence, the *cerl1;cripto* double mutants need only to be compared with Cripto-deficient embryos, greatly simplifying our analysis.

Here we show that the removal of the Nodal antagonist *cerl1* does indeed partially rescue the mouse *cripto-/-* phenotype. *cerl1;cripto* compound mutants recover the orientation of the A-P axis and most of the subsequent gastrulation processes, which are severely impaired in the *cripto* null mutants. Moreover, a subset of *cerl1*$^{-/-}$*;cripto*$^{-/-}$ embryos show the formation of a double axis. All together, these data demonstrate that Cerl1 and Cripto genetically interact in mouse to control embryonic axis development. The rescue of the expression of Nodal target genes observed in *cerl1;cripto* mutants indicates the recovery of Nodal signaling, which is severely compromised in *cripto*$^{-/-}$ embryos. Accordingly, the *cerl1;cripto* rescued phenotype is impaired if we genetically reduce *Nodal* strength. Our results demonstrate that in *cripto*$^{-/-}$ mutants, partial recovery of Nodal signaling is achieved by inactivating the *cerl1* gene. In summary, this work

shows for the first time that in the mouse embryo a Cripto-independent Nodal signaling is able to position the A-P axis correctly and to form both anterior mesendoderm and posterior neuroectoderm.

3.3 RESULTS AND DISCUSSION

3.3.1 *cerl1*$^{-/-}$*;cripto*$^{-/-}$ embryos form an A-P axis

We generated *cerl1;cripto* mouse double mutants by crossing *cerl1*$^{-/-}$ (Belo, Bachiller, et al. 2000) and *cripto*$^{+/-}$ (Liguori, Echevarría, et al. 2003) mice. The resulting *cerl1*$^{-/-}$*;cripto*$^{+/-}$ are apparently normal and fertile and were intercrossed to collect double null mutants to compare with *cripto*$^{-/-}$ embryos. We began by analyzing embryos at 8.5 days post coitum (dpc) by whole mount antisense mRNA in situ hybridization (WISH; Fig 3.1).

At this stage, *cripto*$^{-/-}$ mutants are smaller than wild type (wt) embryos, show a severely compromised embryonic region and form neural territories only anterior to the *gbx2* expression domain; in particular, expression of more caudal markers (*krox20*, *hoxB1* and *hoxB4*) is never observed (Ding, et al. 1998, Liguori, et al. 2003). Moreover, the neural territories do not develop along an A-P but along a P-D axis (Fig 3.1e-g) (Liguori, Echevarría, et al. 2003). In contrast, 70% of the double null mutants express *krox20* which identifies rhombomeres 3 and 5 of the posterior hindbrain (Fig. 3.1j). In addition, 70% of the *cerl1*$^{-/-}$*;cripto*$^{-/-}$ embryos (n=10) express *krox20* and the other neural markers analysed, including *Otx2* (forebrain and midbrain), *gbx2* (anterior hindbrain), and *Wnt1* (dorsal midbrain) along an A-P axis (Fig 3.1i-k) as in the wt embryo (Fig 3.1a-c), not along a P-D axis as in the Cripto null mutants (Fig 3.1e-g).

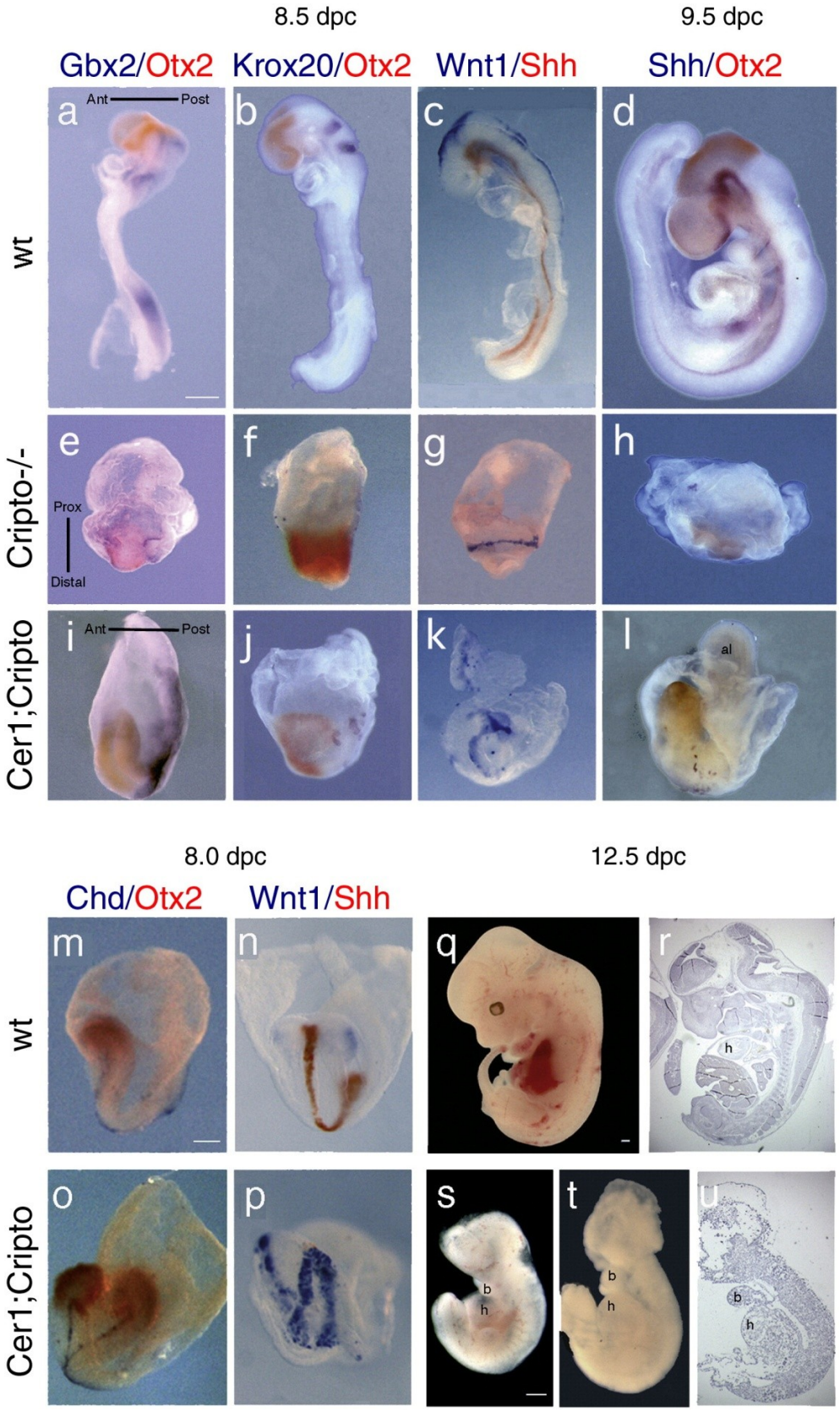

Figure 3.1 - Rescue of posterior neuroectoderm and trunk structures in Cer1;Cripto double mutant embryos.

(a–p) Molecular analysis by double whole-mount *in situ* hybridization (WISH) of 8.5 (a–c, e–g, i–k) and 9.5dpc (d, h, l) wild-type (wt) (a–d), *Cripto−/−* (e–h) and *Cer1−/−;Cripto−/−* embryos (i–l). a, e, i, in

the *cripto* null mutants (e), *otx2* (red) and *gbx2* (blue) are expressed along a P–D axis whereas in the *Cer1−/−;Cripto−/−* double mutants (i) the expression domains are aligned along an A–P axis, as in the wt embryo (a). b, f, j, in the *cripto−/−* embryos (f), the marker of the rhombomeres 3 and 5 *krox-20* is not expressed, in contrast to the double null mutants (j). Concomitantly, *otx2* expression domain is anteriorized in double mutants. c, g, k, in the *Cripto* null mutants (g), the expression of *wnt1* (blue) is radial while in the double null mutants (k), *Wnt1* expression is oriented along the A–P axis. The expression of the ventral neural marker *Shh*(red) is not rescued. d, h, i, *cripto−/−* embryos (h) have almost completely degenerated, although retain *Otx2* expression. In contrast, the double mutants (i) display an embryonic axis, even if reduced respect to the wt embryos (d), with *otx2* domain in one of the extremities and patches of *Shh* expression along the midline. m-p, double WISH of 8.0 dpc wt (m, n) and *cer1−/−;cripto−/−*embryos (o, p), analyzed for *chordin* and *otx2* (m, o) and for *wnt1* and *Shh* (n, p). In some double null mutants, we observed duplication of the embryonic axis (o, p). (q–u) Morphological analysis of 12.5 dpc wt (q, r) and *cer1−/−;cripto−/−* (s–u) embryos. (r, u) Parasagittal sections of the wt embryo in q (r) and of the *cer1−/−;cripto−/−* embryo in t (u). The *cer1−/−;cripto−/−* embryos are significantly smaller than the wt embryos, show anterior head truncations, but form branchial arches and a rudimentary heart. The direction of the axes is shown. Abbreviations Ant: anterior; al: allantoid-like structure; b: branchial arch; h: heart; Post: Posterior; Prox: Proximal. Scale bars represent 300μm.

Interestingly, we also found that 20% (n=10) of the double null mutants analysed at 8.0-8.5 dpc form a secondary anterior neuraxis, revealed by the expression of both *Otx2* and *Wnt1* genes (Fig 3.1m-p). In contrast, *Shh* is expressed in a few cells close to the extremity of only one of the two axes (Fig 3.1p). A similar phenotype has been previously described in the *cerl1*$^{-/-}$*lefty1*$^{-/-}$ mutants in which two Nodal inhibitors are inactivated (Perea-Gomez, Vella FD, et al. 2002). However, while *cerl1*$^{-/-}$*lefty1*$^{-/-}$ embryos also duplicate trunk structures, the *cerl1*$^{-/-}$*;cripto*$^{-/-}$ mutants show a normal trunk with a node and notochord (Fig 3.1o).

At 9.5 dpc, *cripto*$^{-/-}$ mutants consist primarily of extraembryonic tissue (Fig 3.1h); by 10.5 dpc, they are reabsorbed (Xu, et al. 1999). In contrast, double null mutants can be found at 9.5 dpc, in which the embryonic region is well developed and clearly shows an A-P axis, with a head that expresses *otx2* and a morphologically distinguishable allantoid-like structure on the opposite side (Fig 3.1l). These double null mutants appear delayed, resembling 8.0-8.2 dpc (Fig 3.1m) rather than 9.5 dpc (Fig 3.1d) wt embryos, but nonetheless are significantly different from *cripto*$^{-/-}$ mutants, in which no morphological structure is recognizable. *Shh* expression, although defective, is detected in the embryo midline (Fig 3.1l). Strikingly, at 12.5 dpc *cerl1*$^{-/-}$*;cripto*$^{-/-}$ embryos can still

be identified (Fig 3.1s-u). Half of the surviving *cerl1*$^{-/-}$*;cripto*$^{-/-}$ embryos (n=6) are an almost empty yolk sac, but the other half develops the major embryonic axes with distinct head, trunk and tail structures (Fig 3.1s-u). The presence of posterior neuroectoderm and a developing heart in the double mutants is remarkable, since these structures are completely absent in *cripto* null single mutants (Ding, et al. 1998, Liguori, Echevarría, et al. 2003).

To investigate the effects of inactivating a single *Cerl1* allele, we crossed the *cerl1*$^{-/-}$*;cripto*$^{+/-}$ mice to *cripto*$^{+/-}$ mice to obtain *cerl1*$^{+/-}$*;cripto*$^{-/-}$ embryos. We analysed the *cerl1*$^{+/-}$ *;cripto-/-* mutants at both 8.5 and 9.5 dpc (n=10) for the expression of the markers described above. *cerl1*$^{+/-}$*;cripto*$^{-/-}$ embryos also develop an A-P axis (60%; data not shown), essentially like the *cerl1*$^{-/-}$*;cripto*$^{-/-}$ mutants. Thus, the removal of *cerl1*, even one of the two gene copies, rescues significant features of the *cripto*$^{-/-}$ phenotype**.** In summary, we show that double mutant embryos clearly develop further than *cripto*$^{-/-}$ mutants; in particular, they form posterior neuroectoderm and correctly position the A-P axis. These data demonstrate that *cerl1* and *cripto* genetically interact in mouse to control embryonic axis development.

3.3.2 The removal of *cerl1* rescues gastrulation defects of *cripto-/-* embryos

By analysis of earlier embryonic stages, we observed that gastrulation is less impaired in the *cerl1*$^{-/-}$*;cripto*$^{-/-}$ mutants than in *cripto*$^{-/-}$ embryos. At these early stages, we found no significant differences between *cerl1*$^{+/-}$*;cripto*$^{-/-}$ and *cerl1*$^{-/-}$*;cripto*$^{-/-}$ embryos, and therefore both genotypes are included in our analysis (samples referred to as double or *cerl1;cripto* mutants).

At 7.5 dpc, concomitant with the reduction and anteriorization of the *otx2* expression domain (Figs. 3.2c, d, k, l), the double mutants also develop trunk structures (Figs 3.2c, d, g, h, k, l), which are not formed in *cripto*$^{-/-}$ embryos (Figs 3.2b, f, j). *Brachyury* expression domain, which identifies the primitive streak (PS) and the forming mesoderm (Fig 3.2a), is enlarged in 60% (n= 10) of the double mutants (Fig 3.2c) compared to the *cripto-/-* embryos (Fig 3.2b).

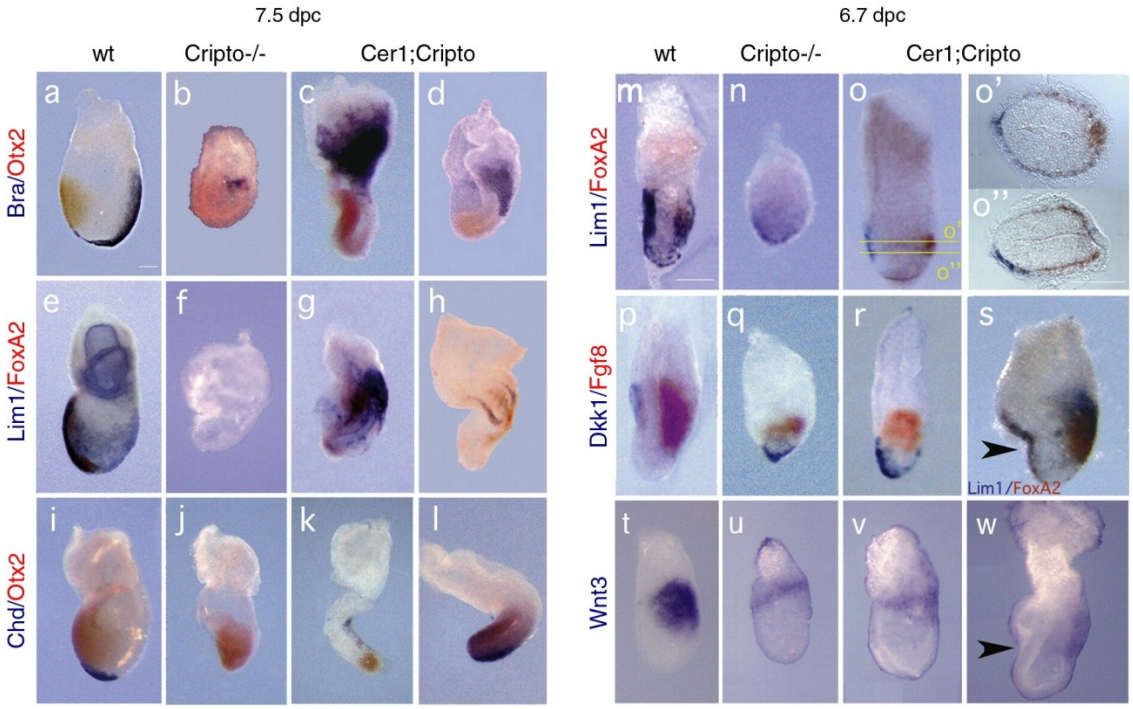

Figure 3.2 - *cer1;cripto* double mutants display rescue of AVE rotation, primitive streak elongation and node derivatives.

Molecular analysis by whole-mount double *in situ* hybridization of 7.5 (a–l) and 6.7 dpc (m–w) wild-type (wt) (a, e, i, m, p, t), *cripto−/−* (b, f, j, n, q, u) and *cer1;cripto* double mutant embryos (c, d, g, h, k, l, o, r, s, v, w). (a–d) The *otx2* (red) domain is anteriorized in the double mutants (c, d) compared to *Cripto−/−* embryos (b), whereas *brachyury* (blue) expression is enlarged (c) and in some double mutants the primitive streak extends toward the distal tip (d). (e–h) *lim1* (blue) and *foxa2* (red) are never detected in *cripto−/−* embryos (f) in contrast to the double mutants (g, h), indicating that a primitive streak, the node and its derivatives are present. (i–l) *chordin* (blue) expression revealed that in the double mutants (k, l) the node and axial mesendoderm are present in contrast to the complete absence in the *cripto* null mutants (j). (m–o, s) *lim1* (blue) and *foxa2*(red) also revealed a correct localization of the A–P axis in the double mutant embryos (o), even though in some cases a constriction in the anterior embryonic region can be observed (s). (o′, o″) Cross sections of the embryo shown in (o) at the indicated levels, show the formation of the primitive streak and the AVE rotation toward the anterior side. (p–r) In the double mutants (r), *dkk* (blue) expression domain is more anterior and *fgf8* (red) expression more distal than in *cripto−/−* embryos (q). (t–w) In the *cripto−/−* embryos, *wnt3* expression is fainter than in the wt embryos and located in the proximal region of the embryo (u). In the *cer1;cripto* mutants, *wnt3* expression remains as weak as in the *cripto−/−* mutants, but is while is located more posterior (v, w), resembling the wt embryos (t). Arrowheads indicate the constriction in the anterior region of double mutants. Scale bars represent 180μm.

In 20% of the double mutants, *brachyury* expression also extends towards the distal tip of the embryo (Fig 3.2d). The analysis at 7.5 dpc revealed that 69% (n=23) of the double mutants also express other markers that are completely absent in the *cripto*$^{-/-}$ embryos, for example *lim1*, which identifies the PS and mesodermal wings and later the node and axial mesoderm (Figs 3.2e-h), *foxa2*, expressed in the node, the midline and anterior definitive endoderm (Figs 3.2e-h), and *chordin* (*chd*), which marks the node and the axial mesendoderm (Figs 3.2i-l). In agreement with previous data, at 6.7 dpc 60% (n=23) of the compound mutants rescue the expression of AVE markers like *dkk* and *lim1* in the anterior of the VE (Figs 3.2m-r), and also of the PS marker *fgf8* in the posterior of the epiblast (Figs 3.2p-r).

We also detected the expression of *wnt3*, marking both posterior epiblast and visceral endoderm in the wt embryo (Fig 3.2t). In both *cripto* single mutants and *cerl1;cripto* double mutants *wnt3* expression is weaker than in wt embryo (Fig 3.2t-w*)*; however, in the 67% of double mutants (n=3), *wnt3* expression domain is shifted posterior, as in the wt, while in the *cripto*$^{-/-}$ embryos, expression stays proximal. Moreover, double mutant embryos express the anterior PS marker *foxa2,* which is never detected in the *cripto* null mutants (Figs 3.2p-s). We note that a small percentage of double null mutants (9%, n=23) show a peculiar characteristic: a marked bend or constriction in the anterior region (Fig 3.2s, w).

Collectively, these data confirm and extend the conclusions reported above that the double mutants have a milder phenotype than the *cripto*$^{-/-}$ embryos. At 6.7 dpc, double mutants have completely converted or are beginning to convert the initial embryonic P-D asymmetry to an A-P axis (Figs 3.2o, r), resembling wt embryos (Figs 3.2 m, p). By contrast, this axis conversion process is completely abolished in *cripto*$^{-/-}$ embryos (Figs 3.2n, q) (Ding et al., 1998; Liguori et al 2003). At later stages, the double mutants form not just posterior and extraembryonic mesoderm (as *cripto*$^{-/-}$ embryos) but also more anterior and later structures, such as the node and its derivatives including the axial mesendoderm (Figs 3.2g, h, k, l).

3.3.3 *cerl1;cripto* mutants rescue Nodal signaling

cerl1;cripto double mutants appear rescued in most of the biological processes that are controlled by Nodal. In fact, *cerl1;cripto* embryos share many phenotypic

characteristics with mutants in which Nodal signaling is only reduced, such as Nodal hypomorphs (Lowe, et al. 2001), asymmetric intronic enhancer (ASE) mutants (Norris, et al. 2002), and double mutants for ActRIIA and ActRIIB (Song, et al. 1999). In order to confirm that Nodal signaling remains active in the *cerl1;cripto* double mutants, we examined the expression of *lefty1* and *lefty2* genes, which mark the AVE and the nascent mesoderm, respectively and are immediate Nodal responsive genes (Fig 3.3a) (Meno, et al. 1998).

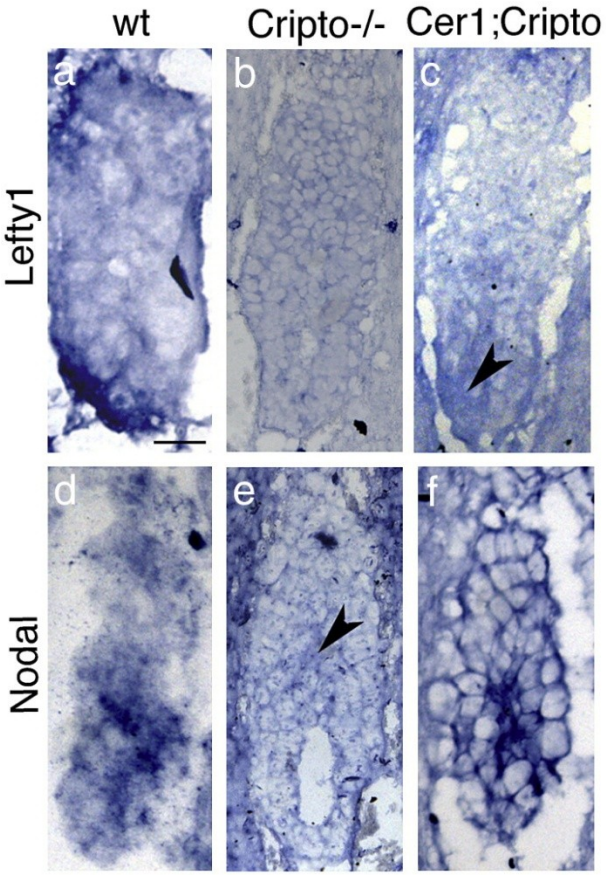

Figure 3.3 - *cer1;cripto* double mutants rescue Lefty1 and Nodal expression before gastrulation.
Molecular analysis by whole-mount *in situ* hybridization (WISH) of 5.5–5.7 dpc wild-type (wt) (a, d), *cripto−/−* (b, e) and *cer1;cripto* (c, f). In the wt embryo, *lefty1* is detected in the distal VE that moves toward the anterior side of the embryo (a).*cripto−/−* embryos lack expression of *lefty1* (b), while *cer1;cripto* embryos show a faint *lefty1* expression, marked by the arrowhead. *Nodal* is expressed in almost all the epiblast of the wt embryo (d) while it is detected only in a proximal cluster of epiblast cells (arrowhead) of the *cripto−/−* embryos (e). Nodal expression in the *cer1;cripto* double mutants (f) resembles the expression on the wt embryo (d). Scale bars represent 50µm.

The expression of both genes is abolished in *cripto*$^{-/-}$ embryos (Fig 3.4b) even though the visceral endoderm and nascent mesoderm are present (Figs 3.2n, q) (Ding, et al. 1998). In contrast, we observed that 60% (n=10) of the double mutants express *Lefty* genes; in about 20% (n=10) of these embryos, the expression domains are also correctly localised, almost resembling a wt embryo (Fig 3.4c).

We also detected the expression of the *Nodal* gene itself, which is controlled by an autoregulatory loop (Varlet, et al. 1997). At 6.7 dpc, *Nodal* is expressed in the posterior epiblast of the wt embryo (Fig 3.4d, d') but only in a proximal ring of epiblast cells in the *cripto-/-* embryo (Fig 3.4e, e'). In contrast, almost 57% (n=7) of the *cerl1;cripto* double mutants ectopically express *Nodal* throughout all the embryonic region (Fig 3.4f, f'). All together, these results indicate that Nodal signaling remains active in the *cerl1;cripto* double mutant embryos and is most likely responsible for the rescue observed. To confirm this, we performed an experiment in which *Nodal* gene dosage is diminished. To this purpose, we crossed the *cerl1*$^{+/-}$*;cripto*$^{+/-}$ double heterozygotes with *Nodal*+/- mice (Lowe, et al. 2001). The resulting *cerl1*$^{+/-}$*;cripto*$^{+/-}$*;Nodal*$^{+/-}$ triple mutants were backcrossed to *cerl1*$^{+/-}$*;cripto*$^{+/-}$ mice to obtain both *cerl1*$^{-/-}$*;cripto*$^{-/-}$*;Nodal*$^{+/-}$ and *cerl1*$^{+/-}$*;cripto*$^{-/-}$*;Nodal*$^{+/-}$ embryos.

The embryos were collected between 8.5 and 9.0 dpc and analyzed by double WISH for the expression of *otx2* and *krox20*. We chose *krox20* as an informative marker because it is expressed in the double mutants but is never expressed in *cripto*$^{-/-}$ embryos. *otx2* was used as control marker. We observed that only 25% (n=20) of the triple mutants express *krox-20*, in contrast to the 59% (n=78) of the double mutants (Fig 3.4g-j, Table 3.1).

Table 3.1 - Percentage of phenotypic rescue observed in the *cerl1;cripto* versus the *cerl1;cripto;Nodal* mutant embryos

Genotype	Rescue of *krox20* expression	%
cerl1$^{+/-}$*;cripto*$^{-/-}$	46/78 (*n* = 78)	59
cerl1$^{-/-}$*;cripto*$^{-/-}$		
cerl1$^{+/-}$*;cripto*$^{-/-}$*;Nodal*$^{+/-}$	5/20 (*n* = 20)	25
cerl1$^{-/-}$*;cripto*$^{-/-}$*;Nodal*$^{+/-}$		

P< 0.01.

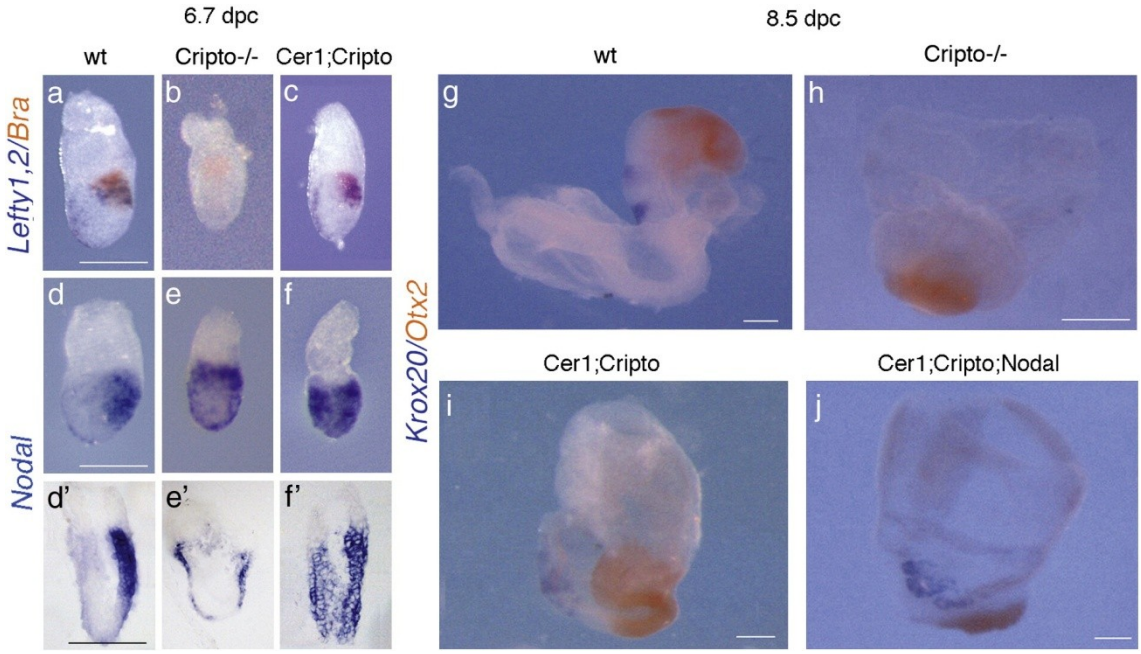

Figure 3.4 - The rescue observed in Cer1;Cripto ouble mutants is due to a recovery of Nodal signaling.

Molecular analysis by double whole-mount in situ hybridization (WISH) of 6.7 dpc (a–f) and 8.5 dpc (g–j) wild-type (wt) (a, d, g), *cripto−/−* (b, e, h), *cer1;cripto* (c, f, i) and *cer1;cripto;Nodal* embryos (j). After hybridization with Nodal probe wt (d′), *cripto−/−* (e′) and *cer1;cripto* (f′) embryos were sectioned. All the sections are sagital. (a–c) In the wt embryo *brachyury* (red) is expressed in the PS, while *lefty1* is detected in the AVE and *lefty2* in the PS (both genes in blue) (a). *cripto−/−* embryos lack expression of Lefty genes (b), while *cer1;cripto* embryos show rescue of the expression and the localization of both *lefty1* and *lefty2* (c). (d–f and d′–f′) *Nodal* is expressed in the AVE and in the posterior epiblast of the wt embryo (d, d′) and is detected in the VE and only in a proximal ring of epiblast cells of the *cripto−/−* embryos (e, e′). *cer1;cripto* double mutants express *Nodal* in almost the entire epiblast (f–f′). (g–k) Double WISH for *krox20* (blue) and Otx2 (red) in wt (g), *cripto−/−* (h), *cer1;cripto* double mutant (i) and *cer1;cripto;Nodal* triple mutant embryos (j). Reduction of *Nodal* gene dosage impairs the amount of rescue in *cer1;cripto* double mutants. Scale bars represent 300 μm.

These data indicate that the c*erl1;cripto;Nodal* triple mutants have a more defective phenotype than the *cerl1;cripto* double mutants. Thus, the reduction of Nodal dosage counteracts the phenotypic rescue found in the double mutants, clearly indicating that Nodal signaling plays a crucial role during the embryonic development of *cerl1;cripto* mutants. Collectively, our data point to the ability of Nodal to signal in the absence of Cripto to mediate both the orientation of the A-P axis and most gastrulation processes.

3.3.4 *cryptic* and *alk7* expression profiles argue against a compensatory role of these factors in *cerl1;cripto* embryos

We also investigated the expression of two other genes involved in the Nodal pathway: *cryptic*, the second EGF-CFC gene present in mouse (Shen, et al. 1997), and *alk7*, the only known Nodal receptor whose activity is diminished but not abolished in the absence of Cripto (Reissman, et al. 2001). However, *cryptic* as well as *alk7* null mutants do not show embryonic lethality and A-P defects (Yan, et al. 1999, Jornvall, et al. 2004).

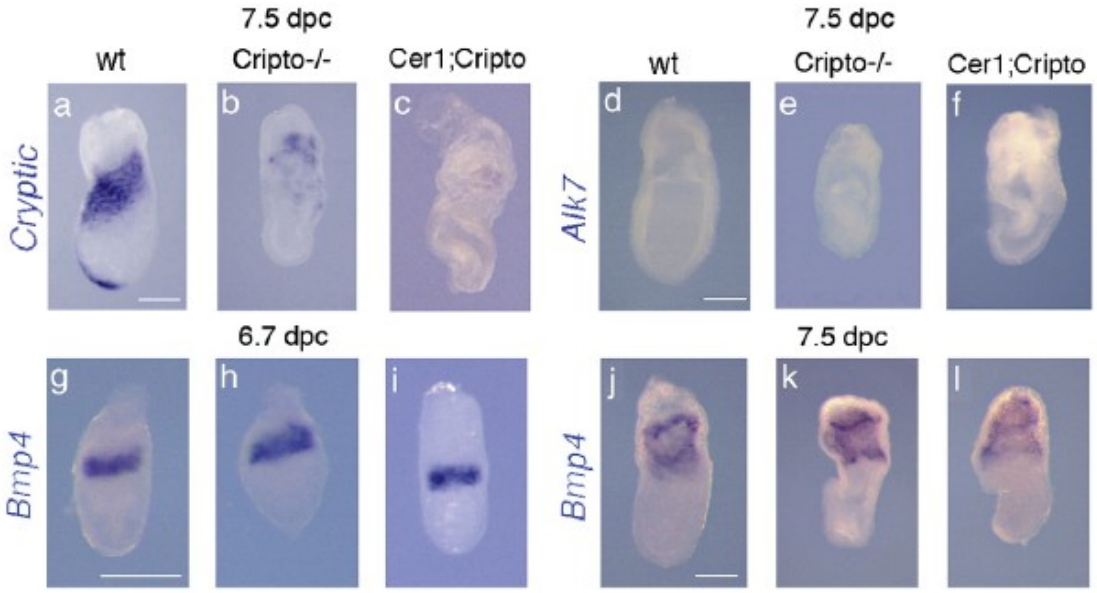

Figure 3.5 Expression profiles of others genes involved the in Nodal pathway.
(a–c) *cryptic* expression in the anterior and lateral mesoderm of the wt embryo (a), in the defective mesoderm close to the extraembryonic region of *Cripto-/-* (b) and *Cer1;Cripto* mutants (c). (d–f) Alk7 expression is not detect either in wt (d), *Cripto-/-* (e) and *Cer1;Cripto* (f) embryos. (g–l) Expression of Bmp4 at both 6.7 (g–i) and 7.5 dpc (j–l). At 6.7 dpc, Bmp4 is expressed in the extraembryonic ectoderm immediately adjacent to the epiblast of wt embryo (g), as well as in both Cripto null (h) and *Cer1;Cripto* double (i) mutants. At 7.5 dpc, *Bmp4* is also expressed in the extraembryonic mesoderm, without any significant difference among wt, *Cripto-/-* and *Cer1;cri* embryos (j–l). Scale bars represent 300 μm.

In the wt embryo, *cryptic* is expressed in the anterior and lateral mesoderm (Fig 3.5a). In *cripto*$^{-/-}$ mutants, due to gastrulation failure, the mesoderm does not migrate and is not correctly specified; however it is possible to detect the expression of *cryptic* in this defective mesoderm, localized close to the extraembryonic region (n=6) (Fig

3.5b). In *cerl1;cripto* double mutants, *cryptic* expression is even more reduced (n=4) (Fig 3.5c). In addition, we could not detect any signal for *alk7,* either in wt, *cripto*$^{-/-}$ (n=4) or *cerl1;cripto* (n=5) embryos (Fig 3.4d-f). Thus, neither *cryptic* nor *alk7* expression appear significantly upregulated in the double mutants relative to the *cripto*$^{-/-}$ embryos, in a manner that might compensate for the lack of Cripto. Finally, since Cerl1 is also a Bmp4 inhibitor, we have analyzed by WISH the expression of *bmp4* at both 6.7 (Fig 3.5g-i) and 7.5 dpc (Fig 3.5j-l). At both stages, we could not detect any difference in *Bmp4* expression among wt, *cripto*$^{-/-}$ (n=9) and *cerl1;cripto* (n=8) mutants.

These data suggest first that the Bmp4 pathway is not directly implicated in *cerl1;cripto* recovery and second that extraembryonic ectoderm (which is fundamental to restrict AVE induction to the distal tip and to initiate its migration anteriorwards; Rodriguez et al., 2005) is specified normally in the *cerl1;cripto* double mutants.

Another factor that could be involved in the signaling activity responsible for the rescue is the TGF-β factor Gdf1. It has been recently described that Gdf1 and Nodal interact during mouse development and that these signals are preferentially transduced through ALK4 and not ALK7 (Andersson, et al. 2006). In our *cerl1;cripto* double mutant model, Gdf1 is unlikely to compensate for Nodal in the initial A-P axis positioning since it was shown to be expressed only after 7.0 dpc. *gdf1* null mutants undergo normal gastrulation (Rankin, et al. 2000) and Gdf1 cooperates with Nodal in midline development but not for A-P axis positioning (Andersson, et al. 2006). Another recently identified member of the TGF-β superfamily, *gdf3,* is expressed during early development, and is essential for AVE induction and A-P axis positioning (Chen and Shen, 2004, Levine and Brivanlou 2006). However, its signaling activity was shown to be Cripto-dependent, being unlikely to compensate for the lack of Nodal signaling in the *Cripto*$^{-/-}$ animals and therefore, in our own experiments (Chen, et al. 2006, Levine and Brivanlou 2006). Nevertheless we cannot discard the involvement of additional signaling molecules, possibly novel TGF-β related signals that may also cooperate with Nodal during early development.

3.3.5 Cripto-independent Nodal signaling guides positioning of the A-P axis

Regional differences in signaling are instrumental in directing the movement of visceral endoderm cells (Tam, et al. 2006). Nodal signaling and the regionalization of its antagonists are required for normal migration of the prospective AVE from the distal tip of the embryo to the anterior side (Yamamoto, et al. 2004). Whereas Nodal activity provides the driving force for AVE migration by stimulating the proliferation of visceral endoderm cells, the antagonists Cerl1 and Lefty1 determine the direction of migration by asymmetric inhibition of Nodal activity on the future anterior (Yamamoto, Saijoh, et al. 2004).

The loss of only one of the two inhibitors does not affect AVE migration and gastrulation, while the inhibition of both *cerl1* and *lefty1* genes causes marked expansion of *Hex* expression domain in the AVE, delayed migration of AVE cells and also formation of multiple primitive streaks (Belo, et al. 2000, Meno, et al. 1998, Perea-Gomez, et al. 2002, Yamamoto, et al. 2004). These data indicate functional redundancy between *cerl1* and *lefty1* in the formation of the A-P axis (Perea-Gomez, et al. 2002, Yamamoto, et al. 2004). Here we report that in the *cerl1;cripto* double mutants, AVE migration to the prospective anterior is significantly rescued compared to the *cripto* single mutants.

In agreement with the model proposed by Yamamoto and coworkers (2004), we find that *cerl1;cripto* double mutants, in contrast to *cripto-/-* embryos, recover Nodal signaling and express *lefty1* gene in the AVE. This suggests that the asymmetry in Nodal activity required for AVE migration is achieved in the *cerl1;cripto* double mutants. Canonical Wnt signaling and its antagonist also regulate A-P axis polarization (Kimura-Yoshida, et al. 2005). Wnt3 and Dkk function as repulsive and attractive guidance cues, respectively, in the migration of visceral endoderm cells (Kimura-Yoshida, et al. 2005).

Recent data on the crosstalk between Nodal and Wnt pathways suggest that *wnt3* is induced by Nodal in a Cripto-independent manner (Ben-Haim, et al. 2006). In agreement with these data, the *cripto* single mutants still express *cnt3*, even though its expression is fainter than in wt embryo and stays as a ring in the proximal region of the embryo. Concomitantly, *dkk* expression, which marks the AVE, has been detected in the distal visceral endoderm of *cripto*$^{-/-}$ embryos. By contrast, *cerl1;cripto* double mutants

show *wnt3* expression shifted towards the posterior of the embryo and *dkk* expression towards the anterior, even though *wnt3* expression remains as weak as in the *cripto* single mutants, These data indicate that both *cripto*$^{-/-}$ and *cerl1;cripto* mutants show an asymmetric distribution of Wnt3 ligand and its antagonist Dkk. However, in the double mutants at 6.7 dpc, this asymmetry is more oriented along the A-P axis. This is not accompanied by an increase in *wnt3* expression with respect to *cripto* single mutants, suggesting that Wnt3 signaling is not the driving force responsible for axial rotation in the *cerl1;cripto* double mutants.

3.3.6 Cripto-independent Nodal signaling is inhibited by Cerl1

Although Cripto has been presented as an essential coreceptor for Nodal signaling, the mouse *cripto* null mutation does not precisely phenocopy the *Nodal* loss of function, being instead less severe (Brennan, et al. 2001, Conlon, et al. 1994, Ding, et al. 1998, Liguori, et al. 2003). These data indicate that, in the mouse embryo, Nodal signals through both Cripto-dependent and independent pathways. Recent data have highlighted an early role of Nodal activity in specifying embryonic visceral endoderm and elongating the egg cylinder, before inducing prospective AVE and germ layer formation (Mesnard, et al. 2006). On the other side, we report that in the mouse embryo Cripto-independent Nodal signaling is able to orient the A-P axis properly and to form both anterior mesendoderm and posterior neuroectoderm. Our data, together with that of Mesnard and coworkers (2006) strengthen the difference between Nodal and Cripto requirements in the mouse embryo and put in evidence an increasing amount of Nodal functions that do not absolutely require Cripto.

Moreover, our data suggest that removal of Cerl1 is able to activate Cripto-independent Nodal signaling. We hypothesize that two different Nodal pathways are active in the early mouse embryo: one that is Cripto-dependent and the other that is Cripto-independent, the latter remaining active until *cerl1* expression.

Our hypothesis provides an adequate explanation for the phenotype of both *cripto* single mutants and *cerl1;cripto* double mutants. In fact, in the *cripto* null mutants, the prospective AVE forms and expresses *cerl1,* but then fails to move anteriorwards. The initial specification of the AVE would thus be due to Cripto-independent Nodal signaling. Subsequently, when Cerl1 starts to be expressed, it inhibits the Cripto-

independent pathway; the resulting absence of a Nodal signaling affects both the anterior AVE movement and gastrulation. In the *cerl1;cripto* mutants, the Cripto-dependent pathway is severely compromised, just as in the *Cripto* single mutants. However, as a consequence of *cerl1* reduction or loss-of-function, the Cripto-independent pathway remains active and is able to mediate not only AVE formation as in the *cripto* single mutants, but also the complete positioning of the A-P axis as well as formation of the mesendoderm.

It is tempting to speculate on how Cerl1 might affect the Cripto-independent Nodal pathway. Ben Haim et al (2006) have recently generated a mouse model producing a mutant Nodal precursor that is resistant to cleavage and processing but which apparently can still signal. One possibility is thus that Cerl1 might antagonize such a Nodal precursor, either by directly blocking its activity or by altering its stability and/or diffusion; loss of Cerl1 activity would thus lead to an increase in Nodal precursor signaling. However, at 6.5 dpc, *cerl1* is not expressed in mutants defective in Nodal processing (Ben-Haim, et al. 2006), making this model an unlikely explanation for the phenotypic rescue observed in the *cerl1;cripto* double mutants.

In conclusion, our data suggest the existence of Cripto-independent signaling mechanisms, by which Nodal controls axis specification and initiates gastrulation in the early mouse embryo. These mechanisms are inhibited by Cerl1. In principle, Cerl1 could antagonize Nodal protein by two (nonexclusive) mechanisms: by blocking Nodal ligand directly and decreasing Nodal signaling activity or by acting on specific components of the Cripto-independent pathway. Interestingly, a dual role as Nodal antagonist has also been described for Lefty (Chen and Shen 2004). Such scenarios in which different antagonists act on different players in Nodal signaling pathways point to additional levels of complexity within the Nodal regulatory network.

4. **Results II -** Comparative Expression of Mouse and Chicken Shisa Homologues During Early Development

Comparative Expression of Mouse and Chicken Shisa Homologues During Early Development

Mário Filipe[1†], Lisa Gonçalves[1,2†], Margaret Bento[1,2†], Ana Cristina Silva[1,2] and José António Belo[1,2]

[1]Instituto Gulbenkian de Ciência, Oeiras, Portugal

[2]Centro de Biomedicina Molecular e Estrutural, Universidade do Algarve, Campus de Gambelas, Faro, Portugal

[†]Drs. Filipe, Gonçalves, and Bento contributed equally to this work.

Published in Developmental Dynamics, (2006) 235:2567–2573.

4.1 ABSTRACT

During vertebrate embryogenesis, fibroblast growth factor (FGF) and Wnt signaling have been implicated in diverse cellular processes, including cell growth, differentiation, and tissue patterning. The recently identified *Xenopus* Shisa protein promotes head formation by inhibiting Wnt and FGF signaling through its interaction with the immature forms of Frizzled and FGF receptors in the endoplasmic reticulum, which prevents their posttranslational maturation. Here, we describe the mouse and chicken homologues of *Xenopus* Shisa. The mouse and chicken Shisa proteins share, respectively, 33.6% and 33.8% identity with the *Xenopus* homolog. In situ hybridization analysis shows that mouse *shisa* is expressed throughout embryonic development, predominantly in the anterior visceral endoderm, headfolds, somites, forebrain, optic vesicle, and limb buds. Cross-species comparison shows that the expression pattern of *cshisa* closely mirrors that of *mshisa*. Our observations indicate that the Shisa family genes are typically expressed in tissues known to require the modulation of Wnt and FGF signaling.

4.2 INTRODUCTION

The establishment of the anteroposterior (AP) axis in vertebrates has been postulated to be under the control of two distinct head and trunk organizing centers (Spemann 1931, Mangold 1933). In mammals, the head-inducing activity is thought to reside in the anterior visceral endoderm (AVE) and later in the axial mesendoderm, whereas trunk-inducing and patterning activities reside in the more posterior primitive streak/node (Belo, et al. 1997, Beddington and Robertson 1999, Bouwmeester and Leyns 1997).

The AVE is an extraembryonic tissue required for early anterior neural specification in the mouse embryo (Thomas and Beddington 1996). The AVE is induced at the distal tip of the 5.5 days postcoitum (dpc) embryo and then migrates to the prospective anterior side, where it imparts anterior identity upon the underlying epiblast (Rivera-Perez, et al. 2003, Yamamoto, et al. 2004, Srinivas 2004, Rodriguez 2005).

Signaling molecules play crucial roles in developmental events, and their actions are highly regulated by endogenous modulators and antagonists to obtain precisely

balanced outputs. The process of neural AP patterning involves the integration of various signals such as retinoic acid (RA), fibroblast growth factors (FGF), and members of the Wnt family. The combined inhibition of bone morphogenetic protein-4 (BMP4), Nodal, and Wnt8 signaling has been demonstrated to be necessary for the specification of anterior neural tissues (Glinka, et al. 1997, Piccolo, et al. 1999, Silva, et al. 2003). Several secreted antagonists of the BMP, Nodal, and Wnt pathways, such as *cerl*, *lefty1*, and *dkk1*, are expressed in the mouse AVE underlying the prospective anterior neuroectoderm (Belo, et al. 1997, Glinka, et al. 1998, Oulad-Abdelghani, et al. 1998). Likewise, the acknowledged topological and functional equivalent of the AVE in chick, the hypoblast, also expresses Nodal, BMP, and Wnt antagonists, such as *caronte*, *dkk1*, and *crescent* (Pfeffer, et al. 1997, Rodríguez Esteban, et al. 1999, Foley, et al. 2000).

Development of the vertebrate limb bud involves a series of cell and axis specification and patterning processes directed by specialized structures such as the zone of polarizing activity (ZPA), the apical ectodermal ridge (AER), and the nonridge ectoderm. The organizing and patterning activities of these regions are mediated by specific genes that have been shown to be regulated by a complex network of transforming growth factor-beta (TGF-β), BMP, FGF, and Wnt signaling pathways (Capdevila and Izpisúa Belmonte 2001). FGFs expressed in the AER, such as FGF2, 4, and 8, promote the proliferation of the mesenchymal limb bud cells in the progress zone and are absolutely required for limb outgrowth. *wnt3A*, initially expressed in the limb surface ectoderm and subsequently restricted to the AER cells, plays an essential role in controlling the induction of the AER. Another Wnt factor, *wnt7A*, is expressed in the dorsal ectoderm and is involved in the specification of dorsal identities in the limb. FGFs also have been shown to oppose TGF-β induced chondrogenesis, and this inhibition is necessary to keep the proliferating mesenchymal cells of the progress zone in an undifferentiated state and maintain limb outgrowth. A strong argument can be made, therefore, for the important role that modulation mechanisms for such signaling pathways must play in the positioning and outgrowth of the limbs.

Metameric organization of the vertebrate body plan is established by somitogenesis, a process by which the paraxial mesoderm becomes segmented into somites, which later will give rise to the vertebrae, skeletal muscles, and part of the dermis (reviewed in Pourquie, 2001). Wnt and FGF signaling pathways are key elements in almost all steps

of this process. Correct specification of paraxial mesoderm, a prerequisite event for somitogenesis, is dependent on Wnt and FGF patterning signals (Deng, et al. 1994, Yoshikawa, et al. 1997, Sun, et al. 1999). The precise spatial and temporal formation of somites relies on the concerted action of two major mechanistic components: the segmentation clock, a molecular oscillator that drives the cyclic expression of a set of genes, setting the periodicity of somite formation; and the determination front, a dynamic morphogen gradient that confers positional responsiveness of the presomitic mesoderm (PSM) cells to the clock signals, thereby defining the segmentation boundaries (Pourquié 2004, Dubrulle and Pourquié 2004, Aulehla and Herrmann 2004). Progression of the determination front involves the establishment of a caudorostral gradient of FGF8/Wnt3A activities along the PSM (Dubrulle, et al. 2001, Aulehla, et al. 2003, Dubrulle and Pourquie 2004).

Furthermore, evidence suggests that the oscillations in notch signaling, which controls the expression of cyclic genes linked to the segmentation clock, are dependent on Wnt3A in the posterior PSM (Aulehla, et al. 2003). The formed somites undergo a maturation process in response to signals emerging from surrounding structures, which leads to the differentiation of three compartments: the sclerotome, the myotome, and the dermatome. The sclerotome gives rise to the vertebrae and ribs and forms from a ventromedial epithelium that has acquired mesenchymal character. The dorsolateral epithelium that remains forms a cap, the dermomyotome, gives rise to the dermatome, from which the dorsal skin dermis originates, and to the myotome, which will form skeletal muscle. Instructive Wnt and FGF signals, among others, are responsible for the specification of the different cell fates in the somite. Particularly, Wnt signaling from the dorsal neural tube and adjacent ectoderm (Stern and Hauschka 1995, Wagner, et al. 2000) and FGFs from the somite itself (Crossley and Martin 1995, Grass, et al. 1996, Pirskanen, et al. 2000) have an important role in the specification and maintenance of myogenic fates.

A recently described *Xenopus* protein termed Shisa, was shown to promote head formation through the inhibition of both Wnt and FGF signaling pathways by a novel ER retention mechanism (Yamamoto, et al. 2005). Secreted antagonists that competitively bind to caudalizing and ventralizing factors (Piccolo, et al. 1996, Piccolo, et al. 1999, Zimmerman, De Jesús-Escobar and Harland 1996) or to their receptors preventing ligand binding (Mao, et al. 2001), play a major role in the head-inducing

activity of the organizer. However, It does so by physically interacting with the immature forms of the Wnt and FGF receptors within the ER and preventing their posttranslational modification and trafficking to the cell surface (Yamamoto, et al. 2005).

Here, we report the identification of the mouse and chicken homologues of *Xenopus* Shisa. We present a detailed description of the expression patterns of *mshisa* and *cshisa* during mouse and chick development and compare them with *Xshisa* expression in *Xenopus*.

4.3 RESULTS AND DISCUSSION

4.3.1 Cloning and Sequence Analysis of Mouse and Chicken *shisa*

To gain further insight into the molecular mechanisms involved in the early steps of forebrain specification, we have carried out a screening for differentially expressed genes in the mouse AVE (Filipe et al., unpublished results). Briefly, a transgenic mouse line was generated in which enhanced green fluorescent protein (EGFP) is expressed in the AVE, under the control of the promoter region of the *cerl* gene (TgN(Cerl-GFP)328Belo; Mesnard et al., 2004). In this transgenic line, the AP axis reorientation could be followed, by the fluorescently labeled AVE cells, even before gastrulation. Gene expression profiling using GeneChips (Affymetrix) identified several new transcripts expressed in the AVE at the very early stages of AP axis establishment.

One of the novel genes identified in this screening and provisory named MAd2 (Mouse Anterodistally expressed gene 2, probe set ID 1423852_at), was found to display a particularly interesting dynamic expression pattern that warranted a more detailed analysis. A BLAST search (Altschul et al., 1990) of the *Xenopus laevis* expressed sequence tag (EST) database using the MAd2 sequence as query, returned a potential homolog, which was reported recently by Yamamoto et al. (2005) as *shisa*. In view of this finding, the MAd2 gene was henceforth designated as mouse *shisa* (GenBank accession no. DQ342342). The EST clone BC057640, obtained from RZPD (IMAGp998G149268Q3), was sequenced and found to contain the entire putative coding sequence (CDS) of *mshisa* as well as 5' and 3' untranslated regions (UTRs). This putative CDS consists of an 888-bp open reading frame (ORF) that encodes a

predicted 295-amino acid protein with a calculated molecular weight of 31.6 kDa, whose sequence is identical to that reported by Yamamoto et al. (2005) for the mouse Shisa homolog.

The cDNA sequence of *mshisa* was then used to Blast the *Gallus gallus* sequence databases for potential homologs. This search led to the identification of two mRNAs (GenBank accession no. NM_204501, AF257354) and three EST clones (GenBank accession no. DR424805, BU205915, BM488505). An 855-bp ORF from the AF257354 RNA was identified as the putative *cshisa* CDS, which encodes for a 284-amino acid protein with a predicted molecular weight of 29.9 kDa. The *cshisa* cDNA sequence was then assembled in silico from the retrieved sequences and submitted to GenBank with the accession no. DQ342343.

Sequence comparison of the Shisa homologs reveals two highly conserved cysteine-rich domains (CRD; Fig. 4.1). The three proteins are also relatively well conserved over their entire sequence, with the murine and chicken Shisa showing, respectively, 33.6% and 33.8% overall identity and 49.5% and 49.2% overall similarity to the *Xenopus* protein. The Shisa proteins of the two amniote vertebrates are even more closely related to each other, sharing 81% identity and 85.8% similarity.

The gene structure of the mouse and chicken *shisa* was deduced from cDNA-genomic alignments and by using the Genscan gene prediction program (http://genes.mit.edu/GENSCAN. html; Burge and Karlin, 1997). The mouse *shisa* gene is composed of two exons, each containing one of the CRDs and separated by a 3,234-bp phase 1 intron, inserted between the first and second base of the codon for the first valine in the conserved sequence VPIYVPFLIV. An identical two-exon gene structure was reported for two other mammalian homologs, the rat and human *shisa* (Katoh and Katoh, 2005). Despite the still preliminary nature of the first draft of the chicken genome assembly, which did not allow the unequivocal determination of the exon structure of the *cshisa* gene, it was nevertheless possible to identify a 1,140-bp intron placed at the exactly same position as the mouse *shisa* intron. Another evidence supporting the homology of the murine and chicken *shisa* comes from the chromosomal location of these two genes, which map to syntenic regions in the mouse chromosome 14C3 and chicken chromosome 1, as annotated in the Ensembl genome databases (v.37 - Feb2006; http://www.ensembl. org/; Birney et al., 2006).

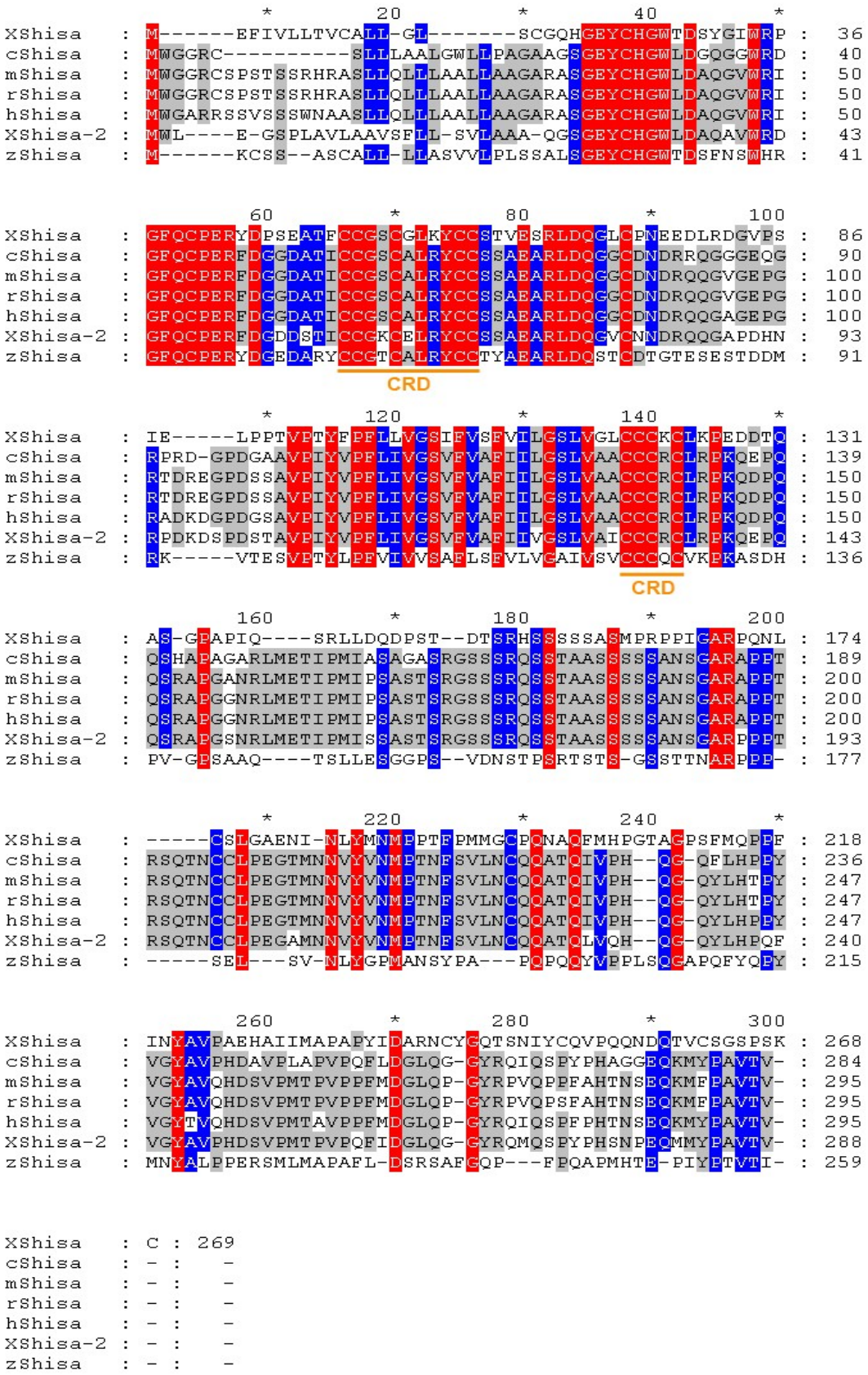

Figure 4.1 - Sequence alignment of XShisa, cShisa, mShisa, rShisa, hShisa, and zShisa.

Predicted amino acid sequences of cysteine-rich domains are underlined in orange. Identical amino acids among all are shaded red, whereas identical amino acids in only two sequences are shaded blue.

4.3.2 Expression of *mshisa* During Mouse Development

In situ hybridization analysis was used to examine the expression of *mshisa* transcripts during mouse embryogenesis. The expression of *mshisa* can be seen as early as 5.5 dpc and continues throughout embryonic development (Fig. 4.2).

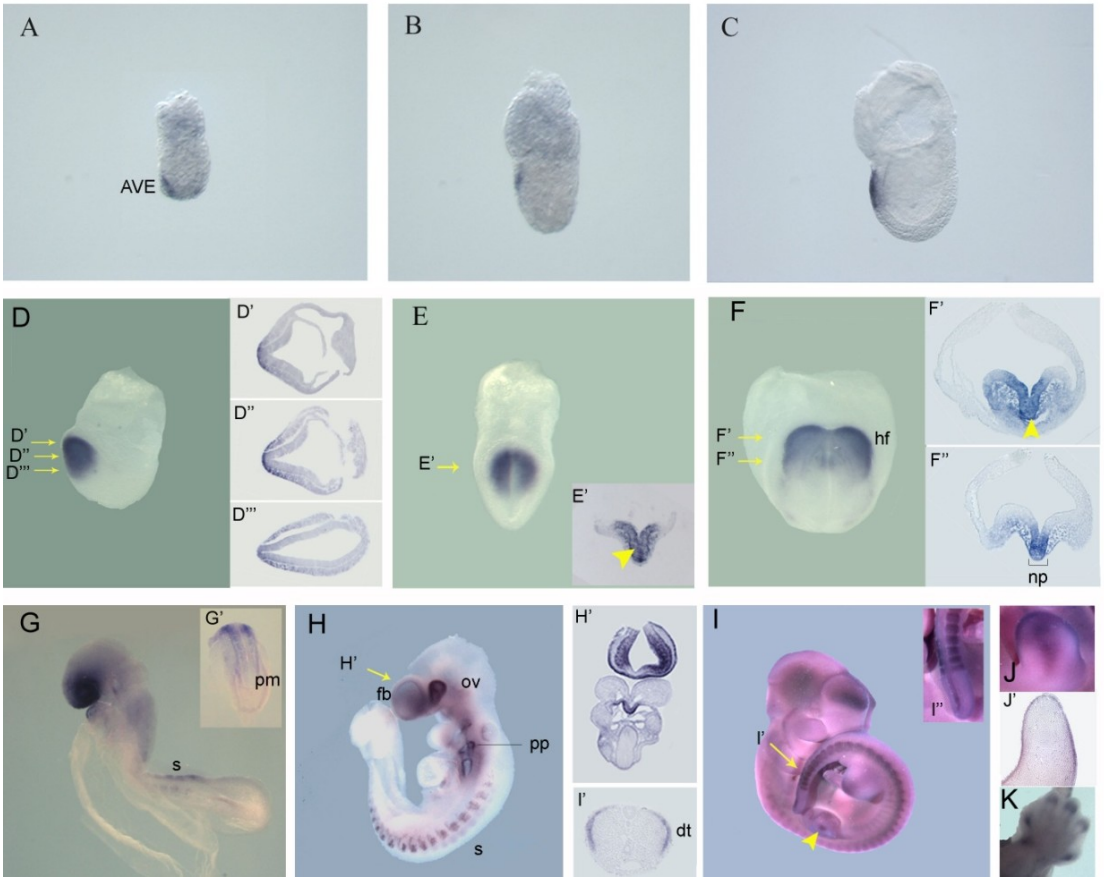

Figure 4.2 - *In situ* hybridization analysis of mshisa expression during mouse development.
All sections are 8-µm. The level at which each section was taken is indicated on panels with yellow arrows and the sections are shown next to the relevant panels. A, B, C: *mshisa* is expressed in the AVE in E5.5, E6.5 and E7.0 mouse embryo. D: At E7.25 mshisa is detected in the prospective head fold. D', D'', D''': Transverse sections of an E7.25 embryo show that *mshisa* is only expressed in the anterior definitive endoderm and subjacent cranial mesoderm. E: In an E7.5 embryo, *mshisa* is expressed in the head folds. E': Transverse section of E7.5 embryo shows that *mshisa* is also induced in the anterior neural plate. F: In an E8.0 embryo mshisa is expressed in the head folds. F', F'': Transverse sections show *mshisa* is present in the cephalic mesenchyme, in the presumptive forebrain neuroectoderm, in the endoderm lining the foregut pocket and in the rostral end of the notochordal plate. G, G': At E8.5 *mshisa* transcripts are expressed in the prospective eye, forebrain and somites. H: At E9.0 *mshisa* is expressed in the eye, in the forebrain, somites and branchial arches. H': Transverse section of E9.0 embryo shows expression of mshisa in the surface ectoderm and in the ventral endoderm of the foregut and immediately adjacent mesenchyme. I: At E11.5 transcripts of mshisa are expressed in the dorsal telencephalon, in the eye, in the somites and limb buds. I': Transverse section of the tail at E11.5 shows *mshisa* in the somite is restricted

to the dermomyotome. I'': Amplification of the tail shows that *mshisa* is absent from the presomitic mesoderm. J: Amplification of the limb bud at E11.5 shows *mshisa* expression. J': Sagital section of the limb bud at E11.5 shows that *mshisa* expression is restricted to the surface ectoderm. K: Amplification of the limb at 13.5 shows *mshisa* is detected in the tip of the forming digits. AVE, anterior visceral endoderm; ba, branchial arches; dt, dermatome; fb, forebrain; hf, head fold; ov, otic vesicle; np, notochord plate; pm, presomitic mesoderm; s, somite.

At pre- to early streak stages, *mshisa* is specifically expressed in the AVE as it migrates to the anterior side (Fig. 4.2A–C). By late streak stage, expression is found in a patch of anterior definitive endoderm (ADE) cells that has replaced the AVE (Fig. 4.2D).

In early allantoic bud embryos (Fig. 4.2E), around embryonic day (E) 7.25– E7.5, *mshisa* transcripts can only be detected in the ADE and subjacent cranial mesoderm (Fig. 4.2E'–E''), while by early headfold stage, *mshisa* is also induced in the anterior neural plate (Fig. 4.2F'). Up to this point, *mshisa* expression seems to be excluded from the midline axial mesendoderm (Fig. 4.2F). As the embryo reaches stage E8.0, *mshisa* is expressed in the cephalic mesenchyme and presumptive forebrain neuroectoderm (Fig. 4.2G–G''). Expression is also present in the endoderm lining the foregut pocket and in the rostral end of the notochordal plate (Fig. 4.2G'').

By E8.5, *mshisa* expression marks the prospective eye and forebrain regions (Fig. 4.2H–H''). Expression of *mshisa* is maintained in the optic vesicles of E9.0–E9.5 embryos (Fig. 4.2I–I', J), and the same is true for the expression in the forebrain, which can be more precisely located to the surface ectoderm and neuroepithelium of the prosencephalic vesicle (Fig. 4.2J'). Other expression domains found at this stage include the pharyngeal pouches (Fig. 4.2J), the lateral region of the invaginating otic pit (Fig. 4.2H'',I'), and the ventral endoderm of the foregut and immediately adjacent mesenchyme (Fig. 4.2J'). Later in development, *mshisa* expression in the forebrain appears to become progressively confined to the dorsal telencephalon (Fig. 4.2K).

With the onset of somitogenesis, *mshisa* starts to be expressed in the forming somites, but is apparently absent from the presomitic mesoderm (Fig. 4.2H–K). Somitic expression of *mshisa* is restricted to the dorsolateral part that constitutes the dermomyotome (Fig. 4.2I'',K'). This expression pattern persists through later stages, albeit gradually decreasing to lower levels in older somites (Fig. 4.2H–K).

Expression of *mshisa* in the developing limb buds can first be seen in a proximal domain (arrowhead, Fig. 4.2K) that subsequently shifts toward the distal tip as the bud grows (Fig. 4.2L). The expression in the limb bud is restricted to the ectoderm, as shown in Figure 4.2L'. At E13.5, *mshisa* expression can still be detected in the tip of the forming digits (Fig. 4.2M), in the region undergoing chondrogenesis.

4.3.3 Expression of *cshisa* During Chick Development

Embryos from prestreak to mid-limb stages of development (Hamburger and Hamilton, 1951) were examined by in situ hybridization (Fig. 4.3). Our observations reveal that the expression pattern of *cshisa* is very similar to that of its murine counterpart.

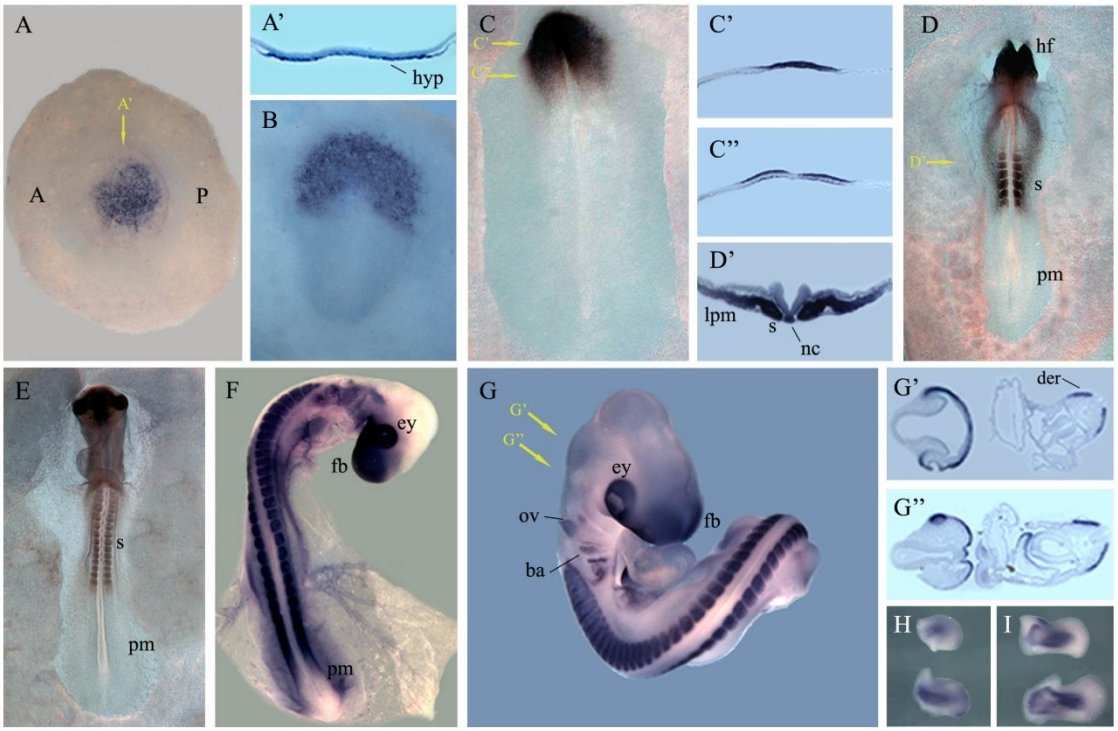

Figure 4.3 - Localization of cshisa transcripts in developing chicken embryos detected by *in situ* hybridization.

A,D and E are ventral views while B and C are dorsal views of whole-mount embryos. All sections are transverse 16-µm cryossections. The level at which each section was taken is indicated on panels with yellow arrows and the sections are shown next to the relevant panels. A: *cshisa* is expressed in the hypoblast in stage HH1 chicken embryo. Anterior is to the left. A': Transverse section of a HH1 chicken

embryo show *cshisa* expression exclusively in the hypoblast. B: *cshisa* transcripts are expressed in the prospective neural plate at HH4. C: At HH6, *cshisa* expression appears restricted to the neural plate and primitive folds. C',C'': Transverse sections a HH6 embryo show that *cshisa* transcripts are locate in the ectodermal cells. D: In stage HH9-, *cshisa* is expressed in the head folds and the somites. There is an absence of *cshisa* transcripts within the presomitic mesoderm of the embryo. D': Section taken at the level of the somites shows *cshisa* expression within the somite and in the lateral plate mesoderm. The notochord is also positive for *cshisa* expression. E: At HH11, *cshisa* transcripts are observed in the forming brain, prospective eye and at the somite level. In the somites *cshisa* expression is strongest in the recently formed somites. F: By stage HH18, *cshisa* can be detected in the forebrain, eye, otic vesicle, branchial arches, somites and the developing limb buds. G: *cshisa* expression in HH25 remains in the otic vesicle, forebrain, branchial arches, eye, somites and limb buds. G',G'': Transverse sections show that *cshisa* transcripts in the somite are restricted to the dermatome. H,I: *cshisa* expression in the early limb buds (H, stage HH22; I, stage HH25) has a very dynamic pattern. *cshisa* starts to be expressed more posteriorly and then migrates towards more distal region. Forelimbs are shown in the top and hindlimbs in the bottom. ba, branchial arches; dt, dermatome; ey, eye; fb, forebrain; hf, head fold; hyp, hypoblast; lpm, lateral plate mesoderm; ov, otic vesicle; nc, notochord; np, neural plate; pm, presomitic mesoderm; s, somite.

At prestreak stages (Hamburger and Hamilton stage 1, HH1), *cshisa* transcripts were strongly detected in the hypoblast (Fig. 4.3A,A'). As gastrulation begins and the primitive streak is formed, *cshisa* expression becomes restricted to the anterior part of the embryo, more specifically to the endodermal layer (stage HH3 ; Fig. 4.3B,B',B''). By stage HH5 (Fig. 4.3C), *cshisa* is expressed in the prospective neural plate tissue. Transverse sections showed that *cshisa* transcripts are still present in the endodermal layer and also start to be expressed in mesodermal cells (Fig. 4.3C',C'',C'''). This expression pattern is consistent with the observation that *Xshisa* is essential for vertebrate head formation (Yamamoto et al., 2005). At stage HH6, *cshisa* mRNA is present in high levels in the head folds and neural plate region (Fig. 4.3D). Transverse sections show that *cshisa* transcripts are localized to the ectodermal cells (Fig. 4.3D',D'').

With the beginning of somitogenesis, *cshisa* starts also to be expressed in the somitic territories. At stage HH7, *cshisa* can be detected in the first forming somite (not shown). By stage HH9^{-} *cshisa* is strongly expressed in the head folds and in the developing somites (Fig. 4.3E). A dynamic expression pattern is observed throughout somitogenesis (Fig. 4.3E–H). *cshisa* transcripts are absent from the posterior region of

the presomitic mesoderm but can be detected at low levels at its rostral end. The expression is strongest in the newly formed somites and gradually decreases as the somites mature. A transverse section at the somite level of a stage HH7 embryo shows that *cshisa* is expressed in the entire somite as well as in the lateral plate mesoderm and notochord (Fig. 4.3E'). Later in development, *cshisa* transcripts are also present in the prospective eye, forebrain, branchial arches, and otic vesicle (Fig. 4.3F–H). As the optic vesicles evaginate, expression is seen in the lens vesicle and anterior surface ectoderm of the frontonasal mass (Fig 4.3H–H''). At stage HH25, *cshisa* expression in the somite is restricted to the dermomyotome (Fig. 4.3H',H''), resembling that of *mshisa* (Fig. 4.2K').

During early limb bud stages, *cshisa* starts to be detected in the more proximal region of the limb buds (not shown) and later, as limbs develop, the expression shifts toward the distal region (Fig. 4.3I,J). This expression pattern in the limb buds resembles the one observed for *MyoD*, a marker of differentiating myogenic cells (Gamer et al., 2001; Fig. 4.3I,J).

As demonstrated above, the murine and chicken *shisa* are very closely related to each other both in terms of their sequence similarity and the evolutionarily conserved expression pattern. The early expression of *mshisa* and *cshisa* in the AVE/hypoblast and anterior neuroectoderm also recapitulates the deep endomesoderm and prospective head ectoderm expression previously described for the *Xenopus shisa*, the founding member of this gene family (Yamamoto et al., 2005). Mouse and chicken *shisa*, however, additionally are expressed in structures such as the somites, pharyngeal region. and the eye.

Being members of the *Xshisa* family, an antagonist of Wnt and FGF signaling (Yamamoto et al., 2005), the conserved expression patterns of both *mshisa* and *cshisa* reflect the importance they may have during embryonic development of the mouse and chick embryos, patterning topologically equivalent regions in these vertebrate embryos.

Assuming, based on their homology with the *Xenopus* protein, that the mouse and chicken Shisa also function as antagonists of Wnt and FGF signaling, then their expression in the AVE and hypoblast may seem, at a first glance, hard to conciliate with the role attributed to these tissues in early neural induction. In fact, recent findings strongly suggest that, at least in chicken, FGF and Wnt signaling are required for neural induction at a very early stage, even before gastrulation. However, it should be taken

into consideration that Shisa acts cell-autonomously; therefore, its expression in the AVE/hypoblast is unlikely to inhibit FGF signaling in the overlying epiblast. Shisa might instead play an indirect role in promoting neural induction by participating in the specification and/or maintenance of the AVE/hypoblast identities, for example through repression of the autocrine action of FGF-8, which is expressed in the AVE (Crossley and Martin, 1995). Later on, Shisa is expressed in the neural plate, and it's plausible then that, like in *Xenopus*, it inhibits the caudalizing Wnt and FGF signals in this tissue. A similar reasoning can be applied to the function of Shisa in the developing limb buds, where Wnt and FGF signaling is known to direct outgrowth and patterning. *shisa* is expressed in the ectoderm layer of the limbs, where most of the Wnt and FGF signaling centers are also located. Again it is conceivable that Shisa is not antagonizing these signaling pathways in the target mesenchymal cells but is instead acting on some of the signaling centers, perhaps protecting them from their own signals. During somitogenesis Shisa might be involved in the process of somite differentiation and condensation through the inhibition the FGF signaling coming from the posterior presomitic mesoderm. Subsequently expression in the dorsolateral compartment of the somite suggests that Shisa could be repressing the FGF and Wnt-mediated myogenic signals in these cells, which as a result will be specified as dermatome. These considerations are purely hypothetical, however, and a more conclusive characterization of the biological function of the mouse and chicken Shisa in embryonic development will require further biochemical and genetic analyses.

5. **Results III -** Functional analysis of the role of the novel gene *mADTK1* during mouse development

Functional analysis of the role of the novel gene *mADTK1* during mouse development

Lisa Gonçalves[1,2], Mário Filipe[2], Moises Mallo[2] and José António Belo[1,2]

[1] IBB-Institute for Biotechnology and Bioengineering, CBME, Universidade do Algarve, Campus de Gambelas, 8005-139 Faro, Portugal;

[2] Instituto Gulbenkian de Ciência, 2781-901 Oeiras, Portugal

Manuscript in preparation (2009)

5.1 ABSTRACT

The AVE plays an essential role during mouse development. Recently in the lab, a differential screening identified several novel genes expressed in the AVE.

One of these genes, ADTK1, encodes for a novel protein with tyrosine and serine/threonine kinase domains. Phosphorylation of different substrates plays important roles switching on and off signaling pathways through embryogenesis. Interestingly, little is known about their role in the AVE.

The human ADTK1 homologue shares 92% identity with mouse. As for the *Xenopus* and chicken, there are two orthologs for each species. XADTK1 share respectively 60 and 42% identity with mADTK1. As for cADTK1, the orthologs share 37 and 28% identity. Preliminary data from work using the *Xenopus* and chick orthologs suggest that this gene may be involved in neural crest migration, neural tube closure, heart formation and development of the eye.

Besides its expression in the AVE, ADTK1 has a singular expression pattern during organogenesis. Although it is in current investigation, its expression pattern suggests that this gene might require the modulation of Wnt, BMP, Shh and FGF signaling, as it is typically expressed in tissues where these signaling pathways are active.

In order to evaluate *ADTK1* biological function, a targeted inactivation was performed. Defects were detected in the eye and ear of some mutants. Skeletal analysis performed in 30 % of *ADTK1* mutants showed defects in bone length, presenting shorter limbs than the wild-type. All *ADTK1* mutant newborn mice analyzed, presented defects in kidney development, kidneys were larger and had a reddish color, comparing to wild-type littermates. Furthermore, medullar region seems to be affected, presenting less glomerular structures that usual, and thus suggesting ADTK1 plays a potential role in kidney development. The process of kidney development is a complex one, not yet fully understood, although many players have been identified, it is not yet completely clear how the different molecules and signaling pathways interact.

Even though, no major conclusions were possible, altogether, these results suggest that ADTK1 is a protein kinase involved in the regulation of more than one signaling pathways, probably Wnt, Shh and BMP.

5.2 INTRODUCTION

The role played by the Anterior Visceral Endoderm (AVE) in the determination of the antero-posterior (A-P) axis and primary induction of the rostral neuroectoderm, has been described (Dufort, et al. 1998, Kimura, et al. 2001, Perea-Gomez, et al. 2001, Shawlot, et al. 1999, Tam and Steiner 1999).

Signaling molecules and transcription factors that play key roles in developmental events, such as induction and patterning of anterior neural tissues, are present in the AVE (Itasaki, et al. 2003, Thomas and Beddington 1996). However, the relative roles of these cascades, the degree to which they are used at any particular axial level and how they are integrated in organizing normal A-P patterning are still poorly understood (Glinka, et al. 1997). In order to understand better these processes, a differential screening has been made in our lab, and several novel genes with expression in the AVE were identified. A novel gene that encodes for a protein with tyrosine kinase and serine/threonine kinase domains, was identified among other genes. This gene was denominated *ADTK1* (Anterior Distal Tyrosine Kinase).

It is widely known that phosphorylation of substrates is essential for regulating biochemical pathways, for instance by activating transcription factors and targeting products for degradation, thus switching on and off different pathways. Proteins with these domains are known to play essential roles through embryonic development, in different pathways: from the Nodal pathway to Wnt signaling (Jones, et al. 2001). For instance, tyrosine kinases often encode for receptors. Receptor tyrosine kinases (RTK) have been shown to be key regulators of normal cellular processes and consequently have a critical role in the development. There are about twenty different classes of RTKs; among them are the EGF, Fibroblast Growth Factors (FGF) and Trk receptor families (Vasiliauskas and Stern 2004).

As for serine/threonine kinases, it has been shown that during early development they have an important role in cell cycle. For instance, the mitogen-activated protein (MAP) kinase signaling cascade is activated by phosphorylation of tyrosine and threonine residues. Once activated, MAP kinases translocate into the nucleus where they phosphorylate several substrates such as DNA-binding proteins and other protein kinases (Haraguchi, et. al 1998, Kassel, et al. 2001).

During development, there are several critical phases that account for a number of birth defects. For instance, failure in neurulation leads to one of most common birth defects. Throughout the process in which the neural plate bends and fuses, giving rise to the neural tube, several different molecules are involved, such as Wnts, FGFs, Sonic hedgehog (Shh), Noggin, Bone Morphogenetic Protein (BMP) family and BMP related molecules (Ybot-Gonzalez, et al. 2007, C. Stern 2005, C. Stern 2006, Kibar, et al. 2007). Particularly, in the case of FGF, it activates the MAPK cascade, which results in the phosphorylation of a crucial linker region of the BMP effector Smad1, which acts as an inhibitor of the BMP pathway.

The combination of Shh and BMPs are essential for the neural tube to close correctly. In the early phase of neurulation, *Shh* is strongly expressed in the notochord, inhibiting *noggin* expression (Shum and Copp 1996). Downregulation of noggin, a BMP signaling antagonist, causes *bmp2* expression to remain high, preventing the tube to close. As Shh levels diminish, *noggin* starts to be expressed, downregulating *bmp2* and causing the neural tube to close (Ybot-Gonzalez, et al. 2007, Stottmann, et al. 2006). However, there probably exists redundant activity with other genes, as in *noggin* null mutants the neural tube closes temporarily, reopening later during development (Stottmann, et al. 2006).

Along with neurulation, also cardiac defects are common birth defects. Congenital heart disease represents the most common birth defects with a rate of about 1 in 100 live births (Hoffman 1995). During early stages of heart development, BMPs and FGFs act as potent inducers of cardiac differentiation, whereas members of the canonical Wnt signaling pathway block cardiac differentiation (Foley, et. al 2000, Foley, et al. 2007, Schneider and Mercola 2001). In mice, null mutations for *chordin* and *tbx1* cause septation defects (Bachiller, et al. 2003, Xu and Baldini 2007). It has been shown that cardiogenesis requires correct L-R patterning of the embryo to be established prior to heart formation (reviewed by Hamada, et al. 2002). Moreover, mutants for *cerl-2*, a Nodal antagonist, also present defects at the level of the heart, showing incomplete atrial-ventricular septation, failure of the outflow tract rotation, hypertrophy of the atrium, ventricular septation defects and strikingly, a severe hyperplasia of the myocardium (Marques, et al. 2004, Araújo, et al. unpublished).

The vertebrate limb development is a complex process that involves several axes specification and patterning processes. Structures such as the zone of polarizing activity (ZPA), the apical ectodermal ridge (AER), and the nonridge ectoderm, are essential in limb development. The organizing and patterning activities of these regions are mediated by specific genes that have been shown to be regulated by a complex network of transforming growth factor-beta (TGF-β), BMP, FGF, and Wnt signaling pathways (Capdevila and Izpisúa Belmonte 2001). The organization of the limb in the three different axes requires interrelated and coordinated action of several signaling molecules.

Shh in the ZPA activates the expression of *fgf4* in the AER. Along with *fgf8, fgf4* promotes the proliferation of the mesenchymal limb bud cells in the progress zone, that are absolutely required for limb outgrowth (Capdevila and Izpisúa Belmonte 2001). Additionally, FGFs in the AER are partially responsible for maintaining Shh in the ZPA (Li and Muneoka 1999). FGFs become restricted to the AER as it migrates distally, because Shh in the proximal region induces a FGF inhibitor, Gremlin (Zúñiga, et al. 1999). Therefore, there is a feedback loop where Shh signaling in the ZPA modulates FGF4 signaling in the posterior AER, which in turn maintains the polarizing region.

Wnt signaling is also critical in controlling the induction of the AER Mouse embryos lacking the *Wnt/* β-*catenin* pathway components, *LRP6* or simultaneously *Lef1* and *Tcf1*, exhibit defects in the formation of the AER (Galceran, et al. 1999). Moreover, Wnt-7a is also required for anterior-posterior patterning

Recently, it was reported a novel gene *Pkdcc* (*ADTK1*) involved in limb formation (Imuta, et al. 2009). According to Imuta, et al. (2009), mutants for this gene present shorter limbs than wild-type littermates. It has been suggested that this novel gene is required for the correctly timed differentiation of flat proliferative chondrocytes. These structures give rise to hypertrophic chondrocytes which, later on, will be replaced by bone cells (Kronenberg 2003).

During organogenesis, at E9.5 the process of kidney development starts with the presence of the nephric mesenchyme, in the region contiguous to the hindlimb. (Mugford, et al. 2009). The definitive kidney, also called metanephros, is not fully developed until approximately the third week after birth. Two previous versions of the kidney are considered during development: the first is the mesonephros, a temporary

structure derived from the intermediate plate mesoderm. The other, which precedes the definitive kidney, is the pronephros, a rudimentary transient kidney (reviewed in Kaufman and Bard, 1999). The pronephros starts to be formed when signals from the somites and surface ectoderm, induce the cells in the intermediate mesoderm to form the nephric bud. (Bouchard, et al. 2002). At E10.5, the metanephric mesenchyme induces a single ureteric bud from the nephric duct near the hind limb (Dressler 2006). Afterwards, the ureteric bud elongates and branches within the metanephric mesenchyme, giving rise to the collecting ducts, pelvis, and ureter (Dressler 2006). At the tip of the ureteric bud, local metanephric mesenchyme is stimulated to condense and differentiate into nephron epithelia. Furthermore, regions of stromal mesenchyme also surround the developing nephrons.

Several genes are involved in the complex process of kidney development. *lim1* and *c-ret* typically pattern the urogenital system (Bridgewater, et al. 2008). *fgf7* and *fgf10* null mutants present small kidneys, whereas *fgf2*promotes condensation of the ureteric tubules (Hains, et al. 2008). *eya1, wt1, pax2, six1* and *gdnf* characterize the metanephric mesenchyme, and in each of these mutants, hypotrophy or agenesis of the kidney is observed (Bouchard, et al. 2002, Yu, et al. 2004, Mugford, et al. 2009).

Wnt signaling also plays a role in regulating the kidney development. It has been demonstrated that β-catenin is critical in controlling the hierarchy of genes responsible for the ureteric branching (Bridgewater, et al. 2008). However, although there are already known several players involved in the process of kidney development, it is not yet clear how the different molecules and signaling pathways interact, in order to correctly form this important organ.

5.3 RESULTS AND DISCUSSION

In order to evaluate the biological role of *ADTK1* during embryonic development, a series of experiments were performed.

5.3.1 ADTK1 Sequence Analysis

ADTK1 encodes for a 493 aminoacid (aa) protein with a genomic distribution consisting of seven exons.

Through bioinformatics analysis of mADTK1 using SMART (Simple Modular Architecture Research Tool) program, it was found that it encodes for a kinase with serine, threonine and tyrosine domains. It appears to have a signal peptide and several transmembrane regions. Also, it has a proline-rich region between aminoacids 75 and 128, and an arginine-rich region between aminoacids 49 and 106. These two last features are shared only with its human homologue.

The presence of serine, threonine and tyrosine kinase domains, suggest an important role during embryogenesis. It is possible that this protein may act in signaling pathways such as BMP or Wnt, as they often require tyrosine kinase or serine/threonine kinase activity in order to proceed with signal transduction. Furthermore, it is also known that these pathways are not fully described, being some intermediate players yet to be identified.

When comparing the sequence homology between several species, one can see that the highest homology is between aminoacids 250 and 400, which is where the higher phosphorylation activity probability occurs (Fig 5.1). However, if only the first ortholog for *Xenopus* and chick is considered, the homology is much higher, being almost all the sequence conserved.

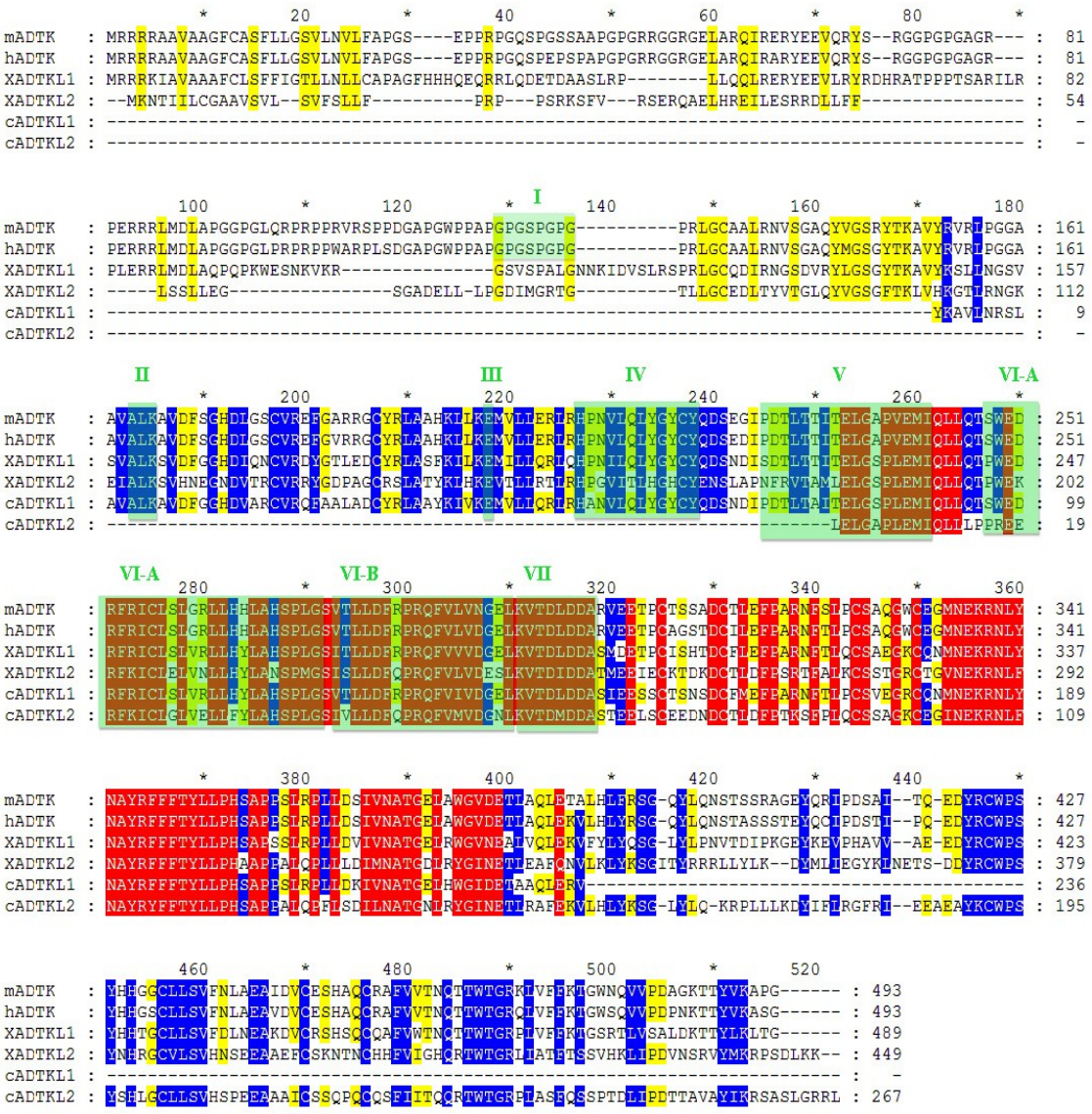

Figure 5.1 - Sequence alignment of: mADTK1, hADTK1, XADTK1-L1, XADTK1-L2, cADTK1-L1 and cADTK1-L2 predicted proteins.

Homologies between the sequences are spotted by shaded amino acids, whereas red shades the highest homology, and yellow the least. m- mouse; h- human; X- *Xenopus*, c- chick. The sequence position and number of the protein kinase subdomains are shaded in green and indicated by roman numerals

Comparison of the different sequences reveal that: mouse ADTK1 shares 92% of identity with human ADTK1, 60 and 42% with Xenopus ADTKL1 and Xenopus ADTKL2, 37% identity with chicken ADTKL1 and 28% identity with chicken ADTKL2 (Fig 5.1, Table 1).

Table 5.1 - Sequence comparison between mADTK1, hADTK1, XADTKL1, XADTKL2, cADTKL1, and cADTKL2

m: mouse, h: human, X: Xenopus, c: chicken. The values shown represent the percentage of homology. The number represent the ratio of homology

	mADTK1	hADTK1	XADTKL1	XADTKL2	cADTKL1
hADTK1	**92**				
XADTKL1	**60**	**62**			
XADTKL2	**42**	**42**	**41**		
cADTKL1	**37**	**37**	**38**	**30**	
cADTKL2	**28**	**29**	**30**	**37**	**29**

It is interesting how mouse ADTK1 sequence resembles the human one, being so different from Xenopus and chick. However, it is important to remember, that both Xenopus and chick have two orthologs for the same gene, and only one gene exists in human and mouse. Moreover, data from the expression pattern of ADTK1 orthologs expression patterns, performed in Xenopus and chick, indicates that overlapping the expression patterns of the two orthologs, it resembles mouse the expression pattern (Bento, Silva and Vitorino, unpublished).

Recently, it has been proposed that *ADTK1* suffers alternative splicing (Imuta, et al. 2009). Part of the coding sequence of the first exon is not transcribed, altering, this way, the first exon into two different exons (Imuta, et al. 2009). Consequently, the new first exon becomes an untranslated (UTR) region. This short ADTK1 version is organized in eight exons, one of them entirely untranslated, and encodes for 293 aa protein (Fig 5.2 B). Curiously, this new protein lacks both proline and arginine-rich regions, that are present in the long version of ADTK1. Using the same program to analyze its sequence, the results differ very much. Whereas the long version is characterized by its serine, threonine, tyrosine kinase activity, this short version looses all characteristic serine threonine, tyrosine domains and is only characterized as a kinase protein. Furthermore, almost all the transmembrane domains predicted for the long version, are absent in the short one, as is the signal peptide.

ADTK1 has ATP-binding and catalytic subdomains which are essential for kinase activity (subdomain I and V, respectively) (Hanks and Hunter 1995), however, the short version of ADTK1 lacks subdomains I, II and III. Therefore, it is probable that only the long version of ADTK1 is functional as a serine/threonine tyrosine kinase.

Preliminary activity assays were performed in our lab, using the *Xenopus* orthologs XADTK1-L1 and XADTK1-L2; however, it wasn't possible to detect any kinase activity using different substrates such as casein, MBP and histones (Silva, et al., unpublished). It is likely that, one of the reasons these experiments didn't work, is due to the fact that, in both *Xenopus* orthologs, the subdomain I is missing. It would be interesting to test whether mouse ADTK1 shows any activity using the same substrates.

In order to verify whether these two forms are co-expressed throughout the embryonic development, RNA was extracted from wild-type embryos at different stages of development, and cDNA was produced. PCRs were performed using several combinations of primers in different exons, with the intention of verifying other potential sites of alternative splicing (Fig 5.2 C).

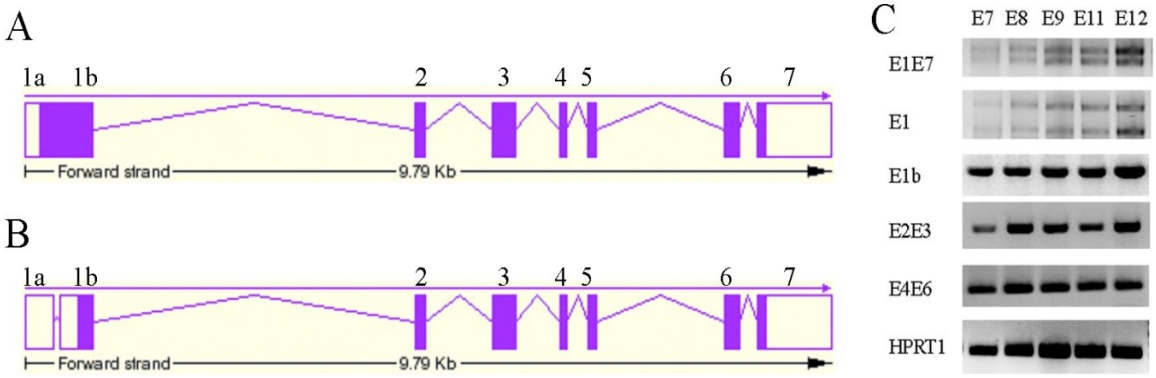

Figure 5.2- Graphic representation of ADTK1

A- Schematic view of the long version of ADTK1 and its exons. B- Schematic view of ADTK short version and ADTK1 exons. C- PCRs with several combinations of primers in the different exons (E1E7- exon1 to exon7; E1- entire exon1; E1b - part b of exon1; E2E3 – exon2 to exon3; E4E6 – exon4 to exon6, HPRT – housekeeping gene) at different stages of embryonic development: E7, E8, E9, E11 and E12.

Analysis of the different PCRs made (Fig 5.2 C), shows that only exon 1 suffers splicing, confirming what had been said before in Imuta et al, 2009. Furthermore, both isoforms are present throughout the embryonic development, and are co-expressed with the same intensity, as no visible differences in the PCRs were observed, using different number of cycles.

Preliminary data from transfection assays, suggest that these two isoforms are not co-localized. Whereas the short isoform seems to be strictly localized inside the cell, possibly membrane bound (Fig 5.3 A), the long isoform seems to be expressed randomly throughout the cytoplasm (Fig 5.3 B). These preliminary data is interesting, as transmembrane domains and a signal peptide was detected in bioinformatics analysis. However, it is known that, sometimes, the predicted transmembrane domains, in fact, correspond to the conformation of the protein itself. Furthermore, the presence of signal peptide has always to be tested, because bioinformatics analysis only gives a probability ratio. As for the potential cytoplasmatic activity, it has to be further tested, because it can also be an artifact of GFP: it is possible that the protein is processed, resulting in GFP cleavage in the cytoplasm, accounting for the homogenous expression.

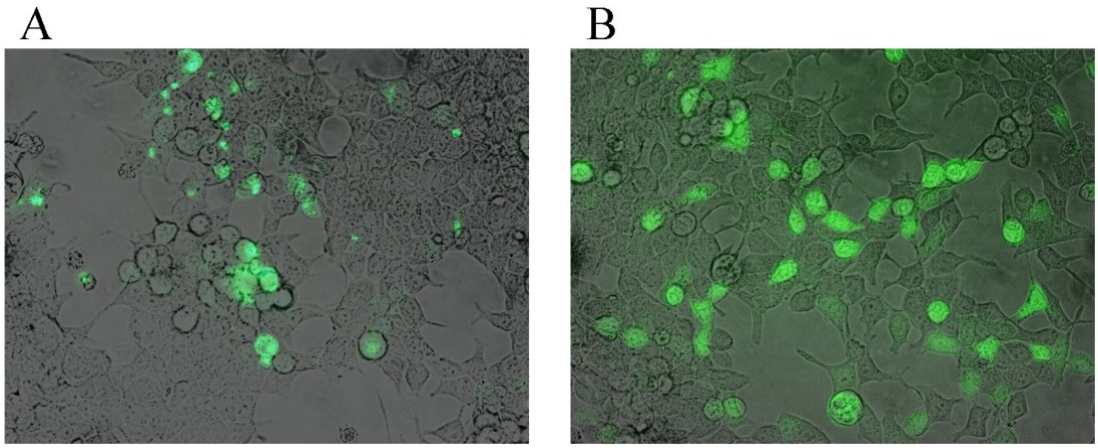

Figure 5.3 - Transfection of ADTK1-GFP protein in HEK 293T cells

A-transfection of ADTK1 short isoform; B- transfection of ADTK1 long isoform.

Cells were tested for autofluorescence, transfecting a non –fluorescent plasmid, and no fluorescence was detected. Thus, it is possible that these two distinct isoforms may have distinct roles during embryonic development. However, these results are not sufficient to take any conclusions, further experiments are necessary.

5.3.2 ADTK1 expression pattern

A set of whole mount *in situ* hybridization analysis was performed in mouse embryos, in several stages of development, so that one could determine the *ADTK1* domains of expression. Later on, embryos were sectioned both sagital and transversely, post *in situ* hybridization, in order to achieve a thorough analysis of its expression pattern.

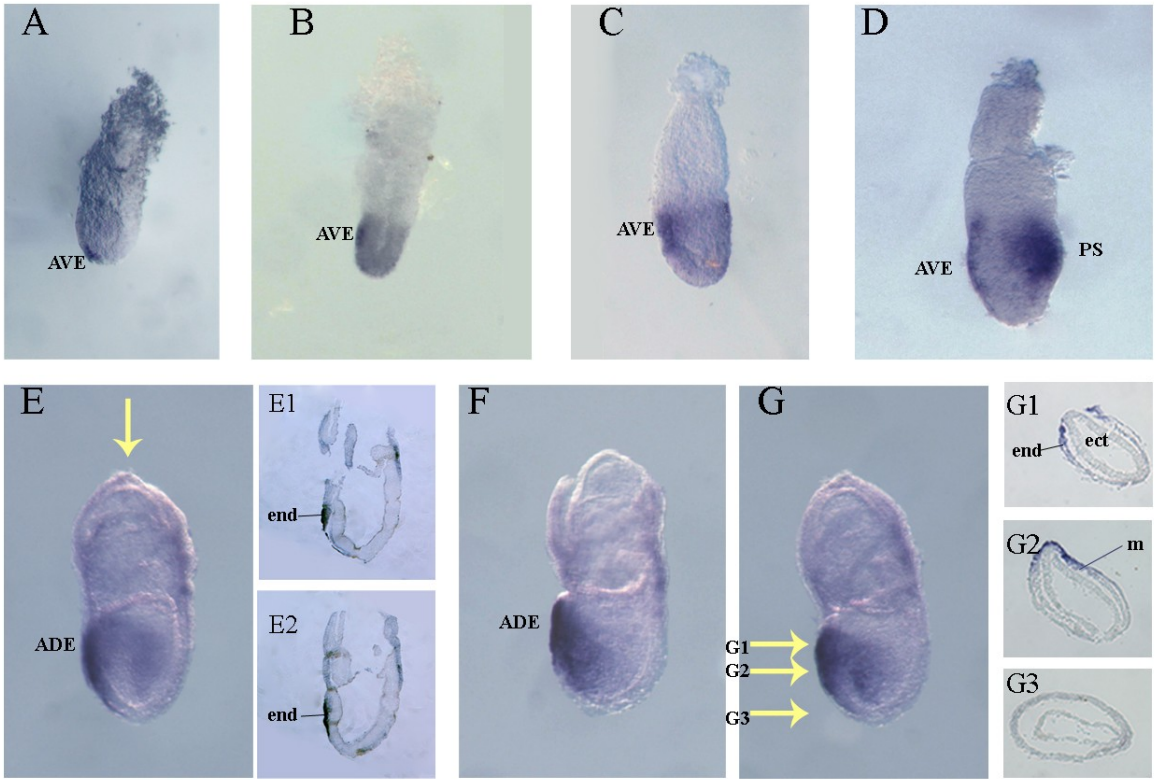

Figure 5.4 - Whole-mount in situ hybridization of ADTK in E5.0–E7.25 wild-type embryos
All sections are 8-µm thick.The level at which each section was taken is indicated on panels with yellow arrows and the sections are shown next to the relevant panels. Left side view of embryos at E5.0 (A); E5.5 (B); E6.0 (C); E6.5 (D); E7.0 (E); E7.25^{-} (F) and E7.25^{+} (G). ADE- anterior definitive endoderm; AVE- anterior visceral endoderm; end- endoderm; ect- ectoderm; m-mesoderm; PS- primitive endoderm.

It is clear that *ADTK1* transcripts are present very early in mouse embryonic development. As early as E5.0, ADTK1 can be detected in the AVE, still very close to the distal tip and it marks the AVE as it migrates anteriorly (Fig 5.1 A, B, C).

During early stages, *ADTK1* is restricted to the endoderm (Fig 5.4 E1, E2), however, at early headfold stage (Fig 5.4 G) *ADTK1* is no longer restricted to the endoderm but it also patterns the anterior region of the mesodermal wings (Fig 5.4 G1, G2).

At early to mid streak stages, *ADTK1* transcripts can be strongly detected, but very transiently in the primitive streak (Fig 5.4 D), and then migrate proximally, towards the extraembryonic region as the streak extends (Fig 5.4 E, E1, F and G). This expression pattern corresponds to the region that will give rise to the heart mesoderm, as well as other tissues, at late streak stage (Tam, et al. 1997). At this stage, as definitive endoderm cells the move anteriorly, the heart mesoderm movement corresponds both spatially and temporally with the movement of the definitive endoderm cells, interestingly, *ADTK1* is present in the definitive endoderm (Fig 5.4 E, F and G). It is possible that, *ADTK1* transient but strong expression in early primitive streak stages, might be necessary for the streak extension or heart mesoderm migration.

As soon as definitive endoderm is formed, *ADTK1* can be detected there (Fig 5.4 D, E, F, G, E1, E2, G1 and G2). Prospective headfolds also show the presence of *ADTK1*, (Fig 5.4F, G) and transverse sections show that, at this stage, *ADTK1* expression is not restricted to the endoderm, but also appears in the mesoderm, being excluded from the ectoderm (Fig 5.4 G1, G2 and G3).

As embryonic development progresses, *ADTK1* transcripts can be detected in the prospective headfolds (Fig 5.5 A) and later in the headfolds (Fig 5.5 B, C, D, E, F, G, and H). Curiously, apart for the transient expression in the primitive streak in early to mid streak stages, *ADTK1* is always restricted to the most anterior part of the embryo. No expression can be detected in the posterior part.

At early headfold stage, sagital sections show that *ADTK1* is present in the endoderm and mesoderm, being absent from the ectoderm (Fig 5.5 C1, C2). Immediately after, transverse and sagital sections show that *ADTK1* transcripts can be detected in the three germ layers (Fig 5.5 D1, D2, E1, F1, E2, and F3).

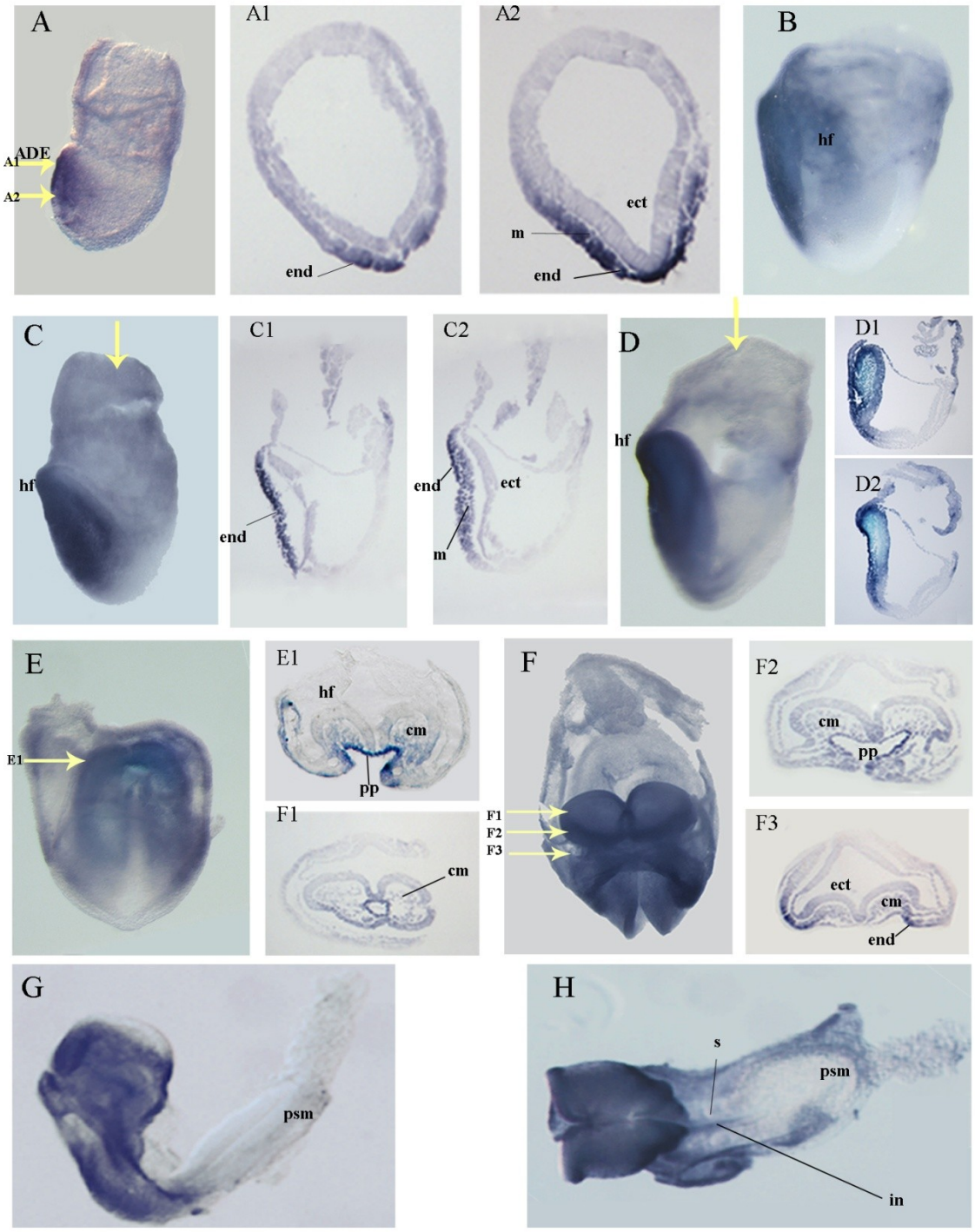

Figure 5.5- Whole-mount i*n situ* hybridization of *ADTK1* in E7.5 to E8.5 wild-type embryos

All sections are 8-µm thick. The level at which each section was taken is indicated on panels with yellow arrows and the sections are shown next to the relevant panels. Left side view of embryos at E7.5 (A), E7.5-7.75 (B-D); E8.0 (E); E8.25 (F); E8.5 (G-H). ADE- anterior definitive endoderm; cm- cephalic mesenchymal cells; end- endoderm; ect- ectoderm; hf- headfolds; in- initial site of neurulation; m- mesoderm; pp- prechordal plate; psm- presomitic mesoderm; s- somite

Furthermore, in early to late headfold stages, *ADTK1* patterns the cephalic mesenchymal cells, prechordal plate, rostral extension of the notochordal plate, and in the endodermal cells lining the junctional zone between the prospective foregut and midgut regions (Fig 5.5 E1, F1, F2 and F3).

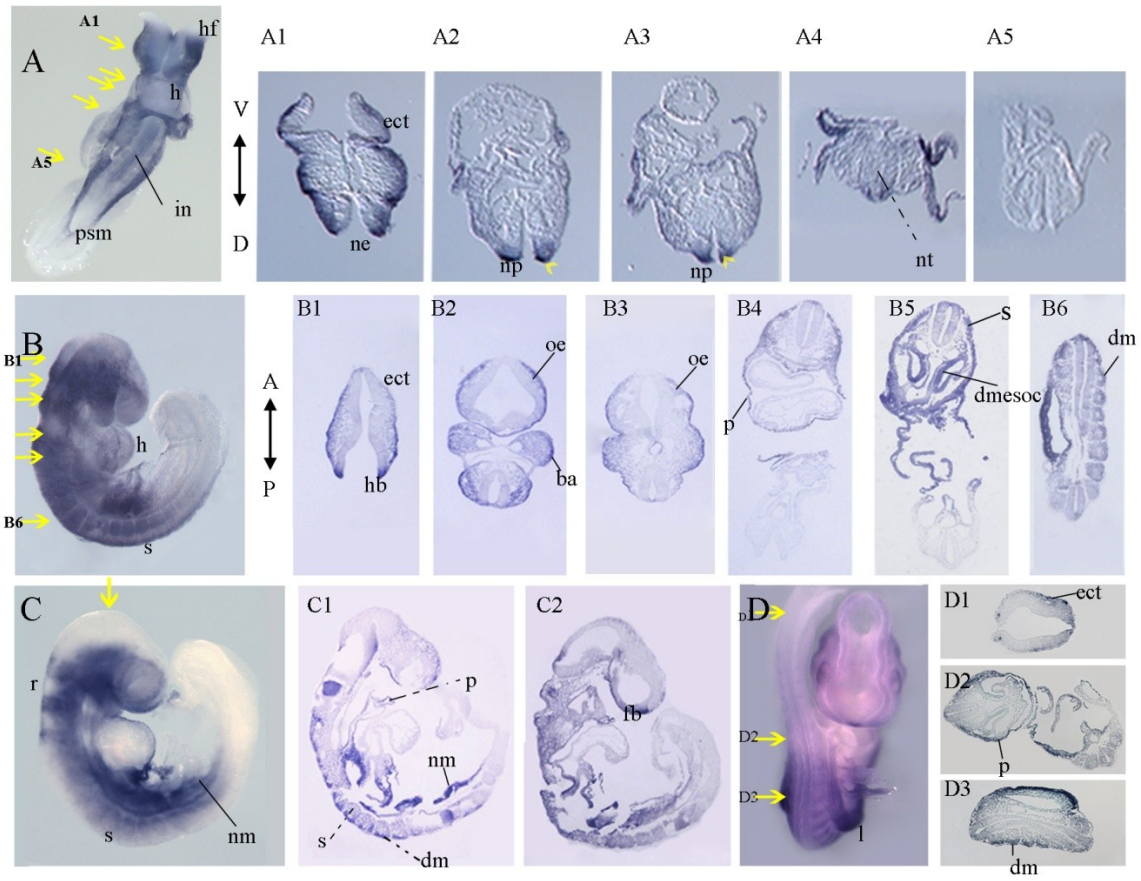

Figure 5.6 – Whole-mount *in situ hybridization* of ADTK1 in E8.75 to E9.5 wild-type embryos

All sections are 8-µm thick. The level at which each section was taken is indicated on panels with yellow arrows and the sections are shown next to the relevant panels. Orientation of the sections of embryos A and B are indicated next to the panels. Ventral view of embryos at E8.75 (A) and E9.5 (D). Right side view of embryos at E9.0 (B); E9.5 (C). ba- branchial arches; dm- dermomyotome; dmesosc- dorsal mesocardium; ect- ectoderm; fb- forebrain; h- heart; hb- hindbrain; hf- headfold; in- initial site of neurulation; l- limb bud; ne- neuroepithelium, nm- nephric mesenchyme; np- neural plate; nt- neural tube; oe- optic eminence; p- pericardium; s- somite. AP- anterior posterior; DV- dorsal ventral.

As the embryo starts the turning, ADTK1 is detected in the headfolds, where it is restricted to the ectoderm and neuroepithelium (Fig 5.6 A, A1), in the somites and at the initial site of neurulation (Fig 5.6 A).

Importantly, between E8.5 and E8.75, *ADTK1* is transiently expressed in the neural ectoderm, in the dorsal tip (Fig 5.6 A2, A3) as well as in the initial site of neurulation (Fig 5.5 H, Fig 5.6 A). This pattern resembles the one of *bmp2* in the same tissue (Ybot-Gonzalez, et al. 2007).

Transverse sections at this stage show that it is present in the most dorsal part of the neural plate (Fig 5.6 A2, A3 and A4). Immediately after turning at E9.0 (Fig 5.6 B) *ADTK1* expression is very strong, being present in the somites, rhombomeres, optic eminence, hindbrain, forebrain and in the pericardium (Fig 5.3 B, B1, B2 and B3) but absent from the heart, midbrain and presomitic mesoderm. As the embryo develops, *ADTK1* transcripts pattern almost all the embryo. Until E9.5, transverse sections show that ADTK1 is present in the most dorsal tip of the neural tube (Fig 5.6 A1, A3, A4, B4, B5, D2).

At E9.5 (Fig 5.6 D, E, F,G) *ADTK1* transcripts are widely present, being always excluded from the presomitic mesoderm, heart and midbrain.

ADTK1 is present in the rhombomeres, the optic eminence (Fig 5.6 C), pharyngeal arches, gut and somites (Fig 5.6 C, D). Both transverse and sagital sections show that *ADTK1* does not pattern all the somite, but only its outer layer, the dermomyotome. It is known that this structure gives rise to the limbs and musculature of the body (reviewed in Buckingham, et al. 2003).

It is widely known the important role played by the AVE during mouse embryogenesis. The results present in figure 5.4, figure 5.5 and figure 5.6 suggest that, as other genes such as *otx2*, *lim1*, *gsc* and *cerl1* (Shawlot, et al. 1999, Perea-Gomez, et al. 2001, Belo, et al. 1998, Belo, et al. 1997), *ADTK1* may be correlated with neural induction and the formation of anterior structures, as *ADTK1* transcripts are detected, and pattern important structures such as the headfolds, prospective forebrain, prospective eye and cephalic mesenchymal cells.

Being present in the optic eminence, as it becomes developed, suggests a potential role in the eye development. Interestingly, *ADTK1* continues to pattern the eye related structures during later development (Fig 5.6 and Fig 5.7).

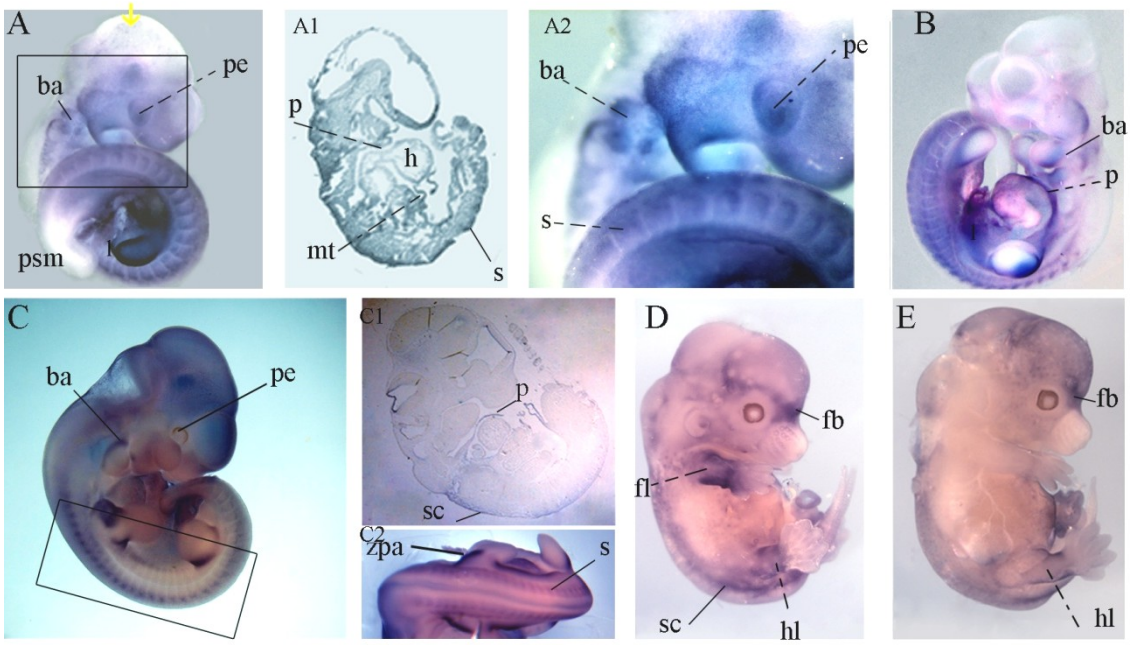

Figure 5.7 - Whole-mount *in situ* hybridization of ADTK1 in E10.5 to E13 wild-type embryos

All sections are 8-µm. The level at which each section was taken is indicated on panels with yellow arrows and the sections are shown next to the relevant panels. Areas of interest are indicated with a black square, magnified and shown next to the relevant panels. Right side view of embryos at E10.5 (A), E11 (C); E12.5 (D); E13.5 (E). Left side view of embryo at E10.5 (B). ba- branchial arches; fb- forebrain; fl- forelimb; h- heart; hb- hindbrain; hf- headfold; hl- hindlimb; l- limb bud; ne- neuroepithelium, mt- ,mesonephric tubules; p- pericardium; pe- prospective eye; psm- presomitic mesoderm; s- somite; sc- spinal chord; zpa- zone of polarizing activity

Consistent with the expression in the dermomyotome, as limb buds start to develop, *ADTK1* can be detected in these structures, being later restricted to the proximal region, including the ZPA (zone of polarizing activity) instead of AER (apical ectodermal ridge) (Fig 5.7A, B, C, C2). This fact suggests that ADTK1 may be playing an antagonistic role for FGFs that are restricted to the AER (Li and Muneoka 1999). Other than playing a direct antagonistic role for FGFs, it might be implicated with Shh activity in the same tissue, activating FGF inhibitor such as *gremlin* (Zúñiga, et al. 1999).

It also interesting that even though *ADTK1* is not present in the heart, it patterns its surrounding membrane, the pericardium (Fig 5.6 B, B4, B5 and C; Fig 5.7 A1, B and C1). It has already been established that pericardium is essential for the correct functioning of the heart, as pericardial pores equilibrate hydrostatic pressures between

the pleural and pericardial cavities and allowing the recruitment of inflammatory cells from the three cavities, the lungs and the heart (Fukuo, et al. 1988). This pattern in the pericardium might be correlated with the initial transient expression in the primitive streak, at early to mid streak stages.

Curiously, at E9.5, *ADTK1* seems to be present in the nephric mesenchyme (Fig 5.6 C, C1 and C2). Later on, sagital sections of embryos at E10.5, show that *ADTK1* transcripts can be detected in the mesonephric tubules (Fig 5.7 A1).

At E11 *ADTK1* expression is still detected in the somites, pharyngeal arches and limbs, but it is clearly starting to diminish, becoming later almost specific for the forebrain, lower limbs (excluding the paws) and spinal chord (Fig 5.7 C, D and I).

Taken together, the thorough analysis of *ADTK1* expression pattern suggests that this gene might play an important role in embryonic processes such as neurulation, head formation, limb and kidney development. Furthermore, the expression in the pericardium implies a possible role in cardiogenesis.

With such a particular expression pattern throughout the different stages of embryonic development, *ADTK1* may play an important role in several processes. Expression of a number of genes in the AVE and initial anterior structures have shown to be important for different crucial steps in development, such as anterior posterior establishment for genes such as *cerl-1*, and *lefty1*, or head formation in case of *otx2, HNF3β* and g*sc* (Shawlot, et al. 1999, Perea-Gomez, et al. 2001, Belo, et al. 1998, Belo, et al. 1997). During mid development stages (Fig 5.5, Fig 5.6), expression in the prechordal and notochordal plates, site of initial neurulation, and most dorsal part of the neural plate, suggest a role in the neural tube closure, possibly in cooperation with genes of the BMP and Wnt signaling pathways. Furthermore, *ADTK1* expression pattern in the neural plate resembles the one of *bmp2* (Ybot-Gonzalez, et al. 2007), which is essential for the correct bending of the neural tube, preventing the tube to close earlier than it should. Moreover, regarding *ADTK1* expression in the neural tube, one can say that it seems to be complementary to the ones described for *Shh* and *HNF3β*: while *Shh* and *HNF3β* (Dufort, et al. 1998, Lei, et al. 2005) pattern the ventral neural tube and notochord, *ADTK1*patterns the neural tube dorsal tip.

A double WISH with *HNF3β* was performed, with the intention of verifying this complementary expression pattern (Fig 5.8).

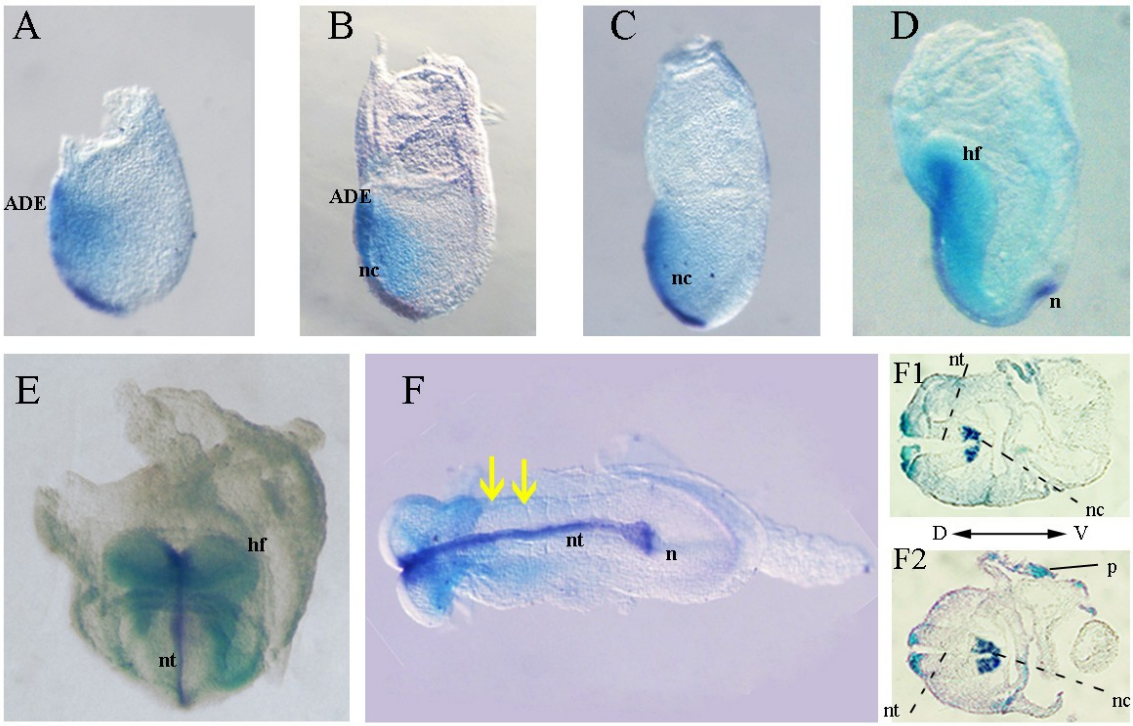

Figure 5.8- Double whole-mount *in situ* hybridization for *HNF3* and *ADTK1* in E6.5 to E8.5 wild-type embryos

ADTK1 expression corresponds to the light blue patterning, whereas *HNF3β* expression corresponds to the dark blue patterning. All sections are 8-µm. The level at which each section was taken is indicated on panels with yellow arrows and the sections are shown next to the relevant panels. Orientation of the sections is indicated next to the panels. Left side view of embryos at E6.5 (A), E7.0 (B), E7.25 (C), E7.5 (D). Ventral view of embryo at E8.0 (E). Dorsal view of embryos at E8.5 (F). ADE- anterior definitive endoderm; hf- headfold; n- node; nc- notochord, nt- neural tube, p- pericardium. DV dorsal ventral.

It is clear that, in early streak stage *ADTK1* and *HNF3β* are not co-localized, while the first patterns the anterior definitive endoderm, the latter patterns the early notochord (Fig 5.8 A). As the notochord extends, both genes pattern the region of the definitive endoderm (Fig 5.8 B and C).

At headfold stage, *HNF3β* transcripts are detected in the notochord, and node, while *ADTK1* expression is expanded in the neural folds (Fig 5.8 D and E). At E8.0, when *ADTK1* patterns the most dorsal tissues of the neural tube, *HNF3β* is expressed in

the complementary region, the ventral part of the neural tube (Fig 5.8 F, F1 and F2). This happens not only in the most anterior part of the neural tube but also in a more posterior region, showing that *ADTK1* expression does not change, as the neural tube closes (Fig 5.8 F2). Interestingly, at this stage, *ADTK1* transcripts are also detected in the body wall overlying the pericardial cavity (Fig 5.8 F1 and F2).

During later stages, *ADTK1* expression in the limb buds is restricted to the most dorsal part of the bud, mimicking the expression of *Shh,* which is also present in the initial ZPA, and is complementary to the expression of *fgf8* which patterns the most ventral region of the limb bud, the AER.

Both these structures act together to promote the correct limb development and growth (Capdevila and Izpisúa Belmonte 2001). The lack of any of this two structures leads to malformation of the limb.

In order to demonstrate these complementary patterns of *ADTK1* and *fgf8*, a double WISH was performed, where it is clear that *fgf8* and *ADTK1* expression patterns are not overlapping in the limb (Fig 5.5 1, B, C). This shows that *ADTK1* is not expressed in the AER, which is characterized by the presence of *fgf8*, but in the limb proximal region and ZPA.

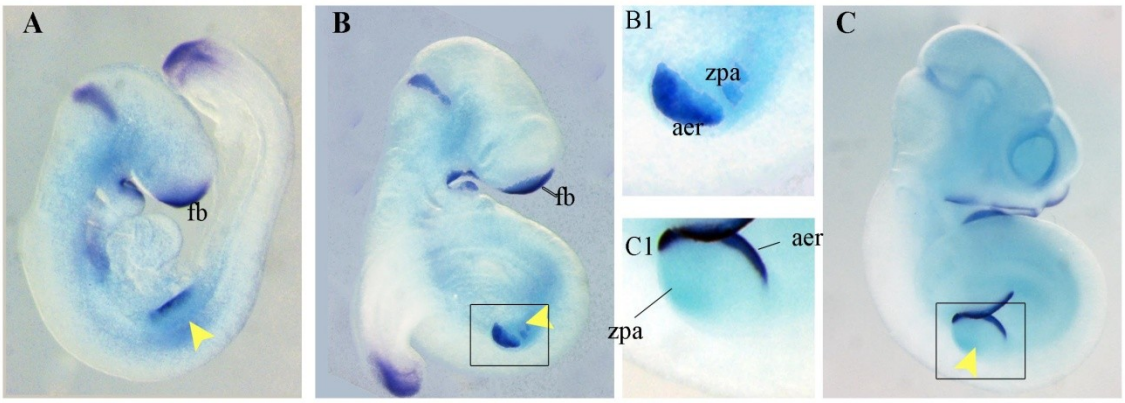

Figure 5.9 – Double whole-mount in situ hybridization for *fgf8* and *ADTK1* in E9.0 to E10.5 wild-type embryos

ADTK1 expression corresponds to the light blue patterning, whereas *fgf8* expression corresponds to the dark blue patterning. Right side view of embryos at E9.0 (A), E9.5 (B), E10.5 (C). Arrowheads indicate the limb buds. Areas of interest are indicated with a black square, magnified and shown next to the relevant panels. aer-anterior ectodermal ridge; fb- forebrain; zpa- zone of polarizing activity.

The expression pattern may or may not be influenced when tested in different mutants, according to the relative position within the different signaling pathways. As we have several different mutants, in order to evaluate in which pathways *ADTK1* might be involved in, it was performed *in situ* hybridization for *ADTK1*, in *cripto*, *Nodal* and *otx2* mutants.

Cripto and Nodal play a major role in establishing the embryonic axes correctly, whereas Otx2 is of great importance for the correct development of anterior structures (Brennan, et al. 2001, Ding, et al. 1998, Perea-Gomez, et al. 2001). As *ADTK1* is expressed in the AVE, a region characterized by the expression of Nodal antagonists, it was enriching information to assess whether *ADTK1* expression pattern was altered in mutants of the Nodal signaling pathway such as *Nodal* itself and *cripto*.

In addition, as seen in figures 5.4, 5.5, 5.6 and 5.7, and discussed above, *ADTK1*, besides being expressed in the AVE, the organizing center for neural structures, it is also expressed in the neural folds and later in the forebrain and hindbrain. For that reason, it was interesting to evaluate *ADTK1* expression pattern in *Otx2* mutants.

In *Otx2* mutants the DVE (distal visceral endoderm) cells do not move to the anterior side, and A-P axis rotation does not take place (Kimura, et al. 2001). *Nodal* mutants lack the primitive streak and most mesoderm (Conlon, et al. 1994), whereas *cripto* mutants lack the primitive streak and additionally fail to migrate the AVE anteriorly, consequently failing to convert the P-D into A-P axis (Ding, et al. 1998).

When analyzing *ADTK1* expression pattern in *cripto, nodal* and *otx2* mutants, the first observation is that *ADTK1* is always expressed, thus the absence of these genes has no effect on *ADTK1* expression. This shows that *ADTK1* is not activated directly by any of these genes. On the other hand, although *ADTK1* expression pattern is altered in all of these mutants, one cannot determine whether *ADTK1* is immediately upstream of *nodal*, *cripto* or *otx2*.

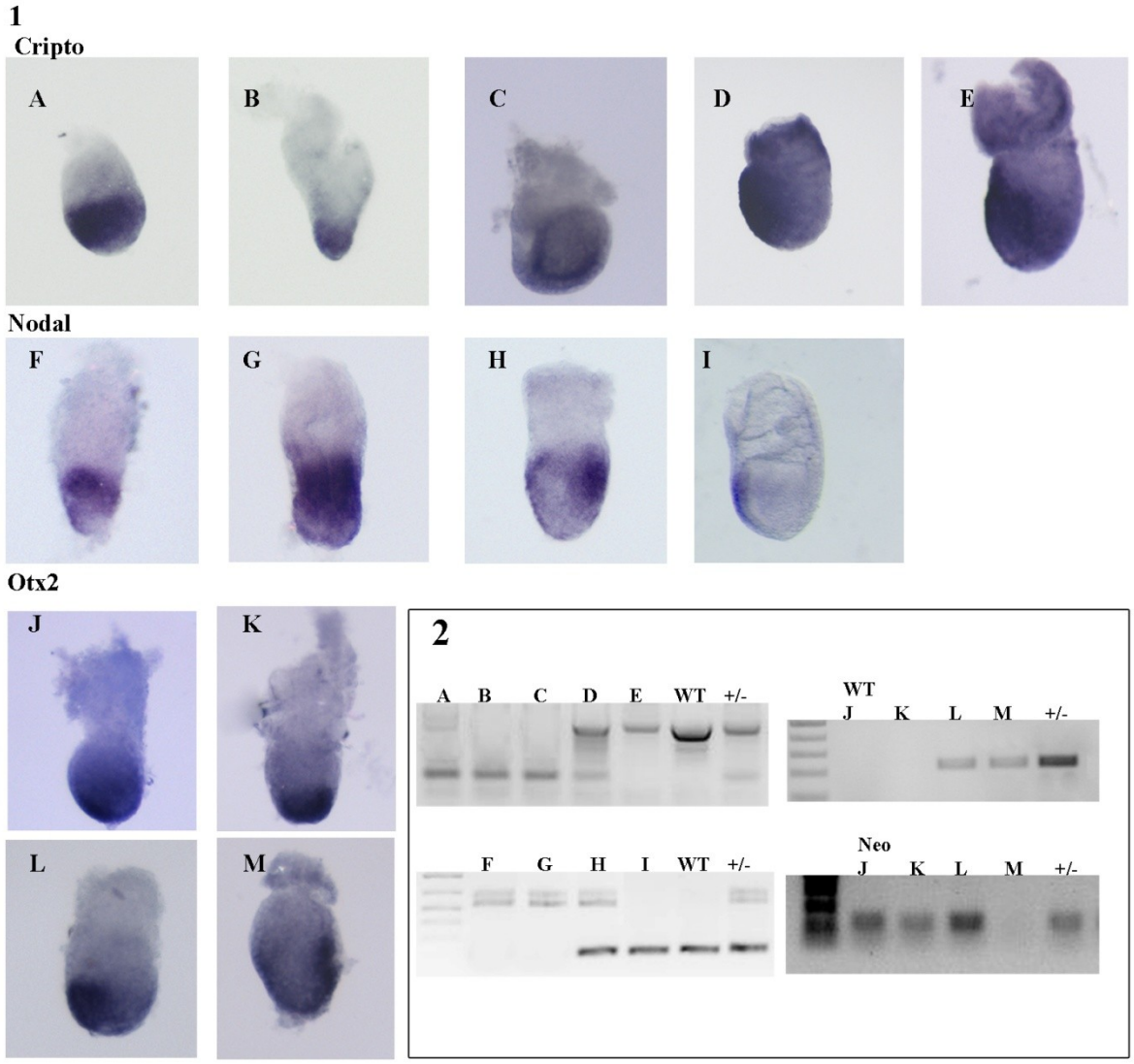

Figure 5.10- Whole-mount *in situ* hybridization of ADTK1 in E6.5 cripto, nodal and otx2 mutant embryos and genotyping

1- Left side view of embryos from Cripto +/- intercrosses (A, B, C, D, E); from Nodal +/- intercrosses (F, G, H, I); and from Otx2 +/- intercrosses (J, K, L, M). 2- Pos- *in situ* embryo genotyping.

These mutant embryos lack important structures as the primitive streak and mesoderm, and fail to correctly establish embryonic axes, thus *ADTK1* expression pattern has to be altered. However as these embryos are during gastrulation process, if *ADTK1* was directly regulating any of these genes, its expression, at this stage, would prevail at the distal tip, consistent with the defects inherent to these mutants.

Nevertheless, only in *ADTK1* mutants one can assess if *ADTK1* is upstream of these genes.

Regarding *cripto* mutants, there seems to be different expression patterns for *ADTK1* in different embryos. *ADTK1* transcripts are detected in almost all the epiblast (Fig 5.10 A); and are also detected at the distal tip of the embryo (Fig 5.10 B), consistent with the failure of VE displacement towards the anterior region; furthermore, *ADTK1* transcripts are also present in a randomized way throughout the epiblast (Fig 5.10 C). Heterozygous embryos do not show any alteration concerning the expression of *ADTK1* (Fig 5.10 D). *Nodal* mutants show differences in *ADTK1* expression pattern which seems to become restricted to a more proximal region (Fig 5.10 F, G). Heterozygous embryos do not show any alteration (Fig 5.10 H). When analyzing the *otx2* null mutants, *ADTK1* becomes restricted to the distal part of the embryo (Fig 5.10 J, K), which is consistent to the fact that these mutants fail to migrate the visceral endoderm anteriorly.

Additionally, analysis of *ADTK1* transcripts in *cripto*, *nodal* and *otx2* mutants, gives the information that *ADTK1* is not directly upstream or being activated by these genes.

5.3.3 ES Cell targeting

To elucidate the biological function of *ADTK1* during development, an *ADTK1* mutant mouse was generated by homologous recombination in ES cells.

In the *ADTK1* targeted allele, exon 1, which includes the transcriptional and translational start sites, and a part of the upstream region and intron 1, was replaced by a PGK neo cassette (Fig 5.11). This mutation eliminates both ADTK1 long and short versions. After ES cell electroporation, and subsequent positive and negative selection with G418 and GANG drugs, respectively, ES cells were cultured in 96 well plates, and their DNA was extracted as described in *Materials and Methods*. Two hundred and forty clones were selected and analyzed for its contents, in order to verify if recombination occurred properly.

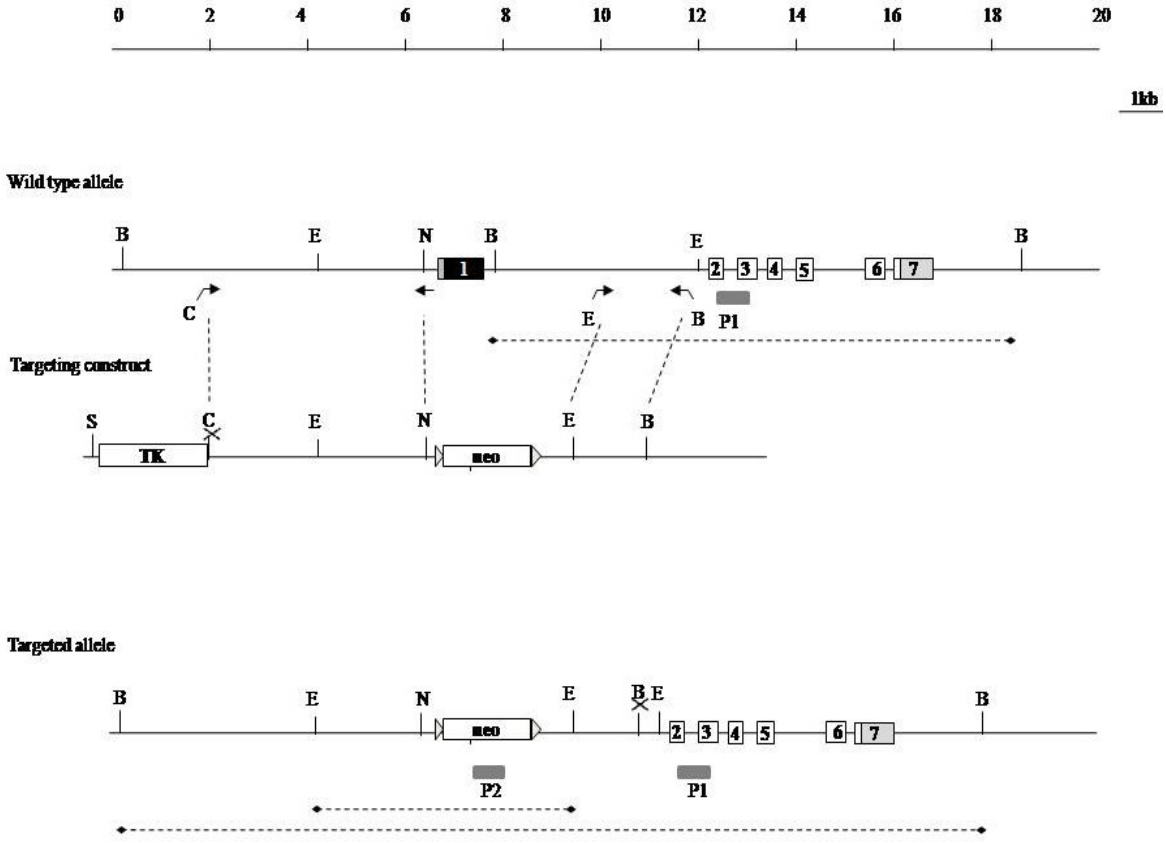

Figure 5.11 - Schematic representation of the targeted deletion of the first exon from *ADTK1* gene
Restriction map of *ADTK1* genomic region, the targeting construct and the recombinant allele. The targeted exon is depicted as a filled box, the remaining exons are depicted as white boxes. UTR regions are depicted in gray. The targeting construct contained a Neo cassette and was flanked by 5' and 3' homology regions. In addition, an HSV-TK cassette was inserted at the end of the 5' arm to allow for negative selection.After BamHI digestion, an external 3' probe and a probe in the neo cassette are used in Southern blot analysis (the targeted allele will give a 17kb band for both probes, as for the wild type allele, it will give a 10.5kb band). The probe that hybridizes in the neo cassette is also used in Southern blot analysis after EcoRV digestion (this originates a 3.6 kb). PCR primers used to amplify the 5' and 3' homology regions are shown as black arrows. B, BamHI; C, Cla I; E, EcoR V; N, Not I; Sal, Sal I; P1, external 3' southern probe; P2, neo cassette internal probe.

If homologous recombination was correct, then the first exon, the targeted exon, was deleted and with it a series of restriction sites were absent. Furthermore, besides deleting the first exon of *ADTK1*, it was replaced with a neo cassette, that carried a

different set of restriction sites (Fig 5.11). This made it possible to identify correct homologous recombination by southern blot hybridization procedures.

The presence of 3'arm of recombination, which was the shorter, was the first to be screened by PCR. From this first screen, only nineteen clones were selected. Even though not all the PCRs worked, possibly because of the DNA extraction process, about 90% of the PCRs with wt genomic DNA as template worked (Fig 5.12; Fig 5.13). In this case, the 3'arm suffered correct homologous recombination in a rate of about 9%.

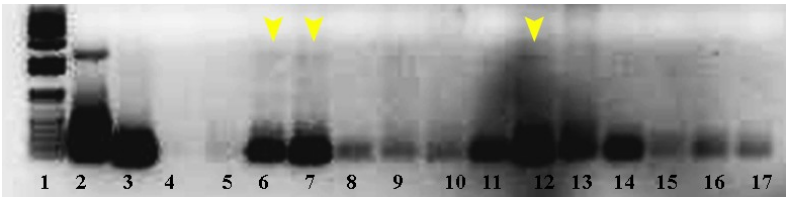

Figure 5.12 - 3' arm PCR screen for neo band

1-1kb+ DNA Ladder; **2**-plasmid control for neo and 3' arm recombination; **3**-wt genomic DNA; **4**- H_2O; **5**- Bacterial Artificial Chromosome for ADTK1 genomic region; **6 to 13**-1A-1H; **14 to 17** – 2A-2D. The expected band for correct recombination is 2200 bps. Positive clones are marked with a yellow arrowhead.

In order to have a positive control for the 3'arm of recombination, it was made a construct containing the neo cassette upstream and the 3'arm sequence, plus 300bp towards the 3' end (Fig 5.12 lane 2).

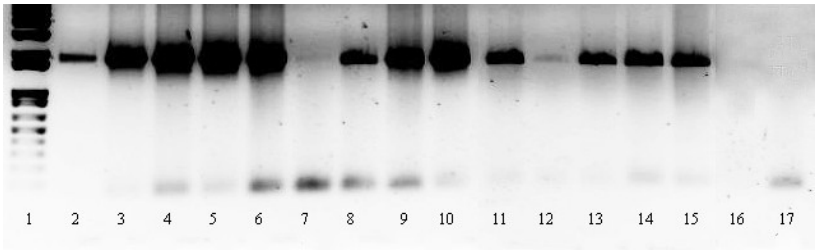

Figure 5.13 - 3' arm PCR screen for wt band

1-1kb+ DNA Ladder; **2**-wt genomic DNA; **3**-Bacterial Artificial Chromosome for ADTK1 genomic region; **4 to 11**-1A-1H; **12 to 15** – 2A-2D; **16**- H_2O; **17**- plasmid control for neo and 3' arm recombination. The expected band for wt genomic band is 1700 bps.

Even though only nineteen clones were positive for the PCR screen, thirty clones were analyzed by southern blot, in order to guarantee that some wild type ES cell controls were present.

It was clear that, even though nineteen clones were positive for the recombination of the 3'arm, the same could not be said for the total recombination of both the 5' and 3' arms, which was screened by southern blot hybridization (Fig 5.14).

When hybridizing with a probe external to the recombination arms, only one positive clone was found.

After performing gel electroforesis, some of the λ-HindIII DNA ladder bands were roughly marked: the 23.1 Kb, the 9.4 Kb and the 6.6 Kb. These correspond to the positive dots in lane 2 of Fig 5.14.

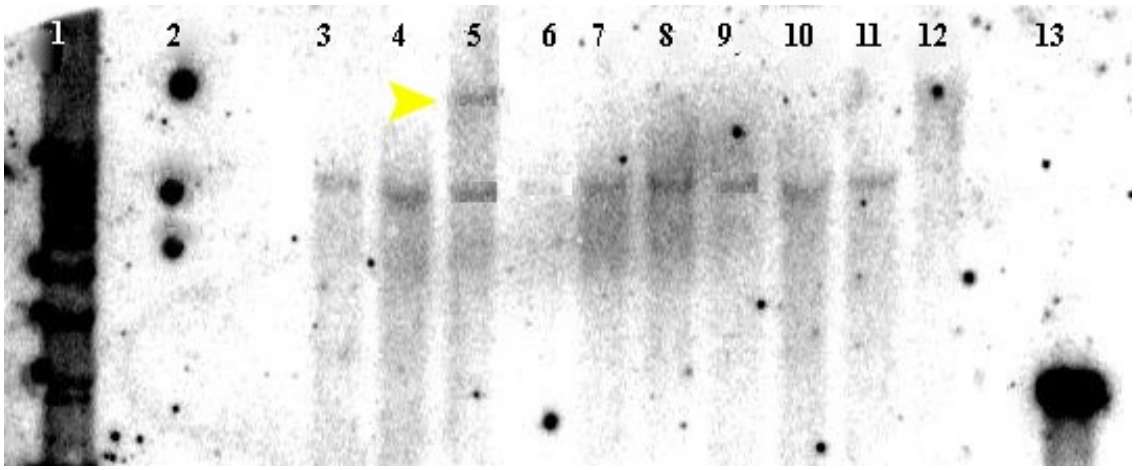

Figure 5.14 - Southern Blot Image using an external 3' probe

1- 1Kb+ DNA ladder; **2**- λ-HindIII DNA ladder; **3 to 10**- ES cell genomic DNA samples cut with BamHI; **11**- wt genomic DNA from tail cut with BamHI; **12**- wt genomic DNA from tail cut with Eco47III; **13**- probe in linearized plasmid. Yellow arrowhead indicate the recombinated band obtained

As can be seen, all the wt bands which are expected to have 10.5Kb, appear slightly above the dot of 9.4 Kb, and are aligned with the wild-type control (lane 11). However, only one appears to have a second band (clone in lane 5) that corresponds to the size of the recombinated band, 17 Kb: in lane 1 the top band corresponds to 12 Kb, and the second (highest) band in lane 5 is between 12 Kb and 23 Kb.

In order to confirm that it was a positive clone, a new southern was performed, this time using an internal probe for the neo cassette. Besides using the BamHI enzyme restriction digestion that would retrieve a 17 Kb band, one other digestion was

performed with EcoRV that cuts inside the 5'arm and cuts just downstream of the neo cassette. This digestion should retrieve a smaller band of 3.6 Kb. A band this size is easy to identify and thus guarantee no other smaller sequences recombinated along with the 5' and 3' recombination arms (Fig 5.15).

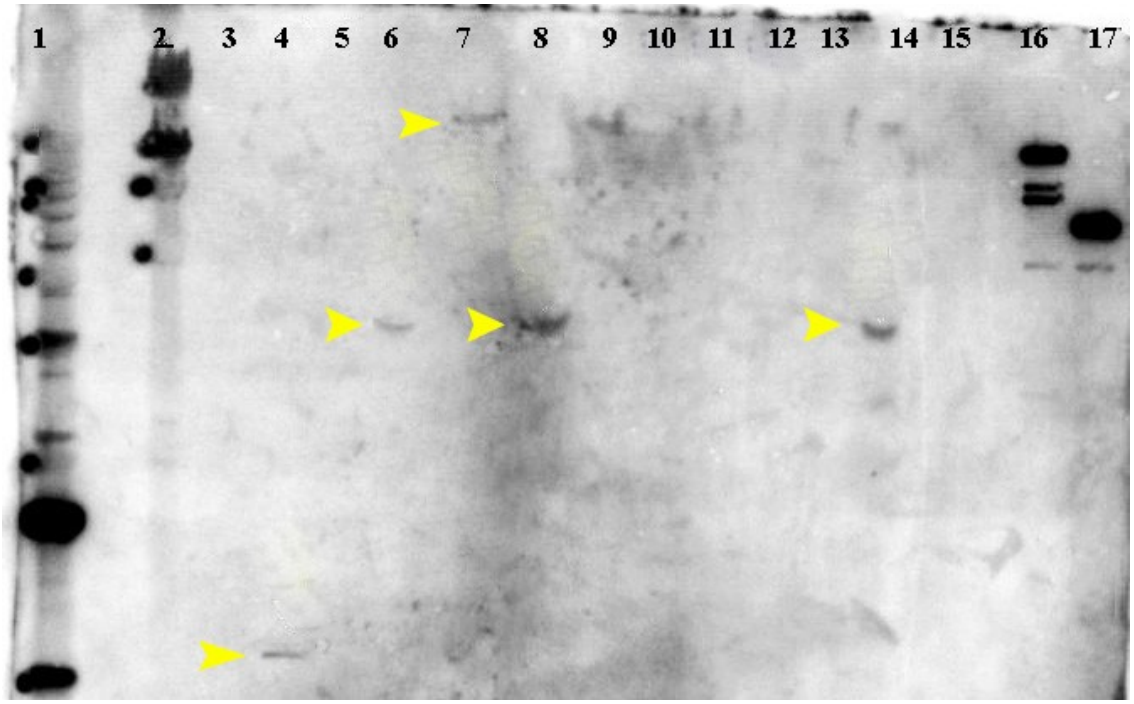

Figure 5.15 - Southern Blot Image using an internal probe for the neo cassette
1- 1Kb+ DNA ladder; **2**- λ-HindIII DNA ladder; **3, 5, 7, 9, 11, 13**- ES cell genomic DNA samples cut with BamHI; **4, 6, 8, 10, 12, 14-** ES cell genomic DNA samples cut with EcoRV; **15-** wt genomic DNA from tail cut with BamHI; **16-** positive control for neo cassette with 14 Kb; **17-** positive control for neo cassette with 6.5 Kb. Yellow arrowheads indicate the bands obtained.

Analyzing the blot, one can observe that more than one clone incorporated the 5' arm together with the neo cassette, having the right size for the digestion with EcoRV, however, again only one clone, the same as before, could fulfill the requirements when digesting with BamHI. One other band could be seen completely out of the expected range; this shows how correct homologous recombination is difficult, and how, although cells survive through the selection process, the neo cassette may be incorporated in wrong sites.

During this screening process, it could be determined that less than 1% of ES cell colonies suffered a correct event of homologous recombination.

After confirmation of the presence of a positive ES cell clone for the correct targeted inactivation of *ADTK1*, the ES cells that had been stored in low concentration were thawed and expanded according to the protocol described in *Materials and Methods*, in order to have a good batch of cells and analyze its viability and growth rate (Fig 5.16). Subsequently, once a good batch of cells was obtained (10 vials, each containing one million cells), one vial of cells was sent to be injected in order to produce mouse chimeras of *ADTK1*.

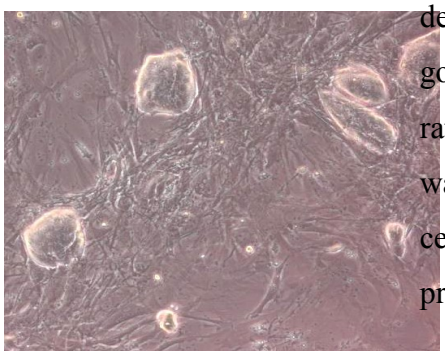

Figure 5.16 - ADTK +/- ES cells
ES cells after three days of being thawed.

5.3.4 Offspring analysis from ADTK1 $^{+/-}$ ES cell injection

The first injections performed at Instituto Gulbenkian de Ciência were on C57Bl/6 black blastocysts, the same background as the the ES cells. Twenty blastocysts were injected and implanted in one foster mother. Five animals were born and genotyped. One of them was a male chimera; however, because these injections were performed on a blastocyst with the same color, one could not assess whether the chimeric contribution was high or low. From mating of this chimera with C57Bl/6 females, twenty four litters were retrieved, and one hundred and twenty three animals were genotyped. None of the offspring mice were positive for the mutated allele, so, it was concluded that this chimera wouldn't pass the mutation to the offspring.

ES cells from the same batch were then sent to be injected in C57Bl/6cBrd (albino) blastocysts which were then implanted in foster mothers. Meanwhile another targeting process was initiated, to guarantee new clones, in case the new injections gave weak chimeras that wouldn't pass the mutation to the germ line. From this new targeting, two

positive clones were screened, however there was no need to inject these cells (data not shown).

In the second injection of ES cells seventy eight blastocysts were injected, and were all implanted in five foster mothers. From these injections, three male chimeras were born. Two of them were about 1% chimeric and the other about 20% (Fig 5.17). The higher the contribution of mutated ES cells to the blastocyst, the higher the probability those cells will populate the germline.

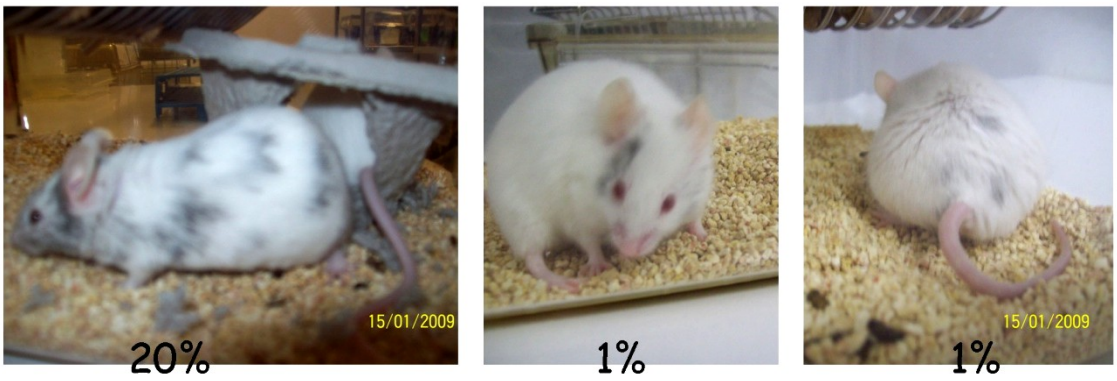

Figure 5.17 - ADTK1 male chimeras

All chimeras were mated with C57Bl/6cBrd (albino) females in order to try to obtain ADTK1 +/- offspring, which will happen if the ADTK1+/- ES cells entered the germline.

Only the 20% chimeric male passed to the germline, producing one black female in his offspring. However, as the injected ES cells were heterozygous, being black , the offspring still had half the probability of being wild type heterozygous. The female was genotyped and proved to be heterozygous (Fig 5.18).

When it reached sexual maturity, the female was crossed in order to expand the ADTK1$^{+/-}$ colony. The heterozygous offspring proved to be viable and fertile without apparent abnormalities in their morphology or behavior.

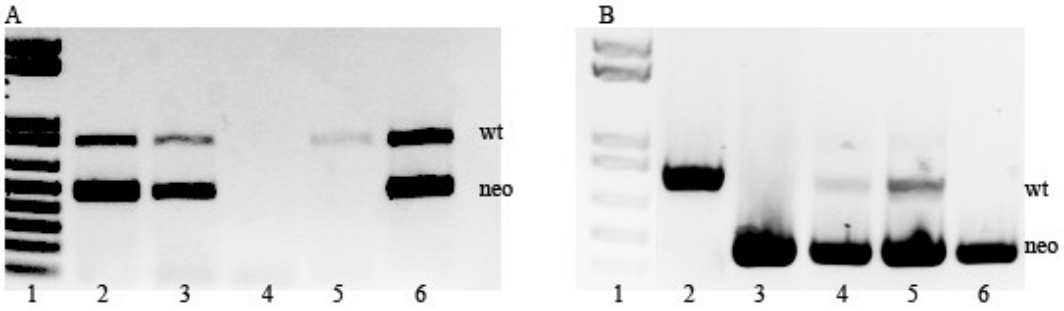

Figure 5.18 - *ADTK1* genotyping

A- ADTK1 chimera and offspring genotype: 1- 1Kb+ DNA ladder, 2- female pup genomic DNA; 3- 20% chimera genomic DNA; 4- H_2O; 5- wt genomic DNA; 6- first chimera genomic DNA; **B**- Offspring genotype from ADTK1 intercrosses: 1- 1Kb+ DNA ladder, 2- wt genomic DNA; 3 – mutated band control; 4, 5, 6- ADTK1 offspring genomic DNA. wt- wild-type band. neo – mutated band.

Heterozygous mutants were intercrossed in order to obtain *ADTK1* null mutants (Fig 5.18; Table 5.1). Except for the embryos recovered at E8.5, *ADTK1* offspring seems to correspond to a mendelian ratio. However, the numbers are still very low to state that for sure.

Table 5.2- Genotype of offspring recovered from eight *ADTK1* +/- intercrosses

E- embryonic day; P- pos-natal day

	+/+ (%)	+/- (%)	-/- (%)	Total
E8.5	5 (38)	8 (62)	0	13
P0-P2	10 (27)	19 (51)	7 (19)	37

The newborn pups obtained from the heterozygous mutants intercrosses, were all alive for the first 12h to 48h. They were collected and sacrificed for posterior analysis. The pups were genotyped, and after, null mutants were thoroughly analyzed, using littermate wild-type pups as control.

Data from *Xenopus* and chick orthologs suggested a potential role in eye development, neural tube closure and cardiogenesis. Furthermore, data from the expression pattern indicated the possibility of ADTK1 being involved in the head

formation, as genes expressed in the AVE such as *otx2*, *lim1*, *gsc* and c*erl1* (Shawlot, et al. 1999, Perea-Gomez, et al. 2001, Belo, et al. 1998, Belo, et al. 1997), often play a role in neural induction and the formation of anterior structures.

The majority of homozygous newborns presented no visible defects. However, about 28% (2/7) presented defects in the eye and ear (Fig 5.19). It seems that anterior iris pigmentation is affected, and the ear seems to be located lower than in the wild-type. Previously, in section 5.3.2, figures 5.6 and 5.7 show that *ADTK1* is expressed in the prospective eye and in the eye.

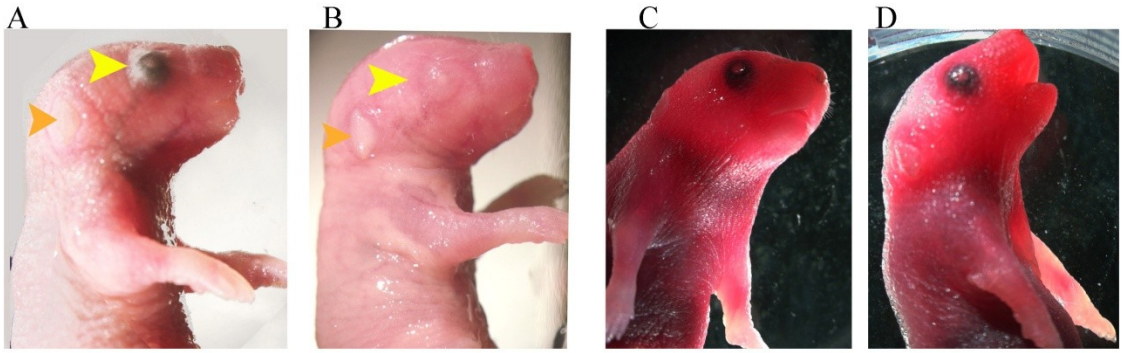

Figure 5.19 - Newborns form ADTK intercrosses

A-wild-type newborn from litter 6; B-*ADTK1* KO newborn from litter 6; C- wild-type newborn from litter 1; D-*ADTK1* KO newborn from litter 6. Yellow arrowheads indicate the eye, while orange arrowheads indicate the ear.

The mutants that presented eye and ear defects were sacrificed 48h after birth. So it is possible that the iris suffered degeneration in the first days, explaining why the other *ADTK1* null mutants did not present these defects. As for the ear, as the newborns were too small, it is possible that the differences were not as emphasized.

Internal organs were evaluated and no significant differences were observed in the heart, lungs, stomach and liver morphology. When analyzing the kidneys, all ADTK1 knockout newborns presented larger kidneys with a dark red color, when comparing with their wild-type littermates (Fig 5.20).

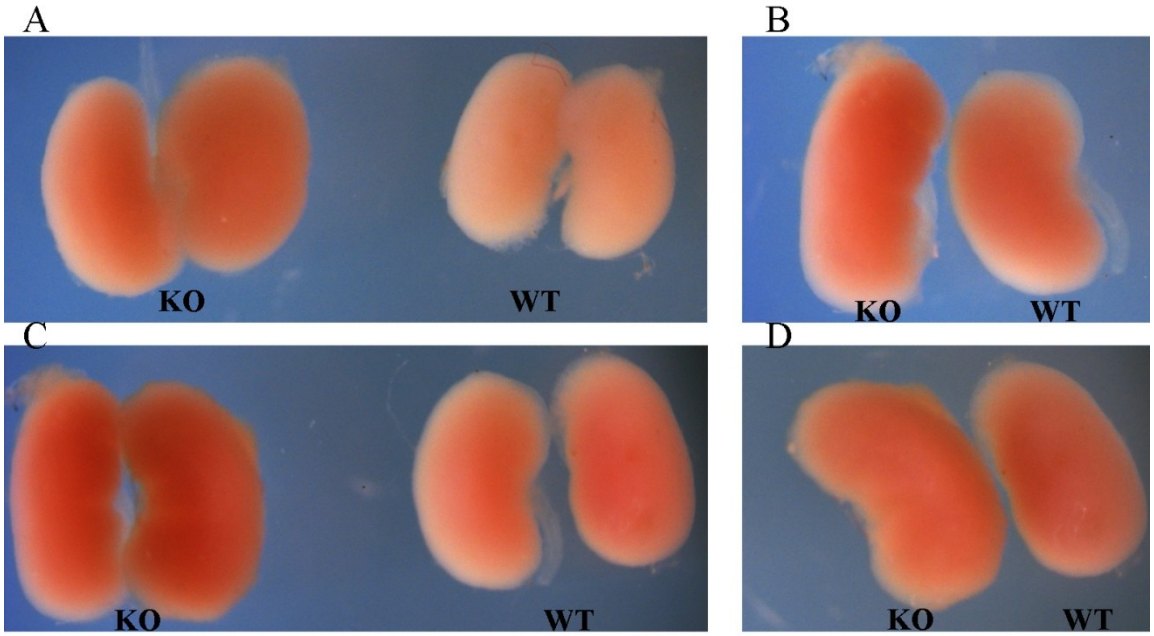

Figure 5.20 - Wild-type and ADTK1 KO kidney comparison

KO - kidney of *ADTK1*-/- newborn pups. WT - kidney of wild -type newborn pups. In all pictures *ADKT1* KO kidneys are presented in the right and wt littermates are presented in the left.A, C- kidneys from the litter 4 and 5; B, D- comparison of right and left kidney, from KO and wt newborns from litter 5.

In order to better understand the defects regarding the kidney morphology, preliminary analysis on histological sections was performed.

Being the kidney constituted by an outer cortex and a inner medulla, it is the inner medulla that seems to be affected. The preliminary data from histological analysis, shows that the *ADTK1* mutant has indeed larger kidneys than its wild type littermate. Both mutants and wild type differentiate the renal pyramids and the cortex region. However, it seems that, comparing with the wild type, *ADTK1* mutants lack part of the medullary tissue (Fig 5.21 B, C, E and F). In fact they just seem to present s-shaped bodies, lacking most the glomeral structures (Fig 5.21 D1, H1 and H2).

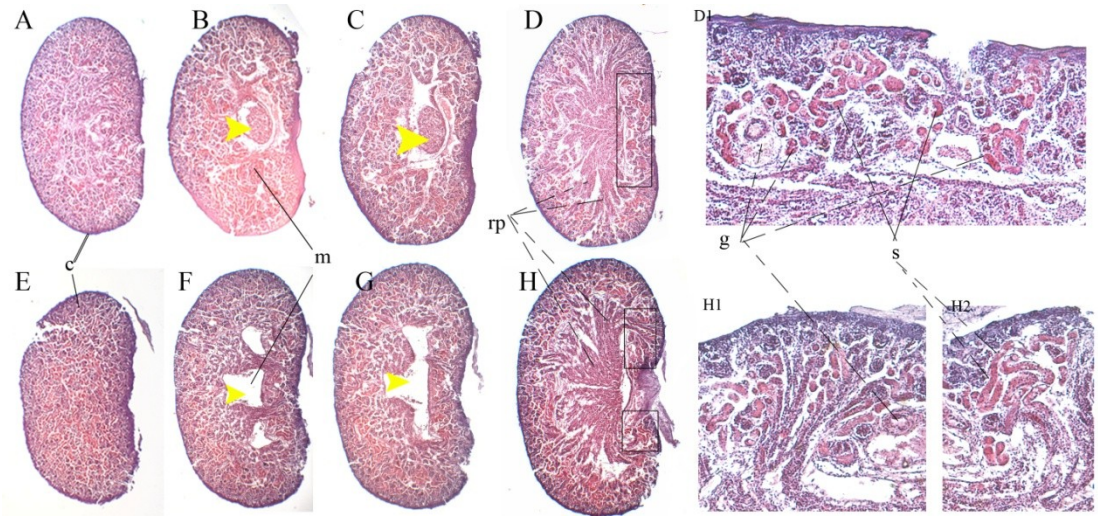

Figure 5.21 - Histological analyses of kidneys from *ADTK1* intercrosses

All sections are sagital and were performed at 12µm. A-D- kidney from wild type newborn mouse, E-H kidney from ADTK1 null newborn mouse. Areas of interest are indicated with a black square, magnified and shown next to the relevant panels c- cortex; g- glomerulus; m- medulla, rp- renal pyramids; s- s shaped body..

Interestingly, morphologically, the *ADTK1* deficient kidneys resemble *wnt4* deficient kidneys, where smooth muscle cell differentiation is perturbed during the embryonic kidney development, when medullary stromal cells and glomeruli, nephron tubules and medulla-like structures are formed (Itäranta, et al. 2006, Kobayashi, et al. 2005). Moreover, in *wnt4* mutant mice *bmp4* expression is completely lost during early nephrogenesis; later, at E16.5 *bmp4* as well as other genes related to kidney development, such as *Shh* and *ptc-1*, are ectopically expressed in the capsular mesenchymal cells, instead of being expressed in the medullary region (Itäranta, et al. 2006). However, these are only preliminary data, and no major conclusions can be taken from these experiments. The majority of papers regarding kidney development, report null mutations for genes involved in the process of nephrogenesis, that instead of originating larger kidneys, give rise to kidney agenesis or hypoplasia. It is possible that *ADTK1* is correlated with *wnt4* and/or with the process of downregulating *six1, gremlin* or *eya1*. Mutants for these genes do not develop the metanephric kidney (reviewed in Yu, et al. 2004), possibly, its overexpression may lead to an overdeveloped, enlarged kidney and, simultaneously, misdevelop medullar structures, which are of great importance for correct kidney function.

Recently this year, Imuta et al. reported bone defects in *Pkdcc* (*ADTK1*) mutants, however, until now all null mutants obtained were roughly the same size as its wild-type littermates and no obvious differences were noticed. However, skeletal analysis with alizarin red and alcian blue provided further and more detailed information. In these limbs, the mineralized regions, which stained red with alizarin red, were significantly shortened compared with its wild type littermates (Fig 5.22, Table 5.3), whereas the size and morphology of the cartilage, which stained blue with alcian blue, were not significantly affected.

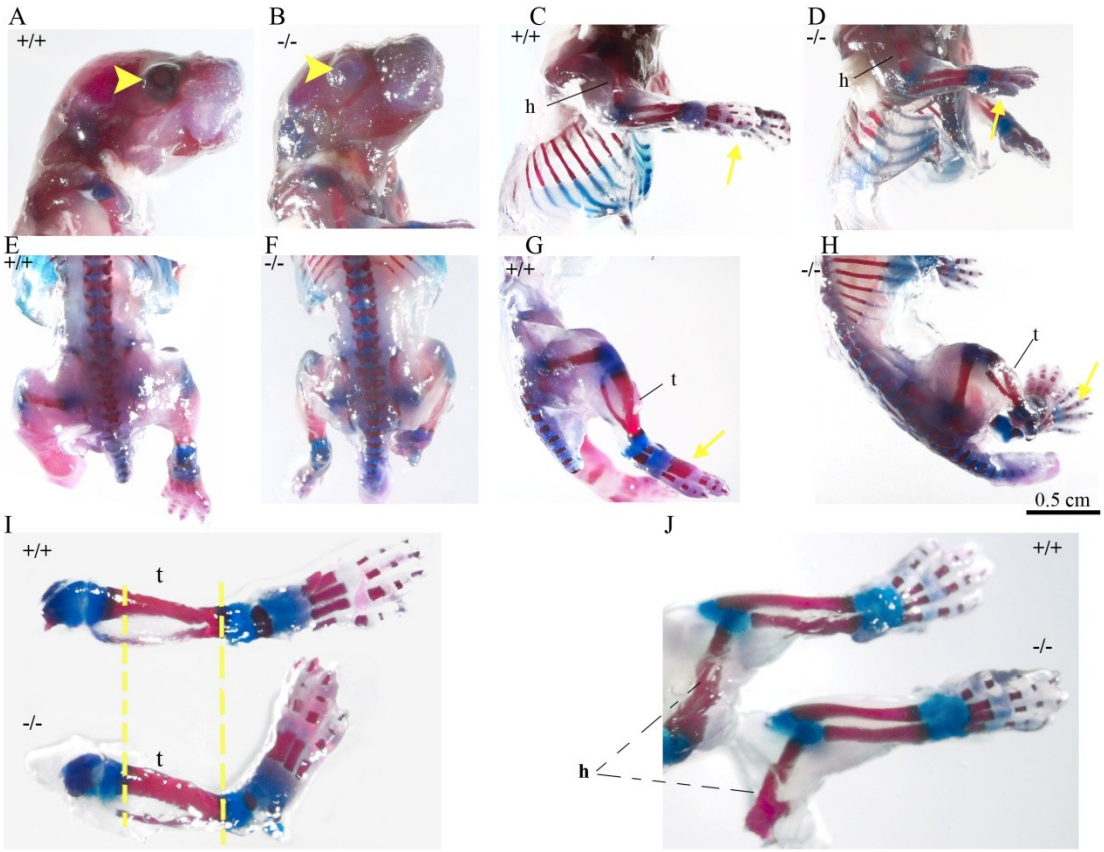

Figure 5.22 - Skeletal analysis of *ADTK1* null mutants and wild type littermates

All skeletons are from the same litter. Panels A, B, C, D, G and H show the right side of the pup. Panels E and F show the dorsal view. Skeletons from wild type newborn pup #32 (A, C, E, G, +/+) and *ADTK1* null mutant newborn pup #35 (B, D, F, H, -/-). I- WT (+/+) and KO (-/-) lower limbs; J- WT (+/+) and KO (-/-) upper limbs. Mineralized regions (bones) are stained red with alizarin red and cartilage is stained blue with alcian blue. The scale bar is equivalent to 0.5 cm and corresponds to panels A-H. Yellow arrowheads indicate the eye. Yellow arrows indicate the paws. Dashed line compares tibia and peroneum lengths, between WT and KO. t: tibia, h, humerus.

Preliminary analysis of 40% of *ADTK1* null mutants generated (3/7), showed that these mutants have indeed shorter hind and forelimbs. In the lower limbs, although the femur is not much affected, the tibia and peroneum sizes are considerably shortened (Fig.5.22 G, H; table 5.3). Regarding the upper limbs, both radio and humerus size are shortened (Fig 5.22 B, C; table 5.3). As for the cervical vertebrae, no significant chances were observed, and no neural tube defects were detected (Fig 5.22 A, B, E and F).

Table 5.3 - Measures of WT and ADTK1 null mutant bones

Measurement of the bones in the upper limbs (humerus, radio and paws) and lower limbs (femur, tibia and paws) in cm. Ratio between ADTK and WT bone length.

	ADTK	WT	ADTK/WT (%)
Humerus	0,273	0,362	75,603
Radio	0,316	0,396	79,748
Upper paws	0,262	0,334	78,497
Femur	0,324	0,331	98,012
Tibia	0,294	0,428	68,700
Lower paws	0,546	0,604	90,333

This data is consistent with *ADTK1* expression in the limbs. It is already known the importance of the correct patterning of the ZPA *vs* AER, and how these two structures together are responsible for the bone formation and extension. Interestingly, *gremlin*, a BMP antagonist for kidney development, also plays a role in maintaining FGFs restricted to the AER, promoting in limb development (Zúñiga, et al. 1999). This could mean that ADTK, that is present in both tissues, could be important for both developmental processes possibly by interaction with gremlin. Furthermore, data from experiments in *Xenopus* orthologs suggest a potential role in the Hedgehog pathway (Silva and Vitorino, unpublished). It is known how both Shh and Ihh play important roles in the eye and limb development, and bone formation, respectively (Chiang, et al. 2001, Ma, et al. 2008), and that Shh is also involved in the process of kidney

development (Yu, et al. 2002). Additionally, during limb development, *gremlin* is activated by Shh. It is possible that ADTK1 is an unidentified intermediate player between these molecules in kidney and limb development.

Interestingly, Imuta et al. also described cleft palate defects in *Pkdcc* (*ADTK1*) mutants, which were not found in during the analysis of *ADTK* mutants. This phenotypical difference can be accounted, possibly, for one of two reasons (or both): the use of TT2 ES cells (Imuta el al., 2009) *vs* pure C57Bl6 ES cells are of different background, which may lead to different phenotypes, as has been extensively reported for other targeted mutations; or it is possible that those results were not obtained yet, due to the low numbers of null mutants obtained so far.

In sum, preliminary analysis of *ADTK1* mutants show defects in bone length, and kidney and eye development. This is consistent with the expression pattern previously described. However, besides the defects in the eye, these results do not mimic the ones obtained in experiments using chick and *Xenopus ADTK1* orthologs, where the use of morpholinos gave rise to several defects in the neural tube closure and heart. Still, the numbers are very low and it is possible that these defects are of low incidence.

The defects obtained in *ADTK1* null mutants, together with data from chick and *Xenopus* orthologs, suggest that ADTK1 is a protein kinase involved in the regulation of more than one signaling pathways, probably Wnt, Hedgehog and BMP.

6. General Discussion

Within developmental biology, axes establishment, head formation, heart and limb development, and neurulation, are subjects of great interest, since the disruption of these processes is responsible for the majority of birth defects.

Regarding axes formation, Nodal signaling pathway is a crucial one, essentially with the asymmetric expression of its antagonists, which force Nodal expression to change from symmetric to asymmetric, during the onset of axes establishment (Hamada, et al. 2002). Nodal itself is responsible for this, as it induces its antagonists and upregulates its own asymmetric expression, through a feedback mechanism. Wrong expression of Nodal signaling targets leads to disruption of axes formation, and misplacement of internal organs (Lowe, et al. 1996, Meno, et al. 1998), originating, sometimes, *situs inversus*, a situation where internal organs are arranged in an inverted way, like a mirror. Before acting on the L-R establishment, *Nodal* is particularly involved in the onset of the A-P axis, in the development of the primitive streak (Conlon, et al. 1994). Lack of Nodal, and some Nodal signaling players such as Cripto, can lead to embryonic arrest, due to gastrulation failure (Conlon, et al. 1994, Xu, et al. 1999). Many advances have been made towards understanding this complex process of axes establishment (Bianco, et al. 2003, Liguori, et al. 2008). Nevertheless, much remains to be explained regarding the meticulous regulation of the signaling pathways involved.

Previous studies report Cerberus as a head inducer in *Xenopus* (Bouwmeester, et al. 1996). *cerberus* homolog in mouse, *cerberus-like1*, is expressed in the AVE and is one of the molecules responsible for restricting Nodal to the posterior part of the embryo, allowing thus for the embryonic axes to develop properly. Howerever, *cer1* is not necessary for anterior patterning, *otx2* expression, or even normal mouse morphogenesis (Simpson, et al. 1999). *cerl1* mutants are viable and fertile animals. Nevertheless, this does not diminish Cerl1 importance. It has already been shown that Cerl1 and Lefty1 have redundant roles in antagonizing Nodal (Perea-Gomez, et al. 2002, Yamamoto, et al. 2004).

During this work it was reported the importance of generating of *cerl1:cripto* double mutants, regarding the study of Nodal signaling during early mouse embryonic development. This work presented the possibility of Nodal transducing its signals through a Cripto-independent pathway. Cripto is important for Nodal activity and, in its

absence, the expression of Nodal target genes, such as *lefty* genes, are downregulated. However, the simultaneous removal of *cerl1* and *cripto*, rescues the expression of Nodal target genes. Moreover, in the absence of Cripto, embryos fail to gastrulate and form the A-P axis correctly, nevertheless, in *cerl1:cripto* mutants, the embryos start gastrulation and have an A-P axis, failing to completely elongate the primitive streak and still missing trunk structures. Although *cripto* and *cerl1* are not co-expressed during development (Belo, et al. 1997, Ding, et al. 1998), it is correct to state that these genes present a complementary or contiguous expression (Belo, et al. 1997, Ding, et al. 1998). It is possible to say that both Cerl1 and Cripto may act on a same group of cells, if it is taken into account that cerl1 is a secreted factor. Thus, in these cells, the absence of *cerl1* and *cripto* results in higher levels of Nodal in the extracellular space, which leads to the rescue of *cripto* null mutants' phenotype.

Interestingly, removing just one copy of *cerl1* the same results can be obtained, suggesting that a Nodal threshold is reached, and that once that threshold is reached it is sufficient to rescue the A-P axis. Higher concentration of Nodal above that threshold causes no effect on the A-P axis rescue.

It is likely that this "non-canonical" Nodal signaling pathway acts through ALK7, a serine/threonine type I receptor. Reissman et al. in 2001, has suggested a signaling pathway alternative to ALK4, proving that Nodal could signal through ALK7 activating phopho-Smad2 and, even though this signaling was enhanced in the presence of Cripto, it also could be transduced independently of Cripto.

However, little is known about ALK7 role during gastrulation and concerning Nodal signaling. It is known that ALK4 mutants fail to produce mesendoderm and die shortly after gastrulation, however, ALK7 mutants show no apparent phenotype, are viable and fertile. Furthermore, *alk7-/-:alk4*+/- double mutants show no differences comparing to wild-type (Jörnvall, et al. 2004). It has already been shown that several genes that, when removed, produce no phenotype are of great importance during development, playing redundant roles in order to assure correct embryonic development, and avoid embryonic arrest.

Without question, the AVE is one of the most important structures during early embryonic development. However, not all of the genes expressed in this tissue, when removed, give evident phenotypes. The topological equivalent of the AVE in *Xenopus*, the anterior dorsal endoderm, expresses much of the same genes. Curiously, much more striking phenotypes are observed when some of these genes are up or downregulated in *Xenopus* than in mouse. This is the case of *cerl1*, which, when microinjected in the ventral side of *Xenopus* embryos, leads to the formation of ectopic head-like structures (Piccolo, et al. 1999), and when knocked-out in mouse, no phenotype is observed (Belo, et al. 1997, Belo, et al. 2000). Again, it also happens with *shisa* (Yamamoto, et al. 2005, Furushima, et al. 2007, Silva, et al. 2006). While *shisa-1* and *shisa-2* in *Xenopus*, when downregulated, present defects at level of the head, eye and somite formation, in the mouse, although the expression pattern corroborates the defects presented in *Xenopus*, the knockout of this gene leads to none of such defects (Furushima, et al. 2007). Furthermore, cross-species comparison between mouse and chick suggest that this gene is conserved: the expression pattern of s*hisa* in mouse resembles the one in chick. Strangely, although mouse *shisa* patterns the same tissue as its *Xenopus* orthologs, tissues which are characteristic of FGF and Wnt activities, the knockout mouse did not present any phenotype.

Once again, some other may be compensating for the loss of *shisa*. It is also possible that defects form at certain stages of development, and are subsequently overcome by the compensation of other genes.

During the course of this work, a thorough analysis of the gene *ADTK1* was performed. Interestingly, two isoforms for this protein were detected, consisting of the complete version and a shortened one. In the latter, the first exon is split in two, and part of it is transformed into an intron, thus originating one more exon, being the full first exon an untranslated region. Curiously, these two isoforms are co-expressed through embryonic development (since E7.0 until E12.0), and no variations in expression levels were detected. However, by carefully analyzing these two isoforms, one can observe that the shorter isoform lacks subdomains I, II and III. Being kinases, subdomain I is crucial for ATP-binding (Hanks and Hunter 1995), thus, it is possible than only the full length protein is a functional one. Curiously, both chick and *Xenopus* orthologs

completely lack or have this subdomain altered (Bento, unpublished; Silva, unpublished; Vitorino, unpublished), suggesting that in these organisms the protein might not have the same function as in mammals, nevertheless the *Xenopus* orthologs and cADTK-L1present the catalytic lysine in subdomain II, which is also crucial for binding to ATP, and may be compensating for the loss of subdomain I (Xu, et al. 2000). As for the subdomain responsible for the catalytic activity, subdomain V, all species analyzed, mouse, human, *Xenopus* and chick, present it. These facts may account for the lack of kinase activity displayed when testing both *Xenopus* orthologs, in preliminary assays.

From the very beginning, the expression pattern analysis suggested an important role for *ADTK1* during embryonic development. This gene is expressed very early in development, in the AVE, at the distal tip as it starts migrating towards the anterior side. It is well documented that the AVE is one of the tissues responsible for the correct establishment of the axes, and formation of anterior structures (Beddington and Robertson 1999, Bielinska, et al. 1999, Perea-Gomez, et al. 2001). However, newborn analysis, regarding the anterior structures in *ADTK1* null mutants, demonstrated no visible defects, except for the eye development in some of the mutants (2/7). This data is consistent with data from downregulation in *Xenopus* orthologs, where some defects in the eye were also detected.

Curiously, recently this year Imuta, et al. published the effect of *ADTK1* (*Pkdcc*) knockout, and reported defects in the palate. When analyzing *ADTK1* mutants, no defects in the palate were detected. However, the ES cells used in that case, were TT2, which are derived from F1 blastocysts obtained from matings between a C57BL/6 females and CBA males (Yagi, et al. 1993). CBA mice, are originated from an A female and a DBA male. The strain A (albino) is characterized by having high incidence of spontaneous cleft palate, which can account for the fact that those mutants presented this defect, and *ADTK1* null mutants, which are pure C57BL/6, did not.

It is known that differences in background, which are characterized by specific single nucleotide polymorphisms (SNPs), can be associated with regulatory variation, affecting gene expression levels, and giving rise to different phenotypes and numbers. Recently in the lab such a case has been detected, when analyzing *cerl2* null mutants in C57BL/6 and 129sv backgrounds (Marques, et al. 2004, Araújo, unpublished).

Furthermore, study of this mutant is still a preliminary one, only few null mutants were still obtained. It is possible that, with more numbers, incidence of cleft palate in *ADTK1* mutants occurs.

Interestingly, BMP2 and BMP4 are involved in several processes such as heart formation, limb development and neurulation. Through the analysis of *ADTK1* expression pattern, the same could be said of this gene.

Moreover, BMP signaling is known to interact with several other pathways, such as Nodal, Wnt and Shh signaling pathways. Even more, *ADTK1* patterns the tissues which are characterized for presenting Shh, BMP and Wnt activities. Analysis of *ADTK1* expression pattern during embryonic development, as well as data from downregulation of chick and *Xenopus* orthologs, suggested that null mutants for *ADTK1* could display defects at the level of heart and limb development, and neural tube closure. Data presented by Imuta, et. al. this year, showed that *ADTK1* (*Pkdcc*) knockout mice exhibited shorter limbs than its wild-type littermates. *ADTK1* mutant specimens analyzed for its skeleton also presented differences in bone length, although mild ones comparing to Imuta (2009); however, the specimens analyzed presented no defects regarding the neural tube closure (as it was suggested by *ADTK1* orthologs experiments). Nevertheless, it is known that during the process neural tube closure many molecules are involved; it is possible that some of these molecules are compensating for the loss of ADTK1, or that there are indeed defects in neural tube development, but mild ones that can be overriden throughout embryogenesis. Furthermore, it has been reported that several genes act synergistically, and when only one is removed, no effect can be detected. It is the case of molecules from Wnt pathway, *JNK1* and *JNK2* (Sabapathy, et al. 1999). Each of these mutants are viable and present no defects, however, the combination of one null mutant with the other, results in unviable embryos with neural tube malformations (Sabapathy, et al. 1999). Possibly, *ADTK1* function in the neural tube is being supported by another gene.

Interestingly, all analyzed *ADTK1* mutants presented larger kidneys than their wild type littermates. Preliminary histological analysis demonstrated that *ADTK1* enlarged kidneys lack medullary structures.

Curiously, *gremlin*, a BMP antagonist essential for kidney development, also plays a role in maintaining FGFs restricted to the AER, promoting in limb development (Zúñiga, et al. 1999). Being ADTK1 present, and presenting defects in both tissues,

limb and kidney, it could be important for both developmental processes possibly by interaction with gremlin. Furthermore, data from experiments in *Xenopus* orthologs suggest a potential role in the Hedgehog pathway (Silva and Vitorino, unpublished). It is known how Hedgehog signaling plays important roles in the eye and limb development, and bone formation (Chiang, et al. 2001, Ma, et al. 2008), as well an in the process of kidney development (Yu, et al. 2002). Additionally, during limb development, *gremlin* is activated by Shh. It is possible that ADTK1 is an unidentified intermediate player between these molecules during both kidney and limb development.

Morphologically, the phenotype obtained in *ADTK1* mutant kidneys is very similar to the phenotype of *wnt4* mutant kidneys described by Itäranta, et al. (2006), suggesting a potential biological role in kidney development. In *wnt4* mutant kidneys, the development of smooth muscle cells in the medullary stroma is compromised, probably due to the absence or misexpression of BMP4, which occurs in those mutants; furthermore, it is already known that *wnt4* in involved in controlling mesenchyme to epithelium transformation that underlies nephron development (Stark et al., 1994) and null mutants for this gene fail to pretubular cell aggregates, thus failing tubule induction (Kispert et al., 1998).

The kidney development is a process not yet fully understood. It is known that molecules from several signaling pathways are involved in the formation of the kidney, however, their relative positions in the pathways remain unclear and intermediate players remain unknown. Additionally, Wnt proteins are known to play important roles in the growth and morphogenesis of organs such as the kidney and lungs, in the regulation of branching morphogenesis (Bridgewater, et al. 2008, De Langhe and Reynolds 2008).

The differentiation of the smooth muscle cell is an important process for the development of several organs other than the kidney; it is also necessary for the correct development of the heart musculature and lungs (Wang 2005). It has been discussed how *ADTK1* is present in the pericardium, and the important role this membrane plays in heart development, allowing the communication with the lungs. Furthermore, data from chick ADTK1 morpholino experiments, strongly suggests an important role in the heart (Bento, unpublished). It is possible that, besides affecting smooth muscle cells differentiation in the kidney, *ADTK1* may be correlated to the differentiation of these cells in the heart, being involved in the development of the heart musculature, although

no apparent defects were detected in the heart during the preliminary analysis of *ADTK1* mutants. The lack of defects in the heart could be justified with the development of the pericardium membrane, which is only complete, about a week after birth (Matsuda, et al. 1990). It is already known that, until the mouse pericardium is fully developed; it consists of a continuous serous membrane that is composed of pericardial and pleural mesothelia, and only later the pericardium becomes fenestrated, and the pericardial and pleural cavities become continuous (Matsuda, et al. 1990). Interestingly, Imuta, et al., suggest that, *Pkdcc* (*ADTK1*) mutants die of respiratory failure due to incomplete lung expansion. Additionally, in the development of heart and lung is also necessary the correct differentiation of smooth muscle cells, where Wnt signaling is also involved (Wang, et al. 2005).

Data from animal caps assays in *Xenopus*, indicate *ADTK1* is correlated to Wnt pathway, as Wnt8 expression is upregulated (Vitorino, unpublished). Furthermore, *Xenopus* ADTK1L2 morpholino experiments show similar defects to what is observed when genes involved in the PCP and Hedgehog pathways are knocked down (Vitorino, unpublished).

Taken together, these set of experiments strongly suggest that ADTK1 may be involved in pathways such as Shh, BMP or Wnt, which play roles in different processes such as kidney development, eye and limb formation, and neural tube development. Furthermore, this data indicates how in the mammalian genome many genes have redundant and synergistic roles, guaranteeing that their removal does not lead to embryonic arrest or birth defects.

7. Future Perspectives

Regarding the experiments related to the study of a Cripto-independent Nodal signaling, it would be interesting to evaluate what happens in *cerl1:cripto:Alk7* triple mutants. It is already known that *Alk7* null mutants present no phenotype, nor do double mutants when combined with *Alk4* heterozygous. Thus, this would be a way to assess whether Nodal can rescue its signaling through Alk7.

Although a large amount of work has been done regarding the study of *ADTK1*, a lot remains to be explained.

Biochemically, correct localization of the two ADTK1 isoforms should be addressed. Co-transfecting cells with fluorescent plasmids containing each of the isoforms together with specific membrane markers, should give a rough notion about where the proteins might be localized, however subsequently, each cell fraction should be separated, and western blots should be performed on each cell fraction in order to correctly identify the cell structures in which, each of ADTK1 isoforms is present. Furthermore, activity assays should be performed on each of the isoforms.

It is widely known how certain genes can compensate the loss of others, having synergistic and redundant activity.

In order to better understand the biological role of *ADTK1*, and the signaling pathways it might be involved in, several experiments could be conducted. First the ADTK1 colony must be expanded so that large numbers of null mutants can be obtained and consistent data can be achieved. Then, it should be tested whether *ADTK1* null mutants survive and if both males and females are fertile, because, although it has been described by Imuta et al. that these mutants die within the first day after birth, it has already been described how different backgrounds can influence.

Whole-mount *in situ* hybridization in null mutants, of *fgf8*, *fgf10*, *bmp2*, *bmp4 shh*, *noggin*, *chordin*, *cerl-1* and *nodal* should be performed at different stages of embryonic development and compared with the corresponding wild-type embryos. These data would provide information regarding several processes during embryogenesis, in which *ADTK1* might be involved in, such as axes determination, neural tube closure, limb formation, and the development of eye, heart and kidney.

Furthermore, as kidney morphology in *ADTK1* mutants is affected, the study of kidney development in these mutants should be addressed. Embryonic development from ADTK1 heterozygous intercrosses should be arrested at different stages, kidneys should be removed and *in situ* hybridization should be performed, using several probes

such as *shh*, *bmp4, wnt4* and *gremlin.* All of these genes participate in kidney development and are essential for its correct formation.

Additionally, as typically the developing medullary stroma differentiates smooth muscle α-actin (α-SMA) adjacent to the developing major vessels, around E14.5; it would be interesting to assess whether smooth muscle α-actin is being formed; this could be achieved by immunostaining with the α-SMA antibody.

It would be interesting to assess whether gremlin, Shh, Bmp4 or Wnt4 directly bind to ADTK1, performing co-immunoprecipitation assays.

RT-PCRs should be performed at different stages of embryonic development, and different genes should be assessed. For instance, *Shh* and *gremlin* expression should be evaluated in *ADTK1* mutants.

A thorough analysis of *ADTK1* mutants should be carried out throughout embryonic development.

8. References

Abu-Issa, R., Smyth, G., Smoak, I., Yamamura, K. and Meyers E.N. "Fgf8 is required for pharyngeal arch and cardiovascular development in the mouse." *Development*, 2003: 129, 4613-4625.

Adkins, H.B., Bianco C, Schiffer SG, Rayhorn P, Zafari M, and Cheung AE. "Antibody blockade of the Cripto CFC domain suppresses tumor cell growth in vivo." *Journal of Clinical Investigation*, 2003: 112, 575–587.

Alvarez-Medina, R., J. Cayuso, T. Okubo, S. Takada, and E. Martí. "Wnt canonical pathway restricts graded Shh/Gli patterning activity through the regulation of Gli3 expression." *Development* , 2008: 135, 237-247.

Anderson, R. M. Lawrence, A. L., Stottmann, R. W., Bachiller, D., Klingensmith, J. "Chordin and noggin promote organizing centers of forebrain development in the mouse." *Development* , 2002: 129, 4975-4987.

Andersson, O., Reissmann, E., Jornvall, H. and Ibanez, C.F. "Synergistic interaction between Gdf1 and Nodal during anterior axis development." *Dev. Biol.*, 2006: 15, 370–381.

Ang, S.L., and Constam, D.B. "A gene network establishing polarity in the early mouse embryo." *Semin Cell Dev Biol*, 2004: 15(5):555-61.

Aulehla, A., and Herrmann, B.G. "Segmentation in vertebrates: clock and gradient finally joined." *Genes Dev*, 2004: 18(17):2060-7.

Aulehla, A., and Pourquié, O. "Oscillating signaling pathways during embryonic development." *Curr Opin Cell Biol*, 2008: 20(6):632-7.

Aulehla, A., Wehrle, C., Brand-Saberi, B., Gossler, A., Kanzler, B and Herrmann, B.G.. "Wnt3a plays a major role in the segmentation clock controlling somitogenesis." *Dev Cell*, 2003: 4:395–406.

Bachiller, D., Klingensmith, J., Kemp C Belo JA Anderson RM May SR McMahon JA McMahon AP Harland RM, Rossant, J. and. De Robertis, E.M. "The organizer factors Chordin and Noggin are required for mouse forebrain development." *Nature*, 2000: 403(6770):658-6.

Bachiller, D., Shneyder N Klingensmith J, Anderson R Tran U, Rossant, J. and De Robertis, E.M.. "The role of chordin/Bmp signals in mammalian pharyngeal development and DiGeorge syndrome." *Development*, 2003: 130:3567–78.

Barembaum, M., and Bronner-Fraser, m. "Early steps in neural crest specification." *Cell & Developmental Biology* , 2005: 16, 642–646.

Baron, M.H. "Early patterning of the mouse embryo: Implications for hematopoietic commitment and differentiation." *Experimental Hematology*, 2005: 1015–1020.

Barrow, J.F., Howell, W.D., Rule, M., Hayashi, S. and Thomas K.R.. "Wnt3 signaling in the epiblast is required for proper orientation of the anteroposterior axis." *Developmental Biology* , 2007: 312, 312–320.

Beddington. "Induction of a second neural axis by the mouse node." *Development*, 1994: 120: 613-620.

Beddington, R. "Cripto-analysis of embryonic codes." *Nature*, 1998: 395(6703):641, 643.

Beddington, R.S.P. "The analysis of cell lineages in th epostimplantation mammalian embryo." *Genetic Approaches to Developmental Neurobiology*, 1981.

Beddington, R.S.P., and Robertson, E.J. "Anterior patterning in mouse." *Trends Genet*, 1998: 14(7):277-84.

Beddington, R.S.P., and Robertson, E.J. "Axis Development and Early Asymmetry in Mammals." *Cell*, 1999: 96:195-209.

Bejsovec, A. "Wnt Pathway Activation: New Relations and Locations." *Cell*, 2005: 120, 11–14.

Bejsovec, A. "Wnt signaling: An embarrassment of receptors." *Current Biology*, 2000: 10:R919–R922.

Belo JA, Silva AC, Borges AC, Filipe M, Bento M, Gonalves L, Vitorino M, Salgueiro AM, Texeira V, Tavares AT, Marques S. "Generating asymmetries in the early vertebrate embryo: the role of the Cerberus-like family." *Int. J. Dev. Biol.*, 2008: 52.

Belo, J.A., Bachiller D, Agius E, Kemp C, Borges AC, Marques S, Piccolo S, **De** Robertis EM. "Cerberus-like Is a Secreted BMP and Nodal Antagonist Not Essential for Mouse Development." *genesis*, 2000: 26:265–270.

Belo, J.A., Bouwmeester T, Leyns L, Kertesz N, Gallo M, Follettie M, and De Robertis EM. "Cerberus-like is a secreted factor with neuralizing activity expressed in the anterior primitive endoderm of the mouse gastrula." *Mech. Dev.*, 1997: 68: 45-57.

Belo, J.A., Leynsa, L., Yamadab, G. and De Robertis, E.M. "The prechordal midline of the chondrocranium is defective in Goosecoid-1 mouse mutants." *Mechanisms of Development*, 1998: 72, 15–25.

Ben-Haim, N., Lu, C., Guzman-Ayala, M., Pescatore, L., Mesnard, D. "The Nodal Precursor Acting via Activin Receptors Induces Mesoderm by Maintaining a Source of Its Convertases and BMP4." *Developmental Cell*, 2006: 11, 313–323.

Bertrand, N., and Dahmane., N "Sonic hedgehog signaling in forebrain development and its interactions with pathways that modify its effects." *TRENDS in Cell Biology*, 2006: 16; 11; 597-605.

Bianco, C., Strizzi, L., Rehman, A., Normanno, N., Wechselberger, C. "A Nodal- and ALK4-independent Signaling Pathway Activated by Cripto-1 through Glypican-1 and c-Src." *Cancer Research*, 2003: 63, 1192–1197.

Bielinska, M., Narita, N. and Wilson, D.B. "Distinct roles for visceral endoderm during embryonic mouse development." *Int. J. Dev. Biol.*, 1999: 43: 183-205.

Blum, M., Gaunt, S.J.,. Cho, K.W.Y., Steinbeisser, H., Bittner D. Blumberg B., and De Robertis, E.M. "Gastrulation in the mouse: the role of the homeobox gene goosecoid." *Cell*, 1992: 69, 1097-1106.

Borges, A.C., Marques, S. and Belo, J.A. "goosecoid and cerberus-like do not interact during mouse embryogenesis." *Int. J. Dev. Biol.*, 2002: 46: 259-262.

Borges, A.C., Marques, S. and Belo, J.A. "The BMP antagonists cerberus-like and noggin do not interact during mouse forebrain development." *Int. J. Dev. Biol.*, 2001: 45: 441-443.

Bouchard, M., Souabni A, Mandler M, Neubüser A, and Busslinger M. "Nephric lineage specification by Pax2 and Pax8." *Genes Dev*, 2002: 16(22):2958-70.

Bouwmeester, T. "The Spemann-Mangold organizer: the control of fate specification and morphogenetic rearrangements during gastrulation in Xenopus." *Int. J. Dev. Biol.*, 2001: 45: 251-258.

Bouwmeester, T., Kim S, Sasai Y, Lu B, and De Robertis EM. "Cerberus is a head-inducing secreted factor expressed in the anterior endoderm of Spemann's organizer." *Nature*, 1996: 382(6592):595-601.

Bouwmeester, T., and Leyns, L. "Vertebrate head induction by anterior primitive endoderm." *Bioessays*, 1997: 10:855-63.

Bovolenta, P., Esteve, P., Ruiz, J.M., Cisneros, E. and Lopez-Rios, J. "Beyond Wnt inhibition: new functions of secreted Frizzled-related proteins in development and disease." *J Cell Sci*, 2008: 121(6):737-46.

Boyles, A.L, Hammock, P. and Speer, M.C. "Candidate Gene Analysis in Human Neural Tube Defects." *American Journal of Medical Genetics*, 2005: 135C:9–23.

Brennan, J., Lu, C.C., Norris, D.P., Rodriguez, T.A., Beddington, R.S. and Robertson, E.J. "Nodal signalling in the epiblast patterns the early mouse embryo." *Nature*, 2001: 411(6840):965-9.

Bridgewater, D., Cox B Cain J, Lau A Athaide V, Gill PS Kuure S, Sainio K, and Rosenblum ND. "Canonical WNT/beta-catenin signaling is required for ureteric branching." *Dev Biol.* , 2008: 317(1):83-94.

Buckingham, M., Bajard L, Daubas P Chang T, Meilhac S Hadchouel J, Rocancourt D Montarras D, and Relaix F. "The formation of skeletal muscle: from somite to limb." *J Anat.*, 2003: 202(1):59-68. Review.

Burke, A.C. "Development and Evolution of the Vertebrate Mesoderm." *Developmental Dynamics*, 2007: 236:2369–2370.

Cadigan, K.M. "Wnt–β-catenin signaling." *Current Biology*, 2008: 18(20):943-947.

Capdevila, J., and Izpisúa Belmonte, J.C.. "Patterning mechanisms controlling vertebrate limb development." *Annu Rev Cell Dev Biol*, 2001: 17:87-132.

Chen, C., and Shen MM. "Two modes by which Lefty proteins inhibit Nodal signaling." *Curr. Biol.*, 2004: 14, 618–624.

Chen, C., Ware, S.M., Sato, A., Houston-Hawkins, D., Habas, R.. "The Vg1-related protein Gdf3 acts in a Nodal signalling pathway in the pre-gastrulation mouse embryo." *Development*, 2006: 133, 319–329.

Cheng, S.K., Olale, F., Brivanlou, A.H. and Schier, A.F. "Lefty blocks a subset of TGF beta signals by antagonizing EGF-CFC coreceptors." *PLoS Biol*, 2004: 2, 215–226.

Cheng, S.K., Olale, F., Bennett, J.T., Brivanlou, A.H. and Schier, A.F. "EGF-CFC proteins are essential coreceptors for the TGF-beta signals Vg1 and GDF1." *Genes Dev*, 2003: 17, 31–36.

Chi, C. L., Martinez, S., Wurst, W. and Martin, G.R. "The isthmic organizer signal FGF8 is required for cell survival in the prospective midbrain and cerebellum." *Development*, 2003: 130, 2633-2644.

Chiang, C., Litingtung, Y., Lee, E., Yong, K. E., Corden, J. L., Westphal, H. and Beachy, P. A. Cyclopia and defective axial patterning in mice lacking Sonic hedgehog gene function. *Nature*, 1996: 383, 407-413

Chiang C, Litingtung Y, Harris MP, Simandl BK, Li Y, Beachy PA, Fallon JF. Manifestation of the limb prepattern: limb development in the absence of Sonic hedgehog function. *Dev Biol.*, 2001 235:421–433.

Chu, J., Ding, J. Jeays-Ward, K., Price, S.M., Placzek, M. and Shen, M.M. "Non-cell-autonomous role for Cripto in axial midline formation during vertebrate embryogenesis." *Development*, 2005: 132, 5539-5551.

Clevers, H. "Wnt/β-Catenin Signaling in Development and Disease." *Cell*, 2006: 127:469-480.

Cohen, E.D., Tian, Y. and Morrisey, E.E.. "Wnt signaling: an essential regulator of cardiovascular differentiation, morphogenesis and progenitor self-renewal." *Development*, 2008: 135, 789-798.

Cohen, M.M. "The Hedgehog Signaling Network." *American Journal of Medical Genetics*, 2003: 123A:5–28.

Conlon, F.L., Lyons, K.M., Takaesu, N., Barth, K.S., Kispert, A. "A primary requirement for nodal in the formation and maintenance of the primitive streak in the mouse." *Development*, 1994: 120(7):1919-28.

Correia, K.M., and Conlon, R.A. "Surface ectoderm is necessary for the morphogenesis of somites." *Mechanisms of Development*, 2000: 91:19-30.

Crossley, P. H., Minowada, G., MacArthur, C.A. and Martin, G.R. "Roles for FGF8 in the induction, initiation, and maintenance of chick limb development." *Cell*, 1996: 84, 127-136.

Crossley, P.H., and G.R. Martin, G.R. "The mouse Fgf8 gene encodes a family of polypeptides and is expressed in regions that direct outgrowth and patterning in the developing embryo." *Development*, 1995: 121(2):439-51.

da Vinci, L. "Studies of Embryos." 1510-1513.

De Langhe, S.P. and Reynolds, S.D. "Wnt signaling in lung organogenesis." *Organogenesis*, 2008: 4(2):100-8.

Deng, C.X., Wynshaw-Boris, A., Shen, M.M., Daugherty, C., Ornitz, D.M. and Leder, P. "Murine FGFR-1 is required for early postimplantation growth and axial organization." *Genes Dev*, 1994: 8(24):3045-57.

Di-Gregorio, A., Sancho, M., Stuckey, D.W. Crompton, L.A. Godwin, J. and et al. "BMP signalling inhibits premature neural differentiation in the mouse embryo." *Development*, 2007: 134, 3359-3369.

Ding, J., Yang, L., Chen, A., Desai, N., Wynshaw-Boris, A. and Shen, M.M.. "Cripto is required for correct orientation of the anterior-posterior axis in the mouse embryo." *Nature*, 1998: 395(6703):702-7.

Dressler, G.R. "The cellular basis of kidney development." *Annu Rev Cell Dev Biol*, 2006: 22:509–529.

Dubrulle, J., and Pourquié, O. "Coupling segmentation to axis formation." *Development*, 2004: 131(23):5783-93.

Dubrulle, J., and Pourquie, O. "fgf8 mRNA decay establishes a gradient that couples axial elongation to patterning in the vertebrate embryo." *Nature*, 2004: 427:419–422.

Dubrulle, J., McGrew, M.J. and Pourquie, O. "FGF signaling controls somite boundary position and regulates segmentation clock control of spatiotemporal Hox gene activation." *Cell*, 2001: 106:219–232.

Dufort, D., Schwartz, L. Harpal, L. and Rossant, J. "The transcription factor HNF3b is required in visceral endoderm for normal primitive streak morphogenesis." *Development*, 1998: 125, 3015-3025.

Echelard, Y., St-Jacques B Epstein DJ, Mohler J Shen L, McMahon, J.A. and McMahon A.P.. "Sonic hedgehog, a member of a family of putative signaling molecules, is implicated in the regulation of CNS polarity." *Cell*, 1993: 75(7):1417-30.

Foley, A.C., Skromne, I. and Stern, C.D. "Reconciling different models of forebrain induction and patterning: a dual role for the hypoblast." *Development*, 2000: 127(17):3839-54.

Foley, A.C., Korol, O.,Timmer, A.M. and Mercola, M. "Multiple functions of Cerberus cooperate to induce heart downstream of Nodal." *Developmental Biology*, 2007: 303:57–65.

Fukuo, Y., Nakatani T, Shinohara H, and Matsuda T. "The mouse pericardium: it allows passage of particulate matter from the pleural to the pericardial cavity." *The Anatomical Record*, 1988: 222(1):1-5.

Furushima, K., Yamamoto, A. Nagano, T. Shibata, M. Kiyonari, H. and Aizawa, S. "Mouse homologues of Shisa antagonistic to Wnt and Fgf signalings." *Developmental Biology*, 2007: 306: 480–492.

Galceran, J., Farinas, I., Depew, M.J. Clevers, H. and Grosschedl, R. "Wnt3a−/−-like phenotype and limb deficiency in Lef1−/−Tcf1−/− mice." *Genes & Development*, 1999: 13: 709–717.

Gilbert, S.F. *Developmental Biology.* 8th. Sinauer, 2006.

Glinka, A., Wu, W., Onichtchouk, W., Blumenstock, C. and Niehrs, C. "Head induction by simultaneous repression of Bmp and Wnt signalling in Xenopus." *Nature*, 1997: 389(6650):517-9.

Glinka, A., Wu, W., Delius, H., Monaghan, A.P. Blumenstock, C. and Niehrs, C. "Dickkopf-1 is a member of a new family of secreted proteins and functions in head induction." *Nature*, 1998: 391: 357-362.

Grass, S., Arnold, H.H. and Braun, T. "Alterations in somite patterning of Myf-5-deficient mice: a possible role for FGF-4 and FGF-6." *Development*, 1996: 122:141.

Gray, P.C., Harrison, C.A. and Vale, W. "Cripto forms a complex with activin and type II activin receptors and can block activin signaling." *Proc. Natl. Acad. Sci. U. S. A.*, 2003: 100, 5193–5198.

Greene, N.D., and Copp, A.J. "Development of the vertebrate central nervous system: formation of the neural tube." *Prenat Diagn*, 2009: 29(4):303-11.

Gritsman, K., Zhang, J., Cheng, S., Heckscher, E.,Talbot, W.S. and Schier, A.F. "The EGF-CFC protein one-eye-pinhead is essential for Nodal signalling." *Cell*, 1999: 97, 121–132.

Hains, D., Sims-Lucas S, Kish K, Saha M, McHugh K, and Bates CM. "Role of fibroblast growth factor receptor 2 in kidney mesenchyme." *Pediatr Res.*, 2008: 64(6):592-8.

Hamada, H., Meno C, Watanabe D, and Saijoh Y. "Establishment of vertebrate left-right asymmetry." *Nat. Rev. Genet*, 2002: 3, 103-113.

Hanks, S.K., and T. Hunter. "The eukaryotic protein kinase superfamily: kinase (catalytic) domam structure and classification." *FASEB J.*, 1995: 9(8):576-96.

Haraguchi, S., Naito, K. and Sato, E. "MAP kinase cascade, but not ERKs, activated during early cleavage of mouse embryos." *Mol Reprod Dev.*, 1998: 51(2):148-55.

Harms, P.W., and Chang, C. "Tomoregulin-1 (TMEFF1) inhibits nodal signaling through direct binding to the nodal coreceptor Cripto." *Genes Dev*, 2003: 17(21):2624-9.

Harris, M.J., and Juriloff, D.M. "Toward Understanding Mechanisms of Genetic Neural Tube." *Teratology*, 1999: 60:292–305.

Hartsoeker, N. "Essai de Dioptrique." 1694.

Hill, R.E., Heaney, S.J. and Lettice, L.A. "Sonic hedgehog: restricted expression and limb dysmorphologies." *Journal of Anatomy*, 2003: 202(1):13-20.

Ho, R. "Axis formation in the embryo of the zebrafish, Brachydanio rerio." *Semin. Dev. Biol.*, 1992: 3:53-64.

Hoffman, J.I. "Incidence of congenital heart disease: I. Postnatal incidence." *Pediatr Cardiol.*, 1995: 16:103–13.

Imuta, Y., Nishioka, N., Kiyonari, H. and Sasaki, H. "Short Limbs, Cleft Palate, and Delayed Formation of Flat Proliferative Chondrocytes in Mice With Targeted Disruption of a Putative Protein Kinase Gene, Pkdcc (AW548124)." *Developmental Dynamics*, 2009: 238:210–222,.

Itäranta, P., Seppänen T Chi L, Tuukkanen J Niku M, Peltoketo H, and Vainio, S. "Wnt-4 signaling is involved in the control of smooth muscle cell fate via Bmp-4 in the medullary stroma of the developing kidney." *Developmental Biology*, 2006: 293(2):473-83.

Itasaki, N., Jones, M. Rowe, A., Domingos, A.M., Smith, J.C. and R. Krumlauf. "Wise, a context-dependent activator and inhibitor of Wnt signalling." *Development*, 2003: 130, 4295-4305.

Jiang, J., and Hui, C.C. "Hedgehog Signaling in Development and Cancer." *Developmental Cell*, 2008: 15(6):801-12.

Jiao, K., Langworthy, M., Batts, L., Brown, C.B., Moses, H.L. and Baldwin, H.S. "Tgfbeta signaling is required for atrioventricular cushion mesenchyme remodeling during in vivo cardiac development." *Development*, 2006: 133(22):4585-93.

Jones, N., Voskas, D. Master, Z., Sarao R, Jones J, and Dumont. D.J. "Rescue of the early vascular defects in Tek/Tie2 null mice reveals an essential survival function." *EMBO Rep*, 2001: 2(5):438-45.

Jörnvall, H., Reissmann E, Andersson O, Mehrkash M, and Ibáñez, C.F. "ALK7, a receptor for nodal, is dispensable for embryogenesis and left-right patterning in the mouse." *Mol. Cell Biology*, 2004: 24(21):9383-9.

Kassel, O., Sancono, A., Krätzschmar, J., Kreft, B., Stassen, M. and Cato, A.C. "Glucocorticoids inhibit MAP kinase via increased expression and decreased degradation of MKP-1." *EMBO J.*, 2001: 20(24):7108-16.

Kawano, Y., and Kypta, R. "Secreted antagonists of the Wnt signalling pathway." *J Cell Sci.*, 2003: 116(13):2627-34.

Kibar, Z., Capra, V. and Gros, P. "Toward understanding the genetic basis of neural tube defects." *Clinical Genetics*, 2007: 71: 295–310.

Kikuchi, A., Yamamoto, H. and Kishida, S. "Multiplicity of the interactions of Wnt proteins and their receptors." *Cellular Signalling*, 2007: 659-671.

Kimura, C., Shen, NMM, Takeda, N., Aizawa, S. and Matsuo, I. "Complementary functions of Otx2 and Cripto in initial patterning of mouse epiblast." *Dev Biol*, 2001: 235, 12–32.

Kimura-Yoshida, C., Nakano, H., Okamura, D., Nakao, K., Yonemura, S.. "Canonical Wnt Signaling and Its Antagonist Regulate Anterior-Posterior Axis Polarization by Guiding Cell Migration in Mouse Visceral Endoderm." *Developmental Cell*, 2005: 9:639–650.

Kirschner, S. "Wilhelm Roux's concept of 'developmental mechanics'." *Wurzbg Medizinhist Mitt.*, 2003: 22:67-80.

Kishigami, S., and Mishina, Y. "BMP signaling and early embryonic patterning." *Cytokine & Growth Factor Reviews*, 2005: 16, 265–278.

Kispert, A., Vainio, S., McMahon, A.P. "Wnt-4 is a mesenchymal signal for epithelial transformation of metanephric mesenchyme in the developing kidney." *Development* 1998: 125, 4225–4234.

Klingensmith, J., Ang, S.L., Bachiller, D. and Rossant, J. "Neural induction and patterning in the mouse in the absence of the node and its derivatives." *Developmental Biology*, 1999: 216:535–549.

Kobayashi, A., Kwan KM, Carroll TJ, McMahon AP, Mendelsohn C, and Behringer, R.R. "Distinct and sequential tissue-specific activities of the LIM-class homeobox gene Lim1 for tubular morphogenesis during kidney development." *Development*, 2005: 132(12):2809-23.

Krebs, L.T., Nonaka, S., Saijoh, Y., O'Brien, O.P,. Hamada, H. and T. Gridley. "Notch signaling regulates left-right asymmetry determination by inducing Nodal expression." *Genes and Development*, 2003: 17: 1207-1212.

Kronenberg, H.M. "Developmental regulation of the growth plate." *Nature*, 2003: 423:332–336.

Lee, J.D., and Anderson, K.V. "Morphogenesis of the node and notochord: the cellular basis for the establishment and maintenance of left-right asymmetry in the mouse." *Developmental Dynamics*, 2008: 237(12): 3464–3476.

Lei, Q., Jeong, Y., Misra, K., Zelman, A.K., Epstein, D.J., and Matise, M.P. "Wnt Signaling Inhibitors Regulate the Transcriptional Response to Morphogenetic Shh-Gli Signaling in the Neural Tube." *Developmental Cell*, 2005: 11, 325–337.

Levine, A., and Brivanlou, A.H. "GDF3, a BMP inhibitor, regulates cell fate in stem cells and early embryos." *Development*, 2006: 133, 209–216.

Levine, A.J., and Brivanlou, A.H. "Proposal of a model of mammalian neural induction." *Developmental Biology*, 2007: 308:247–256.

Li, S., and Muneoka, K. "Cell migration and chick limb development: chemotactic action of FGF-4 and the AER." *Developmental Biology*, 1999: 211(2):335-47.

Liguori, G.L., Borges, A.C., D'Andrea D Liguoro A Gonçalves L Salgueiro AM, Persico M.G., and Belo J.A. "Cripto-independent Nodal signaling promotes positioning of the A–P axis in the early mouse embryo." *Developmental Biology*, 2008: 315:280–289.

Liguori, G.L., Echevarría, D., Improta, R., Signore, M., Martínez, S. and Persico, M.G. "Anterior neural plate regionalization in cripto null mutant mouse embryos in the absence of node and primitive streak." *Dev Biol*, 2003: 264(2):537-49.

Lindsley, R.C., Gill, J.G., Kyba, M., Murphy, T.L. and Murphy, K.M. "Canonical Wnt signaling is required for development of embryonic stem cell-derived mesoderm." *Development*, 2006: 133, 3787-3796.

Liu, P., Wakamiya, M., Shea, M.J., Albrecht, U., Behringer,R.R. and Bradley, A. "Requirement for Wnt3 in vertebrate axis formation." *Nature Genetics*, 1999: 22(4):361-5.

Lowe, L., Yamada, S. and Kuehn, M.R. "Genetic dissection of Nodal function in patterning the mouse embryo." *Development*, 2001: 128, 1831–1843.

Lowe, L.A., Sampath K Supp, K Wright CVE Yokoyama, Potter SS Overbekk P, and Kuehn M.R. "Conserved left-right asymmetry of nodal expression and alterations in murine situs inversus." *Nature*, 1996: 381(6578):158-61.

Lu, C.C., and E.J. Robertson. "Multiple roles for Nodal in the epiblast of the mouse embryo in the establishment of anterior-posterior patterning." *Developmental Biology*, 2004: 273:149– 159.

Lu, C.C., Brennan, J. and Robertson, E.J. "From fertilization to gastrulation: axis formation in the mouse embryo." *Curr. Opin. Genet. Dev.*, 2001: 11, 384–392.

Ma, G., Xiao, Y. and He, L. "Recent progress in the study of Hedgehog signaling." *J. Genet. Genomics*, 2008: 35(3):129-37.

Mangold, O. "Uber die Induktionsfahigkeit der verschiedenen Bezirke der Neurula von Urodelen." *Naturwissenschaften*, 1933: 21:761–766.

Mao, B., Wu, W., Hoppe, D., Stannek, P., Glinka, A. and Niehrs, C. "LDL-receptor related protein 6 is a receptor for Dickkopf proteins." *Nature*, 2001: 411:321–325.

Maretto, S., Aricescu, A.R. Muller, K.W.Y. Cho, E., Bikoff, K., and. Robertson, E.J. "Ventral closure, headfold fusion and definitive endoderm migration defects in mouse embryos lacking the fibronectin leucine-rich transmembrane protein FLRT3." *Developmental Biology*, 2008: 318: 184–193.

Marikawa, Y. "WntB-catenin signaling and body plan formation in mouse embryos." *Cell & Developmental Biology*, 2006: 17:175–184.

Marques, S., Borges, A.C., Silva, A.C., Freitas, S., Cordenonsi, M. and Belo, J.A. "The activity of the Nodal antagonist Cerl-2 in the mouse node is required for correct L/R body axis." *Genes and Development*, 2004: 18: 2342-2347.

Matsuda, T., Fukuo, Y., Shinohara, H., Morisawa, S., Nakatani, T. " The postnatal development of the mouse pericardium; the time and mechanism of formation of pericardial pores." *Okajimas Folia Anat Jpn*. 1990: 67:115-20

McGrath, J., Somlo, S., Makova, S., Tian, X. and M. Brueckner. "Two populations of node monocilia initiate left-right asymmetry in the mouse." *Cell*, 2003: 114:61–73.

McInnes, R.R., and Michaud, J.L. "Toward understanding the genetic basis of neural tube defects." *Clin Genet*, 2007: 71: 295–310.

Mehlen, P., F. Mille, and C. Thibert. "Morphogens and Cell Survival during Development." 2005: 357-366.

Meilhac, S.M., Esner, M., Kelly, R.G., Nicolas, J.F. and Buckingham, M.E. "The clonal origin of myocardial cells in different regions of the embryonic mouse heart." *Dev Cell.*, 2004: 6:685–98.

Meno, C., Gritsman K Ohishi S Ohfuji Y Heckscher E, Mochida K Shimono A Kondoh H., Talbot, W.S., Robertson, E.J., Schier, A.F. and Hamada, H. "Mouse Lefty2 and Zebrafish Antivin Are Feedback Inhibitors of Nodal Signaling during Vertebrate Gastrulation." *Molecular Cell*, 1999: 4, 287–298.

Meno, C., Shimono Y Saijoh, Yashiro K Mochida Ohishi S. K, Noji S Kondoh H, and Hamada, H. "lefty-1 is required for left–right determination as a regulator of lefty-2 and Nodal." *Cell*, 1998: 94, 287–297.

Mercola, M. "Left-right asymmetry: Nodal points." *Journal of Cell Science*, 2003: 16: 3251-3257.

Mesnard, D., Filipe, M., Belo, J.A. and Zernicka-Goetz, M. "The Anterior-Posterior Axis Emerges Respecting the Morphology of the Mouse Embryo that Changes and Aligns with the Uterus before Gastrulation." *Current Biology*, 2004: 14:184–196,.

Mesnard, D., Guzman-Ayala, M. and Constam, D.B. " Nodal specifies embryonic visceral endoderm and sustains pluripotent cells in the epiblast before overt axial patterning." *Development*, 2006: 133, 2497–2505.

Minchiotti, G. "Nodal-dependant Cripto signaling in ES cells: from stem cells to tumor biology." *Oncogene*, 2005: 24:5668–5675.

Mine, N., Anderson, R.M. and Klingensmith, J. "BMP antagonism is required in both the node and lateral plate mesoderm for mammalian left-right axis establishment." *Development*, 2009: 135, 2425-2434.

Mitra, S.M., Hanson, D.A. and. Schlaepfer, D.D. "Focal adhesion kinase: in command and control of cell motility." *Molecular Cell Biology*, 2005: 56-68.

Montcouquiol, M., Crenshaw, E.B. and Kelley, M.W. "Noncanonical Wnt Signaling and Neural Polarity." *Annu. Rev. Neurosci*, 2006: 29:363-386.

Moore-Scott, B.A., Opoka, R., Lin, S.J., Kordich, J.J. and Wells, J.M.. "Identification of Molecular Markers That Are Expressed in Discrete Anterior–Posterior

Domains of the Endoderm From the Gastrula Stage to Mid-gestation." *Developmental Dynamics*, 2007: 236:1997–2003.

Mugford, J.W., Yu J, Kobayahi A, and McMahon AP. "High-resolution gene expression analysis of the developing mouse kidney defines cellular compartments within the nephron progenitor population." *Developmental Biology*, 2009.

Nie, X., Luuko, K. and Kettunen, P. "BMP signalling in craniofacial development." *Int. J. Dev. Biol.*, 2006: 50: 511-521.

Norris, D.P., Brennan, J., Bikoff, E.K. and Robertson, E.J. "The FoxH1-dependent autoregulatory enhancer controls the level of Nodal signals in the mouse embryo." *Development*, 2002: 129, 3455–3468.

Oppenheimer, J.M. "Hans Driesch and the theory and practice of embryonic transplantation." *Bull Hist Med.*, 1970: 44(4):378-82.

Oulad-Abdelghani, M., Chazaud, C., Bouillet, P., Mattei, M.G., Dollé, P. and Chambon, P. "Stra3/lefty, a retinoic acid-inducible novel member of the transforming growth factor-beta superfamily." *Int J Dev Biol*, 1998: 42(1):23-32.

Palmeirim, I., Henrique, D., Ish-Horowicz, D. and Pourquié, O. "Avian hairy gene expression identifies a molecular clock linked to vertebrate segmentation and somitogenesis." *Cell*, 1997: 91(5):639-48.

Perantoni, AO, Naillat F Timofeeva O, Pajni-Underwood S Richman C, Vainio S Wilson C, Dove LF, and Lewandoski, M. "Inactivation of FGF8 in early mesoderm reveals an essential role in kidney development." *Development*, 2005: 132:3859–3871.

Perea-Gomez, A., Lawson, K.A., Rhinn, M., Zakin L Brûlet P, Mazan, S. and Ang, S.L. "Otx2 is required for visceral endoderm movement and for the restriction of posterior signals in the epiblast of the mouse embryo." *Development*, 2001: 128(5):753-65.

Perea-Gomez, A., Shawlot W, Oulad-Abdelghani M. Vella FD, Meno C Chazaud C, Chen L, Robertson E. Pfister V, and Hamada, H. "Nodal antagonists in the anterior visceral endoderm prevent the formation of multiple primitive streaks." *Dev. Cell*, 2002: 3, 745–756.

Persico, M.G., G. Liguori, S. Parisi, D. D'Andrea, and G. Minchiotti. "Cripto in tumors and embryo development." *Biochim. Biophys. Acta*, 2001: 1552, 87–93.

Pfeffer, P.L., De Robertis, E.M. and Izpisua-Belmonte, J.C. "Crescent, a novel chick gene encoding a Frizzled-like cysteine-rich domain, is expressed in anterior regions during early embryogenesis." *Int J Dev Biol*, 1997: 41(3):449-58.

Piccolo, S., Agius, E., Leyns, L., Bhattacharyya, S., Bouwmeester, T. and De Robertis, E.M. "The head inducer Cerberus is a multifunctional antagonist of Nodal, BMP and Wnt signals." *Nature*, 1999: 397(6721):707-10.

Piccolo, S., Sasai, Y., Lu, B., and De Robertis, E.M. "Dorsoventral patterning in Xenopus: inhibition of ventral signals by direct binding of chordin to BMP-4." *Cell*, 1996: 86(4):589-98.

Pirskanen, A., Kiefer, J.C. and Hauschka, J.D. "IGFs, insulin, Shh, bFGF, and TGF-beta1 interact synergistically to promote somite myogenesis in vitro." *Dev Biol*, 2000: 224(2):189-203.

Pourquié, O. "The chick embryo: a leading model in somitogenesis studies." *Mech Dev*, 2004: 121(9):1069-79.

Pourquié, O. "Vertebrate somitogenesis." *Annu. Rev. Cell Dev. Biol.*, 2001: 17:311–50.

Powers, CJ, McLeskey, S.W. and Wellstein, A. "Fibroblast growth factors, their receptors and signaling." *Endocr Relat Cancer*, 2000: 7:165–197.

Qian, D., Jones, C., Rzadzinska, A., Mark, S., Zhang, X. "Wnt5a functions in planar cell polarity regulation in mice." *Developmental Biology*, 2007: 306:121–133.

Rankin, C.T., Bunton, T., Lawler, A.W. and S.J. Lee, S.J. "Regulation of left–right patterning in mice by growth/differentiation factor-1." *Nature Genetics*, 2000: 24:262–265.

Regenerative Medicine. Department of Health and Human Services, 2006.

Reissman, E., Jornvall, H., Blokzijl, A., Andersson, O., Chang, C. and et al. "The orphan receptor ALK7 and the activin receptor ALK4 mediate signalling by Nodal proteins during vertebrate development." *Genes Dev*, 2001: 15, 2010–2022.

Rivera-Pérez, J.A., and T. Magnuson. "Primitive streak formation in mice is preceded by localized activation of Brachyury and Wnt3." *Developmental Biology*, 2005: 288(2):363-71.

Rivera-Perez, J.A., Mager, J. and Magnuson, T. "Dynamic morphogenetic events characterize the mouse visceral endoderm." *Developmental Biology*, 2003: 261:470-487.

Robert, B. "Bone morphogenetic protein signaling in limb outgrowth and patterning." *Develop. Growth Differentiation*, 2007: 49:455–468.

Rodríguez Esteban, C., Capdevila, J., Economides, A.N., Pascual, J., Ortiz, A. and Izpisúa Belmonte, J.C. "The novel Cer-like protein Caronte mediates the establishment of embryonic left-right asymmetry." *Nature*, 1999: 401(6750):243-51.

Rodriguez, T.A., Srinivas, S., Clements, M.P., Smith, J.C., Beddington, R.S. "Induction and migration of the anterior visceral endoderm is regulated by the extra-embryonic ectoderm." *Development*, 2005: 132, 2513-2520.

Rubenstein, J. L. and Beachy, P. A. (1998). Patterning of the embryonic forebrain. *Curr. Opin. Neurobiol.* 8, 18-26.

Sabapathy, K., Jochum, W. Hochedlinger, K. Chang, L. Karin, M. and Wagner, E.F. "Defective neural tube morphogenesis and altered apoptosis in the absence of both JNK1 and JNK2." *Mech Dev.*, 1999: 89(1-2):115-24.

Saloman, D.S., Bianco, C., Ebert AD Khan NI De Santis M Normanno N Wechselberger C Seno M., Williams K Sanicola M Foley S, W, Gullick, J. and Persico, G. "The EGF-CFC family: novel epidermal growth factor-related proteins in development and cancer." *Endocrine-Related Cancer*, 2000: 7:199–226.

Sasai, Y., and De Robertis, E.M. "Ectodermal Patterning in Vertebrate Embryos." *Developmental Biology*, 1997: 182: 5–20.

Schier, A.F. "Nodal Signalling in Vertebrate Development." *Annu. Rev. Cell Dev. Biol.*, 2003: 19:589–621.

Schier, A.F., and M.M. Shen. "Nodal signalling in vertebrate development." *Nature*, 2000: 403(6768):385-9.

Schlange, T., Andree, B., Arnold, H. H. and Brand, T. "BMP2 is required for early heart development during a distinct time period." *Mech. Dev.* 2000: 91,259-270.

Schneider, V.A, and Mercola, M. "Wnt antagonism initiates cardiogenesis in Xenopus laevis." *Genes and Development*, 2001: 15:304–315.

Seidensticker, M.J., and Behrens, J. "Biochemical interactions in the wnt pathway." *Biochimica et Biophysica Acta*, 2000: 1495:168-182.

Shawlot, W., Wakamiya, M., Kwan, K.M., Kania, A., Jessell, T.M. and Behringer, R.R. "Lim1 is required in both primitive streak-derived tissues and visceral endoderm for head formation in the mouse." *Development*, 1999: 126, 4925-4932.

Shen, M.M. "Nodal signaling: developmental roles and regulation." *Development*, 2007: 134(6):1023-34.

Shen, M.M., and Schier, A.F. "The EGF-CFC gene family in vertebrate development." *Trends in Genetics*, 2000: 16(7):303-9.

Shen, M.M., Wang, H. and Leder, P. "A differential display strategy identifies cryptic, a novel EGF related gene expressed in the axial mesoderm during mouse gastrulation." *Development*, 1997: 124, 429–442.

Shi, S., and Stanley, P. "Evolutionary Origins of Notch Signaling in Early Development." *Cell Cycle*, 2006: 274-278.

Shiratori, H., and Hamada, H. "The left-right axis in the mouse: from origin to morphology." *Development*, 2006: 133(11):2095-104.

Shitashige, M., Hirohashi, S. and Yamada, T. "Wnt signaling inside the nucleus." *Cancer Sci*, 2008: 99:631–637.

Shum, AS, and Copp, A.J. "Regional differences in morphogenesis of the neuroepithelium suggest multiple mechanisms of spinal neurulation in the mouse." *Anat Embryol*, 1996: 194, 65-73.

Silva, A.C., Filipe, M., Kuerner, K.M., Steinbeisser, H., and Belo, J.A. "Endogenous Cerberus activity is required for anterior head specification in Xenopus." *Development*, 2003: 130, 4943-4953.

Silva, AC, Filipe M, Vitorino M, Steinbeisser H, and Belo JA. "Developmental expression of Shisa-2 in Xenopus laevis." *Int J Dev Biol.*, 2006: 50(6):575-9.

Simpson, E.H., Johnson DK, Hunsicker P, Suffolk R, Jordan S, and Jackson IJ. "The mouse Cer1 (Cerberus related or homologue) gene is not required for anterior pattern formation." *Developmental Biology*, 1999: 213(1):202-6.

Song, J., et al. "The type II activin receptors are essential for egg cylinder growth, gastrulation, and rostral head development in mice." *Dev. Biol.*, 1999: 213, 157–169.

Spemann, H. "Uber den Anteil von Implantat und Wirtskeim an der Orientierung Embryonalanlage." *W Roux Arch Entwicklungsmech*, 1931: 123:390–516.

Spemann, H., and Mangold, H. "Über induction von embryonalanlangen durch implantation artfremder organisatoren." *Wilhelm Roux Arch. Entwicklungsmech. Org.*, 1924: 100: 599-638.

Srinivas, S., Rodriguez, T., Clements, M., Smith, J.C., Beddington, R.S. "Active cell migration drives the unilateral movements of the anterior visceral endoderm." *Development* , 2004: 131, 1157–1164.

Stern, C.D. "Neural induction: 10 years on since the 'default model'." *Current Opinion in Cell Biology*, 2006: 18(6):692-697 .

Stern, C.D. "Neural induction: old problem, new findings, yet more questions." *Development*, 2005: 132, 2007-2021.

Stern, H.M., and Hauschka, S.D. "Neural tube and notochord promote in vitro myogenesis in single somite explants." *Dev Biol*, 1995: 167(1):87-103.

Stottmann, R.W., Berrong, M., Matta, C., Choi, M. and Klingensmith, J. "The BMP antagonist Noggin promotes cranial and spinal neurulation by distinct mechanisms." *Developmental Biology*, 2006: 295:647–663.

Strizzi, L., Bianco, C., Normanno, N. and Salomon, D. "Cripto-1: a multifunctional modulator during embryogenesis and oncogenesis." *Oncogene*, 2005: 24, 5731–5741.

Sun, X., Meyers, E.N., Lewandoski, M. and Martin, G.R. "Targeted disruption of Fgf8 causes failure of cell migration in the gastrulating mouse embryo." *Genes Dev*, 1999: 13(14):1834-46.

Sweetman, D., Wagstaff, L., Cooper, O., Weijer, C. and Münsterberg, A. "The migration of paraxial and lateral plate mesoderm cells emerging from the late primitive streak is controlled by different Wnt signals." *BMC Developmental Biology*, 2008: 1-15.

Takeuchi, J.K., Bisgrove B.W. Sun X. Lickert H., Chawengsaksophak K. Yamamoto M., Hamada H, Rossant J. Yost H.J., and Bruneau, B.G. "Baf60c is a nuclear Notch signaling component required for the establishment of left-right asymmetry." *PNAS*, 2007: 104(3):846-51.

Tam, P.P., Parameswaran M, Kinder SJ, and Weinberger RP. " The allocation of epiblast cells to the embryonic heart and other mesodermal lineages: the role of ingression and tissue movement during gastrulation." *Development*, 1997: 124(9):1631-42.

Tam, P.P.L., and Loebel, D.A.F. "Gene function in mouse embryogenesis: get set for gastrulation." *Nature Genetics*, 2007: 8(5):368-81.

Tam, P.P.L., and Steiner, K.L. "Anterior patterning by synergistic activity of the early gastrula organizer and the anterior germ layer tissues of the mouse embryo." *Development*, 1999: 126, 5171-5179.

Tam, P.P.L., Loebel, D.A.F. and Tanaka, S.S. "Building the mouse gastrula: signals, asymmetry and lineages." *Current Opinion in Genetics & Development*, 2006: 16:419–425.

Tam, P.P.L., Kanai-Azumay, M and Kanai, Y. "Early endoderm development in vertebrates: lineage differentiation and morphogenetic function." *Current Opinion in Genetics & Developmen*, 2003: 13:393–400.

Tanaka, K., Okabayashi, K., Asashima, M., Perrimon, N. and Kadowaki, T. "The evolutionarily conserved porcupine gene family is involved in the processing of the Wnt family." *Eur. J. Biochem.*, 2000: 267, 4300±4311.

Thomas, P.Q., Brown, A., and Beddington, R.S. "Hex: a homeobox gene revealing periimplantation asymmetry in the mouse embryo and an early transient marker of endothelial cell precursors." *Development*, 1998: 125, 85–94.

Thomas, P.Q., and Beddington, R.S. "Anterior primitive endoderm may be responsible for patterning the anterior neural plate in the mouse embryo." *Current Biology*, 1996: 11:1487–1496.

Tirosh-Finkel, L., Elhanany, H, Rinon, A., and Tzahor, E. "Mesoderm progenitor cells of common origin contribute to the head musculature and the cardiac outflow tract." *Development*, 2006: 133, 1943-1953.

Torres-Padilla, M. E., Richardson, L., Kolasinska, P., Meilhac, S. M., Luetke-Eversloh M., Zernicka-Goetz, M. "The anterior visceral endoderm of the mouse embryo is established from both preimplantation precursor cells and by de novo gene expression after implantation." *Dev. Biol.*, 2007: 309, 97–112.

Uusitalo, M., Heikkila, M, and Vainio, S. "Molecular Genetic Studies of Wnt Signaling in the Mouse." *Experimental Cell Research*, 1999: 253, 336–348.

van Amerongen, R., and Berns, A. "Knockout mouse models to study Wnt signal transduction." *TRENDS in Genetics*, 2006: 678-689.

Varlet, I., Collignon, J, and Robertson, E.J. "Nodal expression in the primitive endoderm is required for specification of the anterior axis during mouse gastrulation." *Development*, 1997: 124, 1033–1044.

Vasiliauskas, D., and Stern, C.D. "Patterning the Embryonic Axis: FGF Signaling and How Vertebrate Embryos Measure Time." *Cell*, 2004: 133-136.

von Baer, K.E. "Ovi Mammalium et Hominis genesi." *Saint-Petersburg's Academy of Science*, 1827.

Waddington, C.H. "Induction by the primitive streak and its derivatives in the chick." *J. Exp. Biol.*, 1933: 10:38-46.

Wagner, J., Schmidt, C., Nikowits, W. Jr. and Christ, B. "Compartmentalization of the somite and myogenesis in chick embryos are influenced by wnt expression." *Dev Biol*, 2000: 228(1):86-94.

Wallingford, J.B. "Neural Tube Closure and Neural Tube Defects: Studies in Animal Models Reveal Known Knowns and Known Unknowns." *American Journal of Medical Genetics Part C (Semin. Med. Genet.)*, 2005: 135C:59–68.

Wang, Z., Shu, W., Lu, M.M., Morrisey, E.E. " Wnt7b activates canonical signaling in epithelial and vascular smooth muscle cells through interactions with Fzd1, Fzd10, and LRP5." *Mol Cell Biol*. 2005: 25(12):5022-30

Watson, J.D., and Crick, F.H. "The structure of DNA." *Cold Spring Harb Symp Quant Biol.*, 1953: 18:123-31.

Wells, J.A., and Melton, DA. "Vertebrate Endoderm Development." *Annu. Rev. Cell Dev. Biol*, 1999: 15:393-410.

Whitman, M. "Nodal signaling in early vertebrate embryos: themes and variations." *Dev Cell*, 2001: 1(5):605-17.

Wodarz, A. "Mechanisms of Wnt Signalling in Development." *Annu. Rev. Cell Dev. Biol.*, 1998: 14:59–88.

Xu, B., English JM, Wilsbacher JL, Stippec S, Goldsmith EJ, and Cobb MH. "WNK1, a novel mammalian serine/threonine protein kinase lacking the catalytic lysine in subdomain II." *J Biol Chem.*, 2000: 275(22):16795-801.

Xu, C., Liguori, G, Persico, MG, and Adamson, ED. "Abrogation of the Cripto gene in mouse leads to failure of postgastrulation morphogenesis and lack of differentiation of cardiomyocytes." *Development*, 1999: 126(3):483-94.

Xu, H., and Baldini, A. "Genetic pathways to mammalian heart development: recent progress from manipulation of the mouse genome." *Semin Cell Dev Biol.*, 2007: 18(1): 77–83.

Yagi, T., Furuta Y Tokunaga T, Yoshida M Nada S, Saga Y Tsukada T, Ikawa Y Takeda N, and Aizawa S. "A novel ES cell line, TT2, with high germline-differentiating potency." *Anal Biochem*, 1993: 214(1):70-6.

Yamamoto, A., Nagano, T, Takehara, S, Hibi, M. and Aizawa, S. "Shisa promotes head formation through the inhibition of receptor protein maturation for the caudalizing factors, Wnt and FGF." *Cell*, 2005: 120(2):223-35.

Yamamoto, M., Beppu, H, Takaoka, K., Meno,C and H. Hamada. "Antagonism between Smad1 and Smad2 signaling determines the site of distal visceral endoderm formation in the mouse embryo." *J. Cell Biology*, 2009: 184(2) 323–334.

Yamamoto, M., Y. Saijoh, A. Perea-Gomez, W. Shawlot, R.R. Behringer, and et al. "Nodal antagonists regulate formation of the anteroposterior axis of the mouse embryo." *Nature*, 2004: 428, 387–392.

Yamanaka, Y., Ralston, A, Stephenson, RO, and Rossant, J. "Cell and molecular regulation of the mouse blastocyst." *Developmental Dynamics*, 2006: 235:2301–2314.

Yan, Y.T., Liu, JJ. Luo, EC, Haltiwanger,RS, Abate-Shen, C, and Shen, M.M.. "Dual roles of Cripto as a ligand and coreceptor in the Nodal signaling pathway." *Mol. Cell. Biol*, 2002: 22, 4439–4449.

Yan, Y.T., Gritsman, K, Ding, J, Burdine, RD, Corrales, JD and et al. "Conserved requirement for EGF-CFC genes in vertebrate left–right axis formation." *Genes Dev*, 1999: 13:2527–2537.

Yang, Y.P., and Klingensmith, J. "Roles of organizer factors and BMP antagonism in mammalian forebrain establishment." *Developmental Biology*, 2006: 296:458–475.

Ybot-Gonzalez, P., Gaston-Massuet, C, Girdler, G, Klingensmith, J; Arkell, R. et al. "Neural plate morphogenesis during mouse neurulation is regulated by antagonism of Bmp signalling." *Development*, 2007: 134, 3203-3211.

Ybot-Gonzalez, P., Savery, D, Gerrelli, D, Signore, M, Mitchell, CE et al. "Convergent extension, planar-cell-polarity signalling and initiation of mouse neural tube closure." *Development*, 2007: 134, 789-799.

Yeo, C., and Whitman, M. "Nodal signals to Smads through Cripto-dependent and Cripto-independent mechanisms." *Mol Cell*, 2001: 7, 949–957.

Yoshikawa, Y, Fujimor, T, McMahon, AP and Takada, S.. "Evidence that absence of Wnt-3a signaling promotes neuralization instead of paraxial mesoderm development in the mouse." *Dev Biol*, 1997: 183(2):234-42.

Yu J, Carroll TJ, McMahon AP. "Sonic hedgehog regulates proliferation and differentiation of mesenchymal cells in the mouse metanephric kidney." *Development* 2002, 129:5301-5312

Yu, J., McMahon, AP, and Valerius, MT. "Recent genetic studies of mouse kidney development." *Curr Opin Genet Dev*, 2004: 14(5):550-7.

Zernicka-Goetz, M. "Cleavage pattern and emerging asymmetry of the mouse embryo." *Nature Reviews Molecular Cell Biology*, 2005: 6(12):919-28.

Zernicka-Goetz, M. "Patterning of the embryo: the first spatial decisions in the life of a mouse." *Development*, 2002: 129, 815-829.

Zernicka-Goetz, M., Morris, SA, and Bruce, AW. "Making a firm decision: multifaceted regulation of cell fate in the early mouse embryo." *Nature Reviews Genetics*, 2009: 10(7):467-77.

Zhao, G.Q. "Consequences of Knocking Out BMP Signaling in the Mouse." *genesis*, 2003: 35:43–56.

Zhu, L., Belo, JA, De Robertis, EM and Stern, CD. "Goosecoid Regulates the Neural Inducing Strength of the Mouse Node." *Developmental Biology*, 1999: 216, 276–281.

Zimmerman, L.B., De Jesús-Escobar, JM, and Harland, RM. "The Spemann organizer signal noggin binds and inactivates bone morphogenetic protein 4." *Cell*, 1996: 86(4):599-606.

Zúñiga, A, Haramis, AP, McMahon, AP and Zeller, R. "Signal relay by BMP antagonism controls the SHH/FGF4 feedback loop in vertebrate limb buds." *Nature*, 1999: 401(6753):598-602.

9. Appendix I

SOLUTIONS

Table 9.1 - List of solutions

Pre-hybridization solution in WISH

50% formamide
5X SSC
0,1% Tween-20
50µg/ml heparin
Prepare it with DEPC treated water

Hybridization solution in WISH

Pre-hybridization solution:
50µg/ml tRNA
50µg/ml salmon sperm DNA (ssDNA)
denatured probe

WISH solution I

50% formamide
4X SSC
1% SDS
H2O

WISH solution II

50% formamide
2X SSC
H2O

SSC 20x

3M NaCl
0.3M $Na_3C_3H_5O(CO_2)_3$ (sodium citrate)
Fill with water and adjust pH to 7.0

MABT

150mM NaCl
100mM $C_4H_4O_4$ (Maleic Acid)
0.1% Tween-20
Fill with water and adjust pH to 7.5

NTMT

0.1M NaCl
0.1M Tris-HCl
0.05M $MgCl_2$
0.1% Tween-20
Fill with water

PBS 10x

80.6mM Na_3PO_4 (sodium phosphate)
19.4mM KH_2PO_4 (potassium phosphate)
27mM KCl
1.37M NaCl
Fill with water and adjust pH to 7.4

α-ES medium

20% FBS
2mM L-Glutamine
Pen/Strep (50U/mL;50µg/mL)
Fill with DMEM (Bicarbonate free/10mM Hepes)

β-ES medium

20% FBS
20% DMSO
Fill with DMEM (Bicarbonate free/10mM Hepes)

MEFs medium

10% FBS
4mM L-Glutamine
0.1mM β-mercaptoethanol
Pen/Strep (50U/mL;50µg/mL)
Fill with DMEM Glutamax

ES cell medium

15% FBS
4mM L-Glutamine
0.1mM β-mercaptoethanol
Pen/Strep (50U/mL;50µg/mL)
0.1 mM Non essential aa
LIF (1000U/mL))
Fill with DMEM Knockout

ES cell 2x freezing medium

20% FBS
20% DMSO
Fill with DMEM

Southern Denaturing Solution

0.5M NaOH
1.0M NaCl
Fill with water and adjust pH to 7.4

Southern Neutralizing Solution

0.5M Tris-HCl
1.5M NaCl
Fill with water and adjust pH to 7.4

Southern Wash Solution I

2x SSC
0.1% SDS

Southern Wash Solution II

0.1x SSC
0.1% SDS

Southern Washing Buffer

0.1 M Maleic acid
0.15 M NaCl
0.3% Tween 20
Fill with water and adjust pH to 7.5

Southern Maleic Acid Buffer

0.1 M Maleic acid
0.15 M NaCl
Fill with water and adjust pH to 7.5

Southern Detection Buffer

0.1 M Tris-HCl
0.1 M NaCl
Fill with water and adjust pH to 9.5

IN SITU PROBES

9.2 – List of *in situ* probes

Clone	Enzyme	RNA polymerase
ADTK1 (ck_624551)	SacI	SP6
ADTK1 (NM_134117)	SacI	T7
BMP4	BamHI	T7
Bra	BamHI	T7
Chd	NotI	T3
Cryptic	EcoRI	T7
cShisa	SalI	T7
Dkk1	EcoRI	T3
Fgf 8	NotI	T7
HNF-3β (FoxA2)	Asp700	T7
Krox20	BamHI	T3
Lim1	HindIII	T7
mShisa (BC05764)	BglII	T7
Nodal	PstI	T7
Noggin	NotI	T7
Otx2	EcoRI	SP6
Shh	HindIII	T3
Wnt3	HindIII	T3

SOUTHERN ASSEMBLY

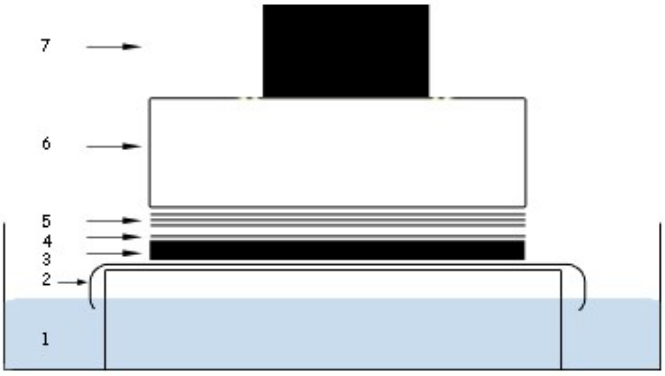

Figure 9.1 - Southern assembly

1-SSC 10x; **2**- Whatmann 3M paper; **3**- agarose gel; **4**- nitrocellulose membrane the size of the gel; **5**- 3 Whatmann 3M sheets the size of the gel; **6**- stack of absorbent paper the size of the gel at least 10cm high; **7**- weight